Masters Theses   Graduate School

8-2023

Development of Domestic Oleochemicals for Coating Applications

Caleb M. Metzcar
Food Science Graduate Student, cmetzcar@vols.utk.edu

To the Graduate Council:

I am submitting herewith a thesis written by Caleb M. Metzcar entitled "Development of Domestic Oleochemicals for Coating Applications." I have examined the final electronic copy of this thesis for form and content and recommend that it be accepted in partial fulfillment of the requirements for the degree of Master of Science, with a major in Food Science.

<div align="right">Tong Wang, Xiaofei Ye, Major Professor</div>

We have read this thesis and recommend its acceptance:

Curtis Luckett

<div align="right">Accepted for the Council:

Dixie L. Thompson</div>

<div align="right">Vice Provost and Dean of the Graduate School</div>

(Original signatures are on file with official student records.)

Development of Domestic Oleochemicals for Coating Applications

A Thesis Presented for the
Master of Science
Degree
The University of Tennessee, Knoxville

Caleb Matthew Metzcar
August 2023

ACKNOWLEDGMENTS

ABSTRACT

The overall objective of the present work is to explore new applications of soybean oil based oleochemicals. Two main applications are developed; one using soybean oil, acrylic acid, and nonthermal plasma (NTP) treatment to dye para-aramids with cationic and non-ionic pigments; the other using fatty acids to synthesize waxes with bound quaternary ammonium compounds (QAC), an antimicrobial functional group, for fruit and vegetable postharvest coating. The color strength of the dyed fabric was quantified and effect of the dyeing on material strength was evaluated to identify the optimal treatment condition. Antimicrobial waxes have been successfully developed that some structures demonstrate strong antibacterial and antifungal activities.

TABLE OF CONTENTS

LIST OF TABLES

LIST OF FIGURES

INTRODUCTION

In 2020 the United States collectively spent $2775 billion on imports of goods and services from the rest of the world[1]. While doing so, the country also set a record on the number of exports of farm and food products, with a total of $177 billion in sales to other countries[2]. Of these farm and food products, one major component is oleochemicals, with vegetable oils specifically reaching a total production of 214.8 million tons globally, an increase of 3.82% from 2020[3]. Also, while in 2020 the United States exported $421 million worth of waxes, another branch of oleochemicals, $195 million was still spent on the import of waxes. Much of these costs are due to the necessity of waxes with desirable traits or characteristics that are only available in other countries, such as carnauba wax.

With the amount of oleochemicals that are produced by the United States, it begs the question, why spend on imports when the available oleochemicals may be modified to achieve desirable characteristics for various applications. Therefore, the goal of this thesis is to explore new methods of utilizing and adding functionality to domestic oleochemicals, specifically soybean oil and fatty acids, for various applications.

The first application to be explored is described in chapters 1 and 2. Aromatic polyamides (para-aramids) are polymers known for their high strength and flame resistance. This is due to the tight orientation of the polymer chains allowing for hydrogen bonding between amide groups, Van der Waals forces from proximity to other chains, and pi stacking from benzene rings, resulting in highly crystalline structures[4]. Due to this, dyeing of para-aramids is very difficult as the structure, first, does not allow for penetration of the polymer chains, and second, is unreactive[5],[6]. To address this, atmospheric nonthermal plasma (NTP), a method of generating and delivering radicals as well as reactive oxygen and nitrogen species, has been

investigated as a pathway to increase the reactivity of para-aramids.[7]. This, along with ultraviolet (UV) or plasma catalyzed polymers, such as acrylated epoxidized soybean oil (AESO), present a possible pathway to increase the amount of interactions between dye molecules and the para-aramid surface, increasing the color strength when dyed[8],[9].

The second application to be explored is described in chapter 3. An estimated 25% of all foods produced globally are lost due to microbial spoilage, with 20% of all harvested fruits and vegetables specifically succumbing to microbial spoilage[10],[11]. In nature, fruits and vegetables synthesize their own waxes to prevent access by microbes as well as prevent moisture loss[12]. The same concept is used in the industry by coating machinery with polymers to prevent access by microbes. However, this does not address when there is contamination. Quaternary ammonium compounds (QAC), are a widely utilized, broad range antimicrobial, that are commonly linked to polymers to provide antimicrobial action along with the coating properties[13]. Therefore, the goal of this work is to provide both physical and antimicrobial protection to coated materials by synthesis of antimicrobial linked waxes.

Literature reviews specific for each topic are presented in the individual chapters.

CHAPTER I
ENHANCING THE DYEING OF PARA-ARAMIDS BY TREATMENT WITH SOYBEAN OIL-BASED BIOPOLYMERS AND NONTHERMAL PLASMA IN A CATIONIC DYE SYSTEM

The following chapter contains the work "Soybean Oil-Based Biopolymers Induced by Nonthermal Plasma to Enhance the Dyeing of Para-Aramids with a Cationic Dye" published in *Polymers* **2022**, *14(3)*, 628. All experiments were completed by me. Co-authors include Dr. Christopher Doona, Dr. Xiaofei Ye and Dr. Tong Wang advised this work.

Abstract

The objective of this study was to identify the individual effect and interactions among pretreatment with soybean oil and acrylic acid as a mixture, glycerol and acrylic acid as a mixture, nonthermal plasma (NTP) treatment time, and NaCl on para-aramid color strength measured by K/S value. It was found that for the soybean oil and acrylic acid pretreatment, the best treatment conditions were a molar ratio of 3.25 acrylic acid to soybean oil, along with a 360 second NTP treatment, and 5% NaCl concentration in the dye bath. For the fastness of the dye, the longest NTP treatment times, 360 seconds, showed the best result. For the glycerol and acrylic acid pretreatment, it was found that the best results for both color strength and fastness were seen when a molar ratio of 1.50 acrylic acid to glycerol and 240 second NTP treatment time were used. Overall, the glycerol acrylate systems showed a lower color strength value as well as higher fastness value.

Abbreviations:

Nonthermal plasma (NTP), acrylated epoxidized soybean oil (AESO), soybean oil and acrylic acid complex (SOAAC), glycerol and acrylic acid complex (GAAC), attenuated total reflectance (ATR), Fourier transform infrared (FTIR), mercury-cadmium-telluride (MCT), dichloromethane (DCM), scanning electron microscopy (SEM)

Introduction

Aromatic polyamides, known by the acronym aramid, consist of benzene rings with amide groups attached at either the meta or para positions, forming long, stacking polymer chains. The organization of this structure allows for hydrogen bonding between amide groups as well as, due to the size and distance of the molecules from each other, pi stacking and Van der Waals forces between benzene rings[4]. These linkages and molecular forces are responsible for the strength and smooth texture of the fabric as well as the unreactive, crystalline structure, making this material difficult to dye and ensure the fastness of dye through common commercial methods[5],[6]. The para formation further increases the difficulty due to a tighter orientation of hydrogen bonding, allowing for even greater Van der Waals forces between benzene rings (Figure 1).

Because of the difficulty in dyeing the para-aramid fabrics, atmospheric nonthermal plasma (NTP) has been investigated as a method to increase the reactivity of the para-aramids by delivery of an electrical field to the atmospheric environment, generating reactive species and free radicals, avoiding the difficulty in maintaining a controlled environment7. When the fabric is treated with plasma, there is potential for the generation of functional groups as well as increased reactivity on the fabric surface due to contact with the generated species. However, it has been observed that plasma treatment of some materials, such as organic dyes, can result in degradation, changing the original color[14].

Along with the generation of functional groups with NTP, polymeric resins may also be used as an intermediate to assist in the binding of dye to the surface. One such resin, acrylated epoxidized soybean oil (AESO) (Figure 2) has sparked excitement for this role due not only to its

Chemical Name	Chemical Structure
Para-Aramid	
Meta-Aramid	

Figure 1. Chemical structure of para- and meta-aramids
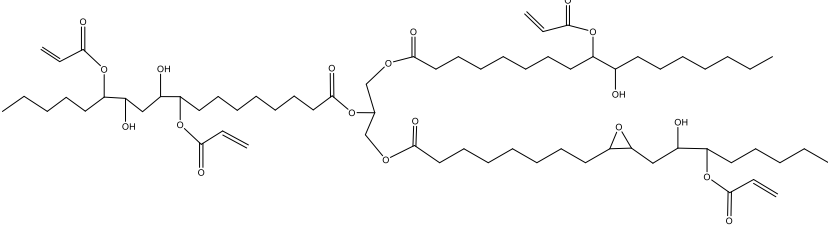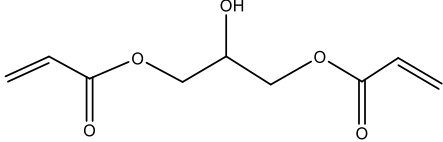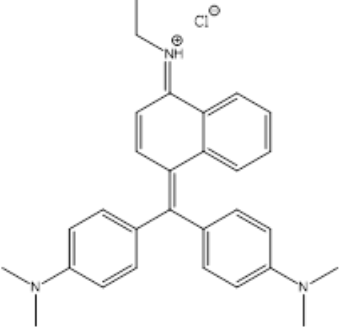
Chemical Name	Chemical Structure
Acrylated epoxidized soybean oil	
Glycerol Acrylate	
Victoria Blue R Dye	

Figure 2. Chemical structure of acrylated epoxidized soybean oil, glycerol acrylate, and Victoria Blue R dye

7

functionality, but also because of its availability as a green alternative compared to petroleum-based resins[8].With the addition of acrylic groups to epoxidized soybean oil, the potential for binding to fabric substrates as well as cross polymerization greatly increases[9]. We hypothesized, however, that the use of AESO can be avoided by the direct formation of a soybean oil and acrylic acid complex (SOAAC) by NTP treatment of soybean oil and acrylic acid on the fabric's surface. In addition, glycerol is believed to react in a similar mechanism by use of acrylic acid with glycerol to form a glycerol and acrylic acid complex (GAAC), similar in structure to glycerol acrylate (Figure 2). Both materials, SOAAC and GAAC, due to their potential to cross polymerize with terminal alkenes, are being utilized as possible dye intermediates for para-aramid fabric. These are specifically of interest as well due to the size of the structures, glycerol presenting a relatively smaller structure compared to the longer alkyl chains in soybean oil. Because of these differences, there is potential for differences in texture of the formed complexes, as well as differences in effectiveness due to the relative amount of hydrophobicity/hydrophilicity of the materials, soybean oil presenting much greater hydrophobicity due to the long alkyl chains compared to the alcohol groups present in glycerol.

Using treatment of the para-aramid surface with soybean oil or glycerol and acrylic acid, along with NTP, the surface may become more receptive to bonding as well as assist with polymerization, of the formed SOAAC and GAAC resins. After the creation of these intermediates, it is hypothesized that treatment of the para-aramid fabric with dyes, such as Victoria Blue R (Figure 2), a water soluble, basic dye, will better adhere to the fabric. This is due to both hydrogen bonding from amine groups present on the dye with the oxygen of the SOAAC and GAAC, as well as potentially formed covalent bonds between the fabric, intermediate, and dye. The dye may also adhere to the para-aramid surface through dispersion forces from

proximity to the polymer chains to an extent. Also, due to the charged nature of the dye, NaCl, an electrolyte, is also investigated due to the potential to assist with the bond between the material and dye by stabilization of ionic interactions[15]. Therefore, the objectives of this study are to evaluate effective treatment strategies using NTP as a treatment, SOAAC and GAAC as intermediate reactive components, and NaCl to maximize the color strength and fastness of dye to para-aramid fabric.

Materials and Methods

Experimental Design

Due to the number of variables being investigated in this study, sequential full factorial designs for screening of variable impact were utilized. The results of these experiments were then analyzed, and variables were included or removed in further experiments based on effectiveness. Consequently, the variables that produced the best results were selected for further experimental optimization trials using response surface designs. Central composite designs were utilized when a broader range of two individual variables were to be investigated, while box Behnken designs were utilized when three variables with 3 levels were to be investigated for interactions. Anchor points of box Behnken designs were determined by increasing the range around conditions presenting the best color strength during full factorial observation. The results of these experiments were analyzed using Design Expert software (Stat-Ease Inc., Minneapolis, MN, USA) to present the combination of variables with the best possible outcome. The coefficient of determination (r^2) was utilized as a measure of fit for generated models.

Para-aramid treatment

The complete treatment and dyeing process for para-aramids can be observed in Figure 3. Two pretreatment solutions were prepared to soak para-aramid samples overnight. The first

pretreatment solution, the soybean oil and acrylic acid solution, was made by combining acrylic acid (Sigma-Aldrich, St. Louis, MO, USA, CAS #: 79-10-7) and soybean oil from a local grocery store (Crisco Pure Vegetable Oil) at the molar ratios of 1.50, 3.25, and 5.00 acrylic acid to soybean oil. To aid in the even distribution of the solution components onto the para-aramid surface, ethyl acetate (Sigma-Aldrich, St. Louis, MO, USA, CAS #: 41-78-6) was used as a solvent at the molar ratios of 6.9, 3.0, and 2.6 ethyl acetate to acrylic acid respectively, added until all components were dissolved. The second solution, the glycerol and acrylic acid solution, was made by combining glycerol (Sigma-Aldrich, St. Louis, MO, USA, CAS #: 56-81-5) and acrylic acid at the molar ratios of 0.60, 1.05, and 1.50 acrylic acid to glycerol based on the results of preliminary experiments. To aid in the even distribution of these solutions, ethanol was used as a solvent at the molar ratios of 1.9, 2.4, and 3.0 ethanol to acrylic acid respectively, added until all components were dissolved. Para-aramid fabric samples were then individually cut into one-inch pieces and immersed in their respective pretreatment solution for 20 h.

Three 0.1 wt.% Victoria Blue R dye (Sigma-Aldrich, St. Louis, MO, USA, **CAS #:** 2185-86-6) in distilled water solutions were prepared using either 2, 5, or 8 wt.% NaCl (by mass of dye solution). Dye solutions were placed into 5mL glass conical vials with a stir bar included, and placed in a reaction vial stirrer and heater (React-Thermo, Fisher Scientific, Waltham, Massachusetts, USA) for continuous agitation at 60°C.

After soaking for 20 h, para-aramid samples were removed from the pretreatment solutions and solvent evaporated. Samples were placed on a plexiglass platform for treatment with nonthermal plasma. This was done through rotation of the samples underneath a coplanar dielectric barrier which generated plasma on the surface of the barrier when the parallel electrodes embedded were powered (Figure 4). The samples were rotated to promote even

10
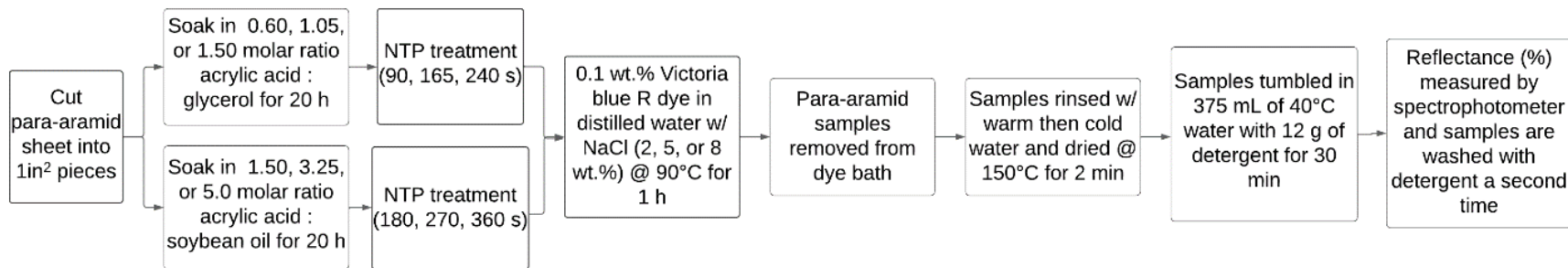
Figure 3. Flowchart for the dyeing and washing of para-aramid with both soybean oil and glycerol – acrylic acid system
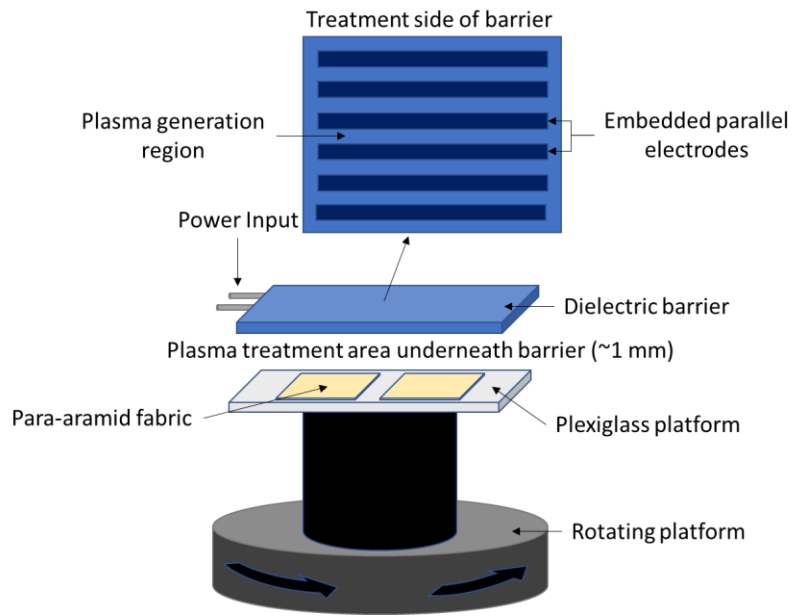
Figure 4. Nonthermal plasma treatment diagram

treatment by the NTP discharge due multiple individual discharge channels. The SOAAC

pretreatments were given 3, 4.5, or 6 min NTP treatments, determined through preliminary trials,

for observation of maximum color strength results, with the GAAC treatment times varying

among 1.5, 2.75, and 4 min. Directly after NTP treatment, dye baths were raised to 90°C, and

treated para-aramid samples were placed in dye vials while stirring for one hour.

Para-aramid washing and fastness tests

After dyeing, the water rinse process was done to remove excess dye. This was done by

rinsing with first warm, then cold water, for 5 min total to remove any loose dye that remained.

The wet samples were collected in a wire mesh container and placed in a convective oven heated

at a rate of 35°C /min until 150°C was reached and maintained for 2 min to dry. Samples were

placed in a plastic bottle for a detergent wash by adding 12g of detergent (ECOS Plus Stain-

Fighting Enzymes) along with 375 mL of 40°C water and tumbled for 30 min. The water rinse

and drying process was then repeated, dried samples were removed, and their images recorded

by flatbed scanner for visual observation. The face side (NTP treated side) of the dyed samples

were recorded for quantitative measure by a spectrophotometer (Spectro 1, Variable,

Chattanooga, TN, USA). The same detergent washing method was repeated once more for a total

of two detergent washes.

K/S Measurement for Color Strength

Effectiveness of the dyeing process was based on the color strength of the samples,

measured by the K/S value, the ratio of light absorption (K) to light scattering (S), with the

greater the K/S value, the darker the sample. This was obtained from the spectral reflectance (R)

of the para-aramid sample at 615 nm, Victoria Blue R's maximum absorption wavelength,

according to product specifications. The measurement was converted to K/S using the Kubelka-Monk equation (Equation 1). The spectral reflectance (R) is measured using a spectrophotometer. The dye fastness was measured by comparison of the percent change in K/S value between detergent washes (dK/S)[16].

$$\frac{K}{S} = \frac{(1-R)^2}{2R}$$

Equation 1. Kubelka-Munk equation used to calculate K/S from spectral reflectance (R)

Tensile Strength Analysis of NTP Treated and Dyed Para-aramid Yarn

The effect of NTP treatment and dyeing process on para-aramid yarn was investigated through tensile strength analysis using TA.XT plus texture analyzer instrument (Stable Micro Systems, United Kingdom) based on modification of ASTM D7269. For observation of the NTP treatment effect, 12-inch long para-aramid yarn with finest fiber diameter of 11 µm was treated with 0, 60, or 180 s of NTP and then placed in sealed bags for 3 d for conditioning.

The effect of the dyeing process was observed through dyeing para-aramid yarn with the SOAAC and GAAC system conditions where the greatest color strength occurred. AESO pretreated yarn was treated with NTP for 4 min before dyeing by the explained para-aramid treatment method. Dyed yarn was rinsed with water to remove unbound dye, dried at 150°C for 2 min, and then placed in sealed bags for 3 d for conditioning.

After conditioning, one end of the yarn was wrapped around an electrical wire to minimize slipping, and placed into the top clamp of the TA.XT system. The bottom, hanging end of the yarn, was wrapped around another electrical wire and placed into the bottom clamp, totaling a gauge length of 10 in, decided due to length limitations of the TA.XT plus texture. The yarn was then pulled apart with a pre-test speed of 0.5 mm/s, trigger force of 30 g, and test speed

of 2 mm/s until the break point force (g) was observed. Each sample was completed in triplicate and results compared by student's t-test comparison of means.

FTIR Analysis for Identification of Chemical Changes

Attenuated total reflectance (ATR) - Fourier Transform infrared (FTIR) analysis was performed to obtain an IR spectrum for reactants as well as samples to observe what chemical changes may have occurred throughout the treatment process on a solid sample. A liquid nitrogen cooled Mercury-Cadmium-Telluride (MCT) detector was used along with a germanium crystal for ATR readings, and potassium bromide used as background for the samples.

Extraction of Dyed Para-aramid Fabric for Characterization of the Interactions Among Para-aramid Fabric, Formed Resin, and Victoria Blue R Dye

To investigate the relationship among para-aramid fabric, formed resin, and Victoria Blue R dye, extraction of dyed para-aramid fabric was completed using solvents of varying polarity. Color strength was first recorded for three, 1 in^2 dyed para-aramid fabric before being placed in 40 mL of either hexane, a nonpolar solvent, ethanol, a polar solvent, or 2:1 chloroform methanol (v/v), containing both polar and nonpolar solvents, for 16 h. After extraction, samples were dried at 150°C for 2 min before color strength was recorded.

Extract solutions were dried through rotary evaporation before being dissolved in 20 mL of hexane and 20 mL of distilled water for the observation of dye movement in the phase separation. Undissolved material was then dissolved by 20 mL of dichloromethane (DCM), followed by 2 0 mL of distilled water for the observation of dye movement in the phase separation. The experiment was completed in triplicate for verification of observed results.

16

Scanning Electron Microscopy (SEM) for Observation of Para-Aramid Surface Morphology

Untreated and NTP treated, or AESO, SOAAC, or GAAC pretreated and dyed 1 in^2 para-aramid fabric was observed with scanning electron microscopy (SEM; Zeiss Auriga 40) for investigation of each's effect on the fabric as well as observation of the surface morphology of formed resins. Samples were prepared by application of a thin layer of Iridium before attachment to an aluminum pin with copper tape to assist in charge dissipation during imaging.

Results and Discussion

Full Factorial Design for Multiple Variable Screening

To understand the potential effectiveness of SOAAC, as well as investigate the potential effect of NTP treatment, an initial central composite design was completed with varying concentrations of AESO and NTP treatment time (Table 1). It was found that overall color strength increased as both AESO concentration and NTP treatment time increased, obtaining a maximum color strength of 7.2 (Figure 5).

After obtaining the baseline and observing the trend with NTP, the initial SOAAC investigation began. This was completed by a two-level full factorial design investigating the acrylic acid to soybean oil molar ratio, NTP treatment time, solvent utilized for dyeing, and NTP treatment after dyeing (Table 2). Because of the linear trend observed with NTP, the treatment time points were increased. Glycerol was included as a solvent as it has been shown to be an effective alternative to ethanol for assisting in dye uptake in synthetic fibers[17]. A post-dye NTP treatment was also investigated as a potential method to assist in fixing the dye to the para-aramids. It was found that each of these factors was significant (Figure 6).

Table 1. Central composite experimental design for AESO as a pretreatment solution and different NTP treatment time

AESO Pretreatment (wt.%)	NTP Treatment Time (s)	K/S	Std Dev*
0.85	75.0	2.5	0.086
0.85	138.6	2.5	0.049
4.97	30.0	3.6	0.016
4.97	120.0	4.0	0.008
15	11.4	3.8	0.072
15	75.0	5.3	0.066
15	75.0	4.4	0.127
15	75.0	4.7	0.116
15	75.0	5.2	0.065
15	75.0	5.5	0.125
15	75.0	5.8	0.104
15	138.6	5.5	0.017
24.96	30.0	5.1	0.008
24.96	120.0	7.2	0.090
29.09	11.4	3.6	0.032
29.09	75.0	6.8	0.126

*Standard deviation based on triplicate analysis
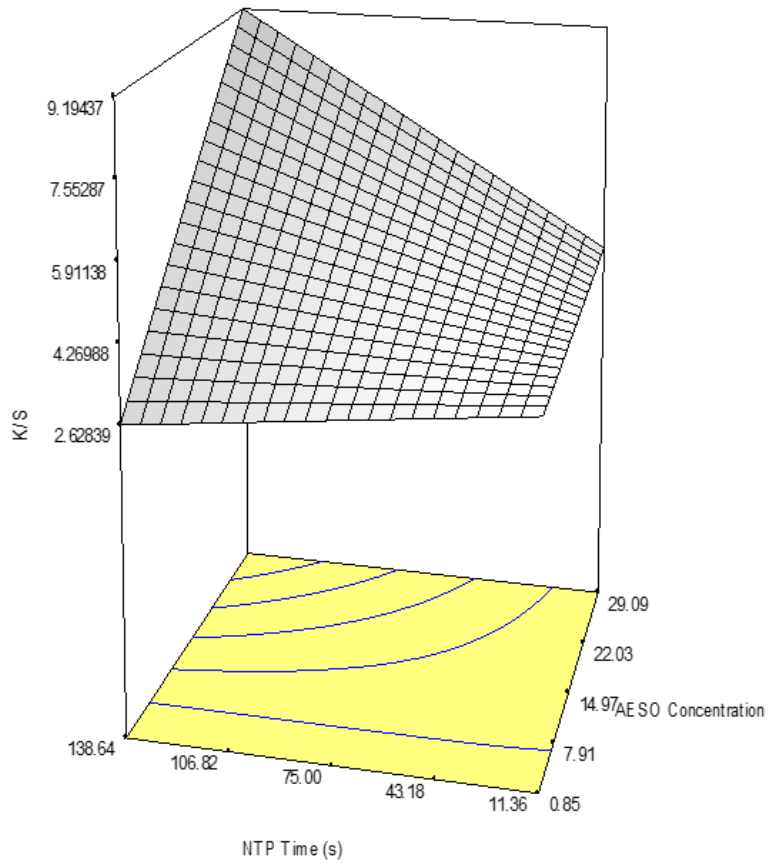
Figure 5. K/S values surface plot of acrylated epoxidized soybean oil (AESO) pretreatment concentration and nonthermal plasma (NTP) treatment time ($r^2 = 0.8922$)

Table 2. Two level full factorial experimental design for acrylic acid to soybean oil molar ratio, NTP treatment time, solvent utilized for dyeing, and NTP treatment after dyeing

Acrylic acid : Soybean oil Molar Ratio	NTP Time (s)	Dye Solvent	Post-dye NTP Time (s)	K/S	Std Dev*
1.60	240	Distilled Water	0	7.7	0.087
1.60	240	Distilled Water	30	4.0	0.054
1.60	240	Glycerol	0	1.0	0.032
1.60	240	Glycerol	30	1.0	0.059
1.60	360	Distilled Water	0	9.6	0.175
1.60	360	Distilled Water	30	6.8	0.012
1.60	360	Glycerol	0	0.7	0.026
1.60	360	Glycerol	30	1.6	0.084
3.99	240	Distilled Water	0	7.7	0.056
3.99	240	Distilled Water	30	8.8	0.039
3.99	240	Glycerol	0	1.2	0.066
3.99	240	Glycerol	30	1.1	0.017
3.99	360	Distilled Water	0	9.6	0.113
3.99	360	Distilled Water	30	8.3	0.023
3.99	360	Glycerol	0	1.4	0.039
3.99	360	Glycerol	30	1.2	0.005

*Standard deviation based on triplicate analysis
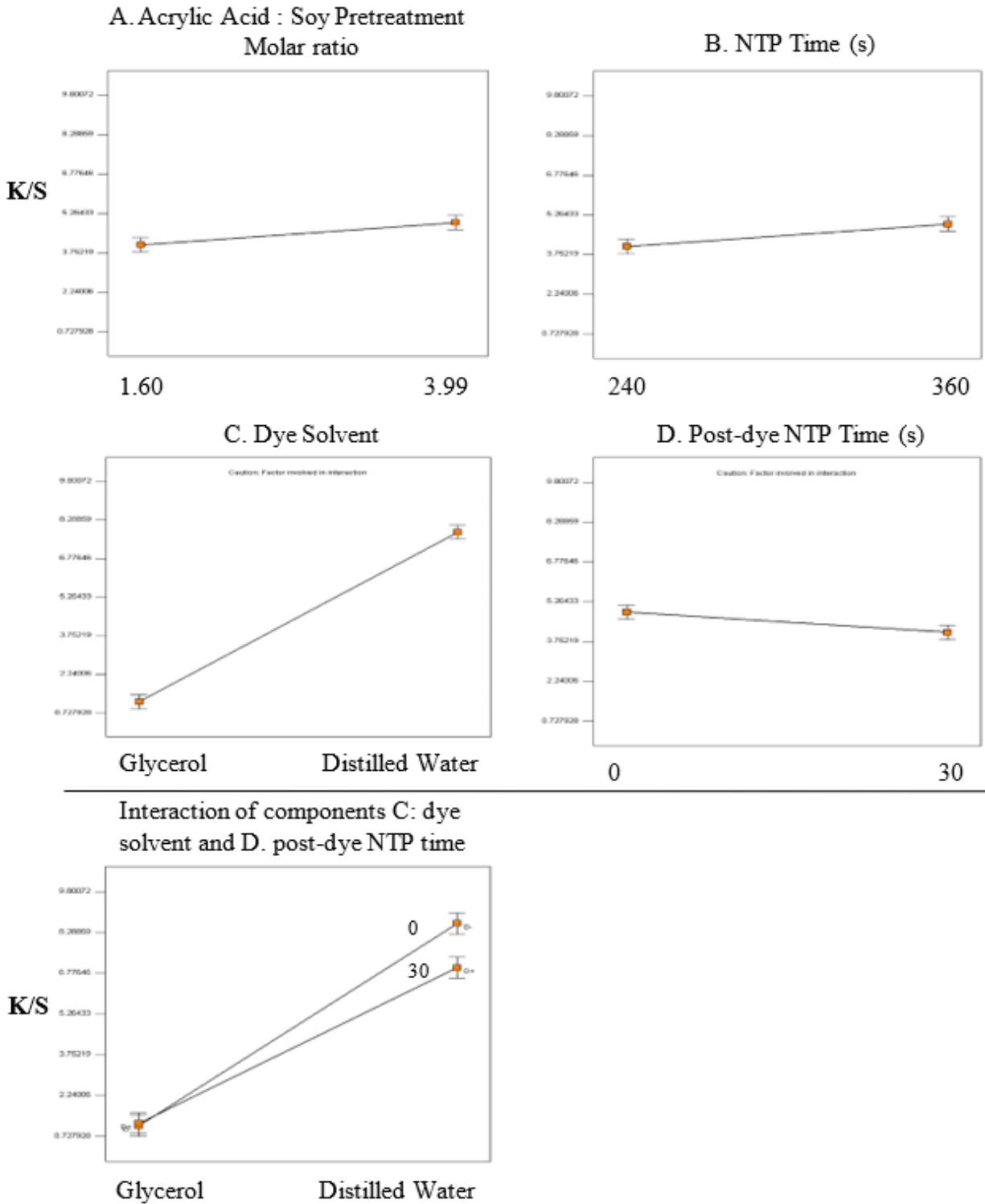
Figure 6. Main effect and interaction plots of acrylic acid and soybean oil pretreatments, NTP treatment times, dye solvent, and post-dyeing NTP time

The SOAAC pretreatment was effective, with higher molar ratios of acrylic acid to soybean oil presenting a greater effectiveness. The NTP treatment showed the same trend that was observed prior, with increasing treatment time resulting in greater color strength. However, glycerol presented a significant decrease in the color strength relative to water dyeing, as well as the post dye NTP treatment resulting in lower color strength values, believed to be due to degradation of the dye, as observed from the darkening of the samples after treatment. From this experiment, it was found that a maximum color strength of 9.6 was obtained, surpassing the previously investigated AESO. With this experiment complete, the focus was placed on the GAAC system.

The GAAC system containing different functional groups compared to the SOAAC system resulted in utilization of a wider range of NTP treatment times compared to the prior experiment (Table 3). Due to glycerol containing three hydroxyls, molar ratios of 0.68 and 1.38 acrylic acid to glycerol were utilized. These ratios were selected to observe both the possibilities of a mono-addition of acrylic acid to the glycerol backbone, as well as the possibility of both di and tri-addition of glycerol to the glycerol backbone. This results in better observation of the effect of further hydrogen bonding due to remaining hydroxyl groups on the glycerol backbone of the mono-addition, as well as observation of the effect of greater polymerization in the di and tri-additions. Because of the increased potential for hydrogen bonding, and therefore ionic interactions, NaCl was included in the dye bath to facilitate interactions between the GAAC and Victoria Blue R. NTP treatment prior to pretreatment was investigated as a method to increase the interactions between the para-aramid fabric and GAAC, resulting in greater color strength. Each of these variables was significant (Figure 7).

Table 3. Two level full factorial experimental design for glycerol and acrylic acid as a pretreatment solution

Acrylic acid : Glycerol molar ratio	NTP Time (s)	NaCl in bath (wt.%)	NTP Time Before Pretreatment (s)	K/S	Std Dev*
0.68	180	0	0	1.7	0.294
0.68	180	0	60	6.6	0.056
0.68	180	5	0	4.0	0.244
0.68	180	5	60	4.9	0.368
0.68	360	0	0	1.7	0.011
0.68	360	0	60	2.2	0.011
0.68	360	5	0	3.4	0.220
0.68	360	5	60	2.5	0.183
1.38	180	0	0	4.2	0.350
1.38	180	0	60	6.5	0.011
1.38	180	5	0	7.6	0.111
1.38	180	5	60	5.4	0.468
1.38	360	0	0	2.3	0.017
1.38	360	0	60	3.0	0.112
1.38	360	5	0	4.4	0.231
1.38	360	5	60	3.9	0.140

*Standard deviation based on triplicate analysis
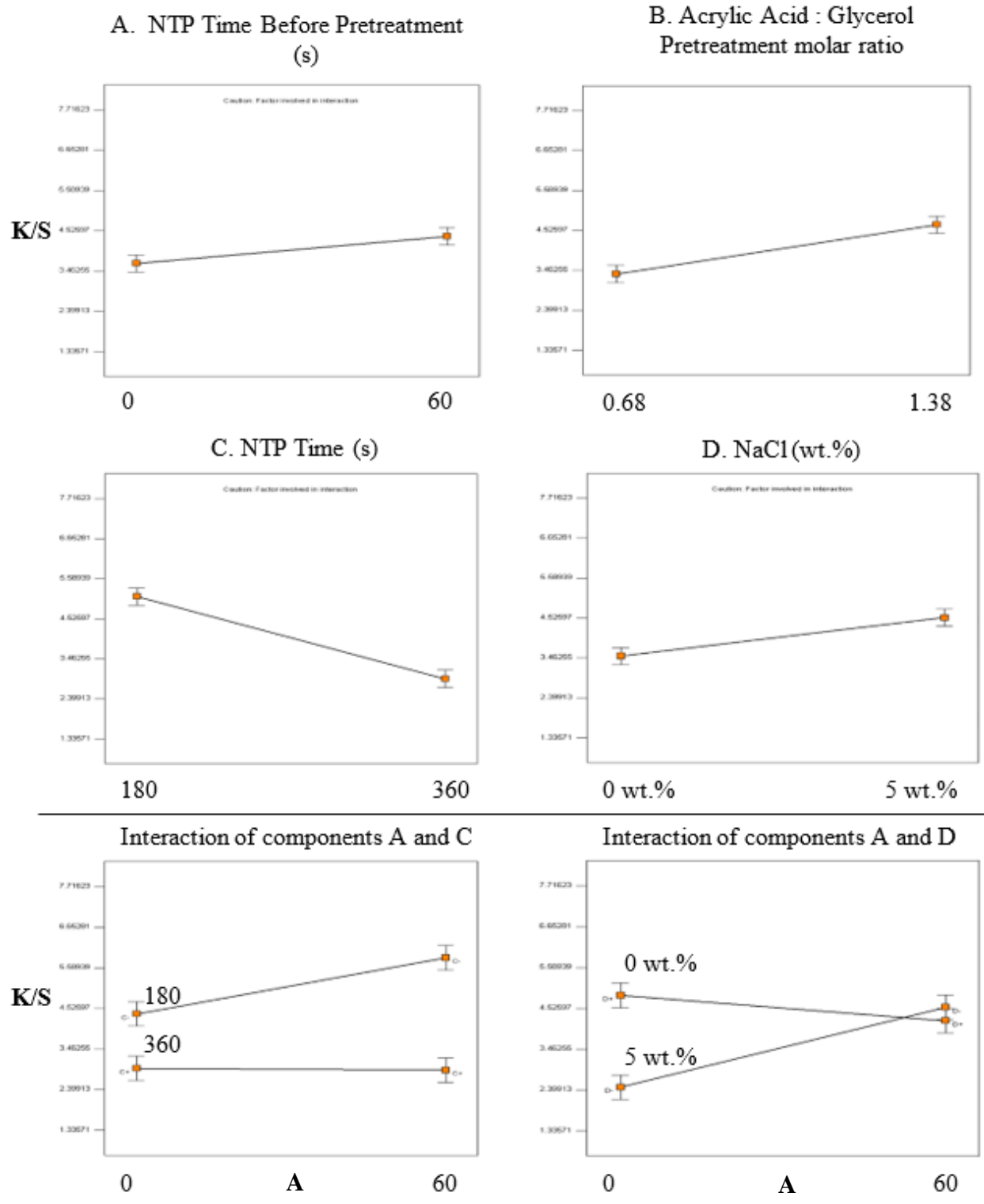
Figure 7. Main effect and interaction plots of NTP before pretreatment, acrylic acid and glycerol pretreatments, NTP treatment times, and NaCl concentration

NTP treatment time before pretreatment, the acrylic acid to glycerol molar ratio, and NaCl concentration all presented positive trends, with increasing effectiveness resulting from higher concentrations utilized. However, because of the negative interaction between NaCl and NTP treatment prior to pretreatment, only NaCl was continued to be used moving forward. A major change in GAAC system compared to what was observed in the SOAAC system was the effect of increased NTP treatment time. With longer NTP treatment, the color strength of the para-aramid decreased, potentially due to degradation of the GAAC. Upon completion of these preliminary experiments, the SOAAC and GAAC systems were further investigated for experimental optimization.

Experimental optimization of the SOAAC pretreatment system by Box Behnken response surface design

The effect of soybean oil to acrylic acid molar concentration in the SOAAC pretreatment, NTP treatment times, and NaCl concentrations in the dye bath were investigated for the ideal combination to obtain maximum color strength values. The soybean oil to acrylic acid molar concentrations of 1.5, 3.25, and 5.0 were used along with 180, 270, and 360 s NTP treatment times, and 2, 5, and 8 wt.% NaCl (Table 4). After completion of the dyeing process and the first detergent wash, color strength values were recorded and compared among samples (Figure 8). The greatest color strength was at the experimental conditions of a molar ratio of 3.25 acrylic acid to soybean oil, 360 s NTP treatment, and 5 wt.% NaCl concentration in the dye bath.

The observed results are believed to be due to the interactions between the formed SOAAC intermediate with the Victoria Blue R dye. With addition of acrylic groups at the internal alkene locations, it allowed for polymerization of the resin, assisting in adherence to the para-aramid structure. The factor that is believed to contribute greatly on the dye adhering to the

Table 4. Box Behnken response surface experimental design for SOAAC molar concentrations, NTP treatment time (s), and NaCl concentration in the dye bath

Acrylic/Soy molar ratio	NTP Time (s)	NaCl in bath (wt.%)	KS	Std Dev*	dK/S† (%)
1.5	180	5	10.6	0.02	21.2
1.5	270	2	5.6	0.21	33.1
1.5	270	8	7.4	0.57	22
1.5	360	5	10.5	0.39	4
3.25	180	2	8	0.19	29.9
3.25	180	8	9.6	0.04	31.4
3.25	270	5	13.2	1.16	2.8
3.25	270	5	8.9	0.05	4.7
3.25	270	5	13.4	0.22	14.8
3.25	270	5	12.3	0.26	16.1
3.25	270	5	12.2	1.56	13.1
3.25	360	2	11	0.13	6.3
3.25	360	8	10.7	0.06	12.3
5	180	5	9.6	0.34	5.3
5	270	2	10.9	0.18	5.3
5	270	8	9.8	0.13	25.1
5	360	5	10.9	0.76	-1.9

*Standard deviation based on triplicate analysis

†"dK/S" indicates percent reduction in color strength from first to second detergent wash
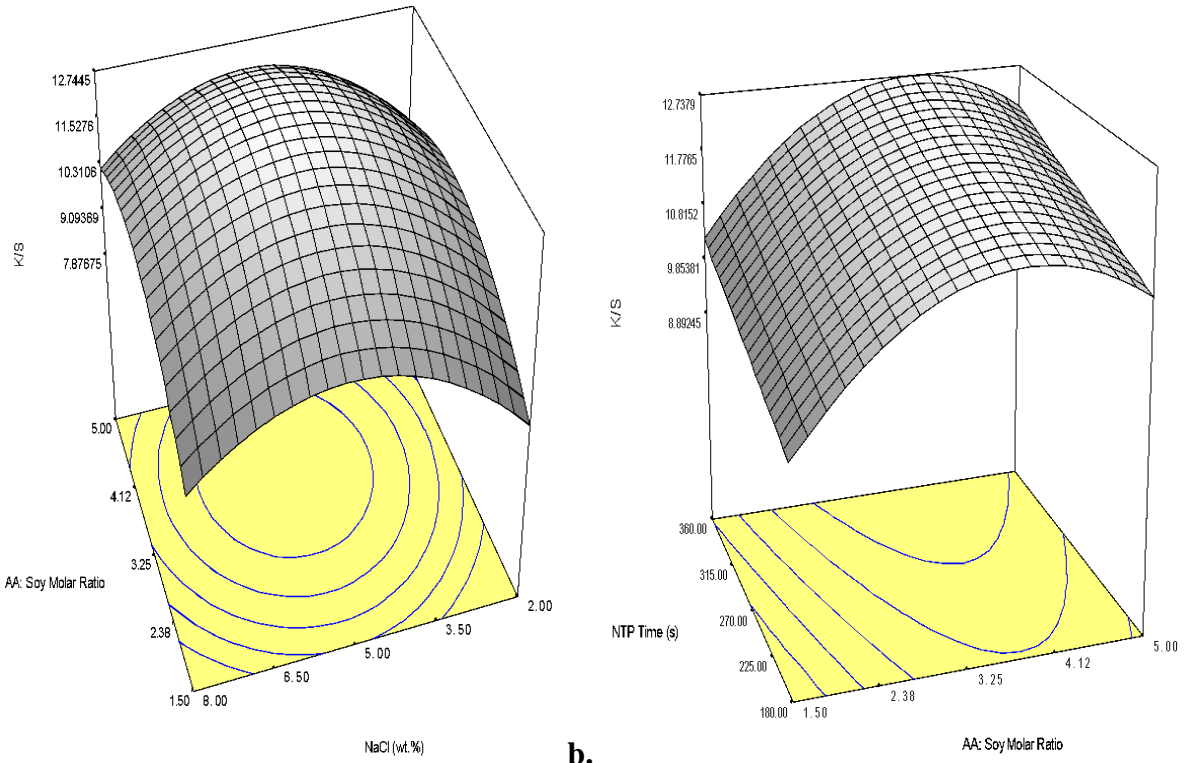
Figure 8. K/S value surface plot of molar ratio of soybean oil to acrylic acid , NaCl concentration, and NTP time after the first detergent wash with a. NTP treatment time held constant at 360 s and b. NaCl concentration held constant at 5.0 wt.%
($r^2 = 0.8065$)

fabric is hydrogen bonding between the intermediate and dye. Due to the availability of both hydrogen bond donators and acceptors on both the dye and SOAAC, multiple opportunities to form hydrogen bonds are available. With longer NTP times showing better fastness, it presents an increase in the degree of bonding between the para-aramid fabric and SOAAC, as well as increased polymerization within the SOAAC. This allows for a surface that is harder to remove, and therefore less likely to be removed through washing.

Experimental optimization of the GAAC pretreatment system by Box Behnken response surface design

For the GAAC pretreatment system, molar ratios of 0.6, 1.05, and 1.50 acrylic acid to glycerol, 90, 165, and 240 second NTP treatment times, and 2, 5, and 8 wt.% NaCl concentrations in the dye bath were used (Table 5). In this system, a relatively increased stiffness compared to SOAAC, believed to be polymerization of the resin after NTP treatment, was observed. This is believed to occur due to the smaller monomer size of GAAC, as well as the potential for all three terminal ends polymerizing. This causes increased rigidity compared to the flexibility of the longer alkane chains in soybean oil. Reduced NTP treatment times compared to SOAAC were used in this system as it was found that longer times would begin to degrade GAAC and present a loss of rigidity and color strength.

Higher molar ratios of acrylic acid to glycerol and longer NTP treatment times had a significant effect on the color strength of the dyeing after the first detergent wash (Figure 9). This is believed to be similar to the mechanism predicted in the SOAAC system. With more acrylic acid to form bonds with the glycerol, it is possible for more polymerization within GAAC, as well as with increased time, more energy to facilitate these reactions. However, a greater color strength is observed in the SOAAC system, attributed to GAAC's possible lack of

Table 5. Box Behnken response surface experimental design for GAAC molar concentrations, NTP treatment time (s), and NaCl concentration in the dye bath

Acrylic/Glycerol molar ratio	NTP time (s)	NaCl in bath (wt.%)	KS W1	Std Dev*	dK/S[†] (%)
0.6	90	5	1.5	0.02	26.3
0.6	165	2	3.6	0.19	31.6
0.6	165	8	3.7	0.01	39.0
0.6	240	5	3.7	0.08	39.5
1.05	90	2	3.3	0.04	29.8
1.05	90	8	3.0	0.10	34.5
1.05	165	5	2.2	0.02	25.9
1.05	165	5	2.1	0.01	29.7
1.05	165	5	4.0	0.09	37.6
1.05	165	5	4.4	0.11	15.9
1.05	165	5	3.8	0.07	36.1
1.05	240	2	5.1	0.18	19.2
1.05	240	8	5.6	0.15	14.3
1.5	90	5	3.4	0.11	22.5
1.5	165	2	5.0	0.07	14.9
1.5	165	8	5.1	0.06	28.1
1.5	240	5	6.2	0.12	16.7

*Standard deviation based on triplicate analysis

[†]"dK/S" indicates percent reduction in color strength from first to second detergent wash
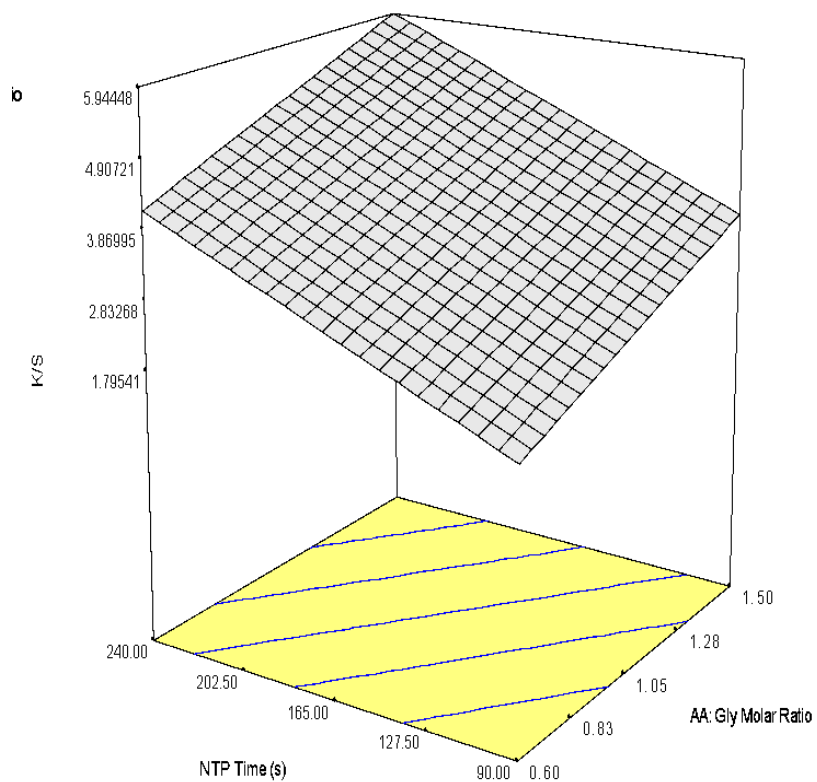
Figure 9. Surface plot of GAAC pretreatment after the first detergent wash with NaCl held constant at 2% and effect of treatment time and acrylic acid to glycerol molar ratio ($r^2 = 0.8014$)
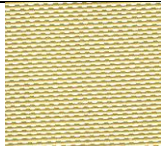
hydrogen bond donators when glycerol is fully reacted with acrylic acid. This completed reaction may also be indicated by the rigid structure, due to polymerization among the smaller monomer units of the GAAC. With the difficulty to bond with dye fully polymerized, but easier to be removed when not, the results observed are predictable. The color difference between the raw para-aramid material and para-aramid dyed under the best conditions for both SOAAC and GAAC can be observed in table 6.

Tensile Strength Analysis of NTP Treated and Dyed Para-aramid Yarn

To investigate the impact of NTP treatment and dyeing on the strength of para-aramid fabric, a tensile strength analysis was completed. For NTP, untreated para-aramid yarn was treated with either 0, 1, or 3 min of NTP. It was observed that there was significant difference between 0 and 1 min of treatment, as well as when treated for 3 min. This is believed to be due to continued exposure to reactive species and radicals, causing breakdown and changes in the chemical structure of the fabric[7].

For the dyeing process and individual pretreatments, SOAAC with a 3.25 molar ratio of acrylic acid to soybean oil dissolved in a 3.0 molar ratio of acrylic acid to ethyl acetate, GAAC with 1.50 molar ratio of acrylic acid to glycerol dissolved in a 3.0 molar ratio of acrylic acid to ethanol, and 25 wt.% AESO in ethyl acetate were investigated, both with and without 5 wt.% NaCl included in the dye bath (Figure 10). The various pretreatments were included for observation of the impact that each of these materials may have on the strength of the yarn, and NaCl included to observe potential degradation that is reported in hypochlorite solutions[11]. It was observed that there was no significant difference between the untreated para-aramids and any of the AESO treated samples, the only SOAAC treated, and GAAC with NaCl. Because of this, it points that the use of these coatings may provide a barrier to the para-aramids

Table 6. Untreated and dyed para-aramid samples prepared with SOAAC or GAAC

Treatment Conditions	Scanned Sample
Raw Para-Aramids	
3.25 molar ratio acrylic acid : soybean oil 3.0 molar ratio ethyl acetate : acrylic acid 270s NTP Treatment 5 wt.% NaCl	
1.50 molar ratio of acrylic acid : glycerol 3.0 molar ratio ethanol : acrylic acid 240s NTP Treatment 5 wt.% NaCl	
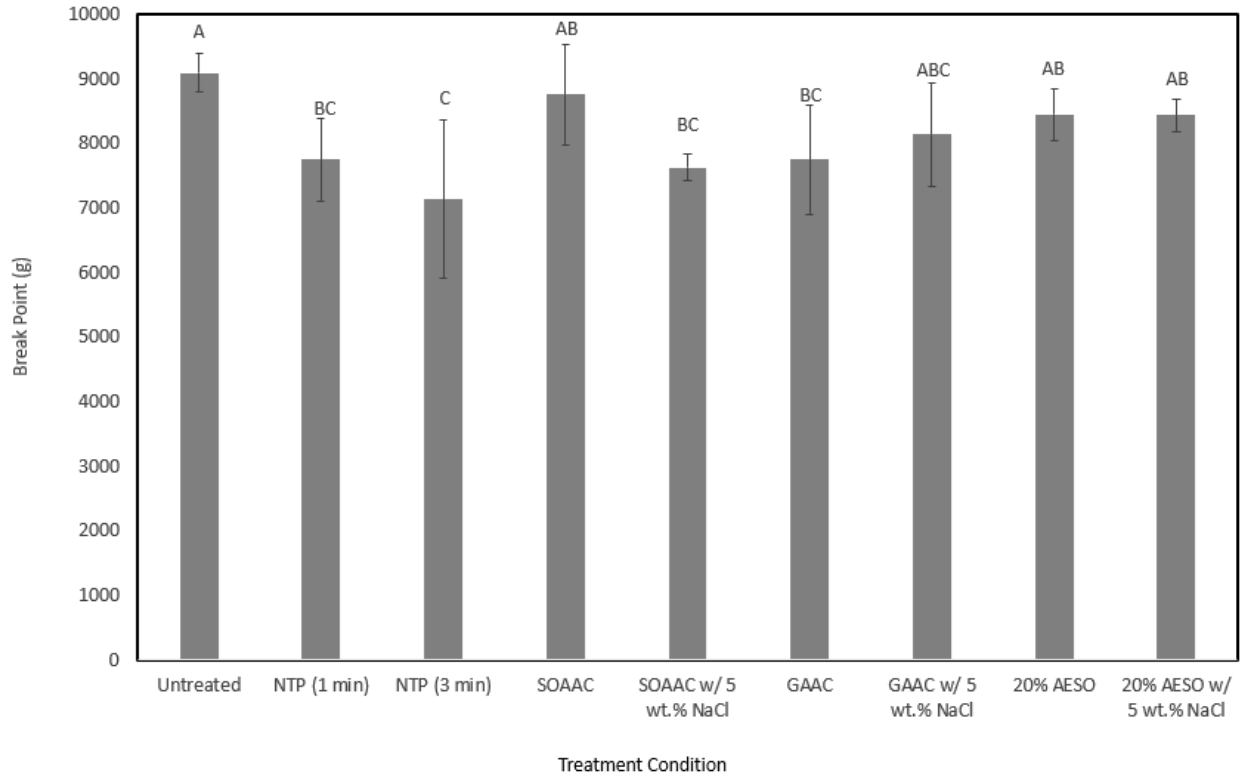
Standard deviation based on triplicate analysis
Significance determined by student's t-test

Figure 10. Break point (g) comparison of untreated, NTP treated, and Victoria Blue R dyed para-aramid fabric with SOAAC, GAAC, and AESO pretreatments

from the NTP, allowing for less of a breakdown when in contact with this material. This is

further indicated by the fact that the SOAAC yarn was treated for 6 min total, and still did not

present a significant reduction in break point.

FTIR Analysis to determine chemical changes during NTP treatment

To determine what chemical changes may have occurred, FTIR analysis was used to

observe the change in peaks by NTP treatment for both systems. When observing the SOAAC

system (Figure 11), the predicted reactions, specifically the ester formation between oxidized

alkenes and acrylic acid, as well the loss of alkenes due to polymerization, are potentially visible

in three regions specifically. The first and most clear region is 1695 cm^{-1} and 1740 cm^{-1}. This

region represents, first, the conjugated carboxylic acids of acrylic acid at 1695 cm^{-1}, and second,

esters at 1740 cm^{-1}. After 6 min of NTP, there was decrease in carboxylic acids with an increase

in esters. This represents the bonding of the acrylic acid groups to the soybean oil backbone,

showing that the reaction necessary for polymerization is occurring.

It can be observed that after the 6 min NTP treatment time, there was a decrease in the

intensity of the peak of amide bonds (1636 cm^{-1}). This may indicate the reduction in these free

amide bonds and instead formation of interactions with the soybean oil intermediate or other

reactive species in the atmosphere. This could be supported with the slight intensity increase in

the 1362 cm^{-1} region. This region can present aromatic amine bonds, which, if the carbonyl of

the amide were interacting with the SOAAC intermediate, could cause an increase.

Another main peak of interest is the increased intensity at 1466 cm^{-1}, a representative

area for alkanes[13]. This peak shows the formation of the polymerization between the SOAAC

intermediate. The terminal alkenes that can be found on the intermediate, when under NTP
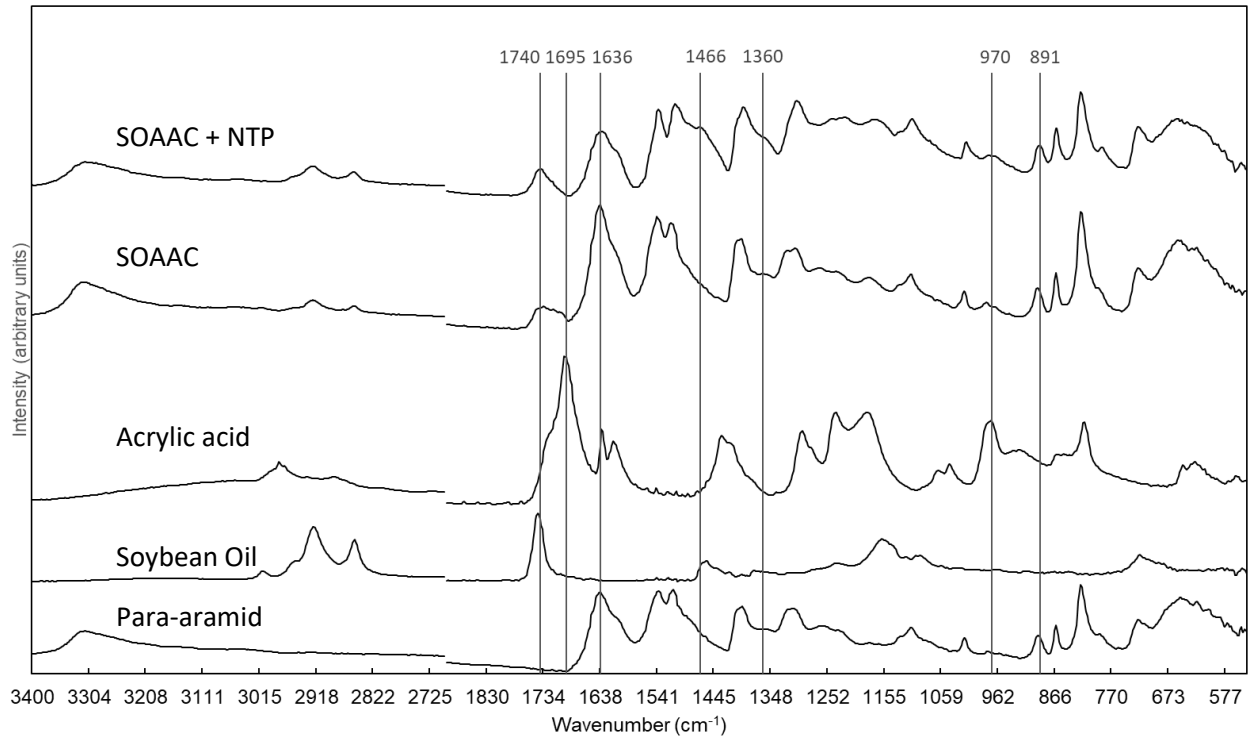
Figure 11. FTIR of para-aramid fabric, soybean oil, acrylic acid, and soybean oil and acrylic acid pretreatment on the surface of para-aramids before and after NTP treatment

treatment, can react to polymerize with each other, forming alkanes where the alkene previously was. This could also be supported by the reduction in the peak around the 970 cm^{-1} region. This area has the potential to show many different forms of alkene, in this scenario the monosubstituted alkene which is expected from terminal alkenes. This may also provide evidence for formation of epoxides by the NTP treatment, as these are commonly around the 915 cm^{-1} region[14]. Also, with the increased width of the peak around 1360 cm^{-1}, it is possible to observe alcohol formation. The potential structure of AESO, which is also a potential structure for the SOAAC intermediate created during NTP treatment, it is possible that alcohol groups bonded to the alkene locations are being observed, both reducing alkene readings while also increasing this peak.

At 885 cm^{-1} on the spectrum of the SOAAC system, a widening of a peak can be observed. This potentially could indicate the attachment of a group to the benzene ring of the para-aramid structure as this region is an indicator for 1,2,4 trisubstituted carbons[15]. If this were accurate it could partially explain the greater color strength obtained through these treatments. With the attachment of groups at these locations, the very tight, crystalline structure could be partially opened due to the space the new addition occupies, allowing easier access for dye.

In the GAAC system, the changes due to the NTP are believed to be similar. The same bonding of the acrylic acid groups to the backbone can be observed at 1695 cm^{-1} and 1740 cm^{-1} (Figure 12). However, in this system, this represents the ester formation by the acrylic acid and hydroxyls of the glycerol. The FTIR also presented a small peak generated at 1485 cm^{-1}, potentially showing the same polymerization that was predicted for SOACC. Lastly, at 891 cm^{-1}, a peak sharpening was observed, presenting the same potential for attachment of a group to the benzene ring of the para-aramid structure.

36
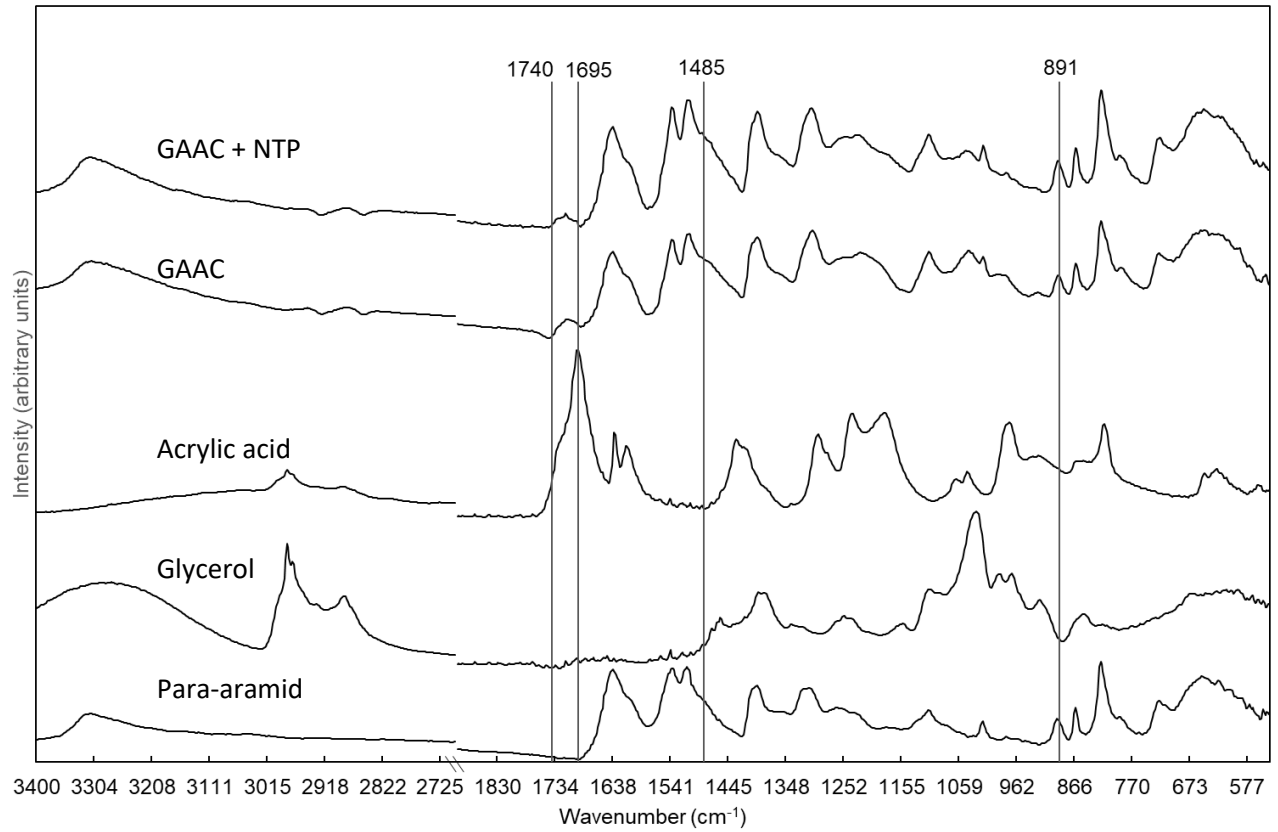
Figure 12. FTIR of para-aramid fabric, glycerol, acrylic acid, and glycerol and acrylic acid pretreatment on the surface of para-aramids before and after NTP treatment

Extraction of Dyed Para-aramid Fabric for Characterization of the Interactions Between

Para-aramid Fabric, Formed Resin, and Victoria Blue R Dye

Dyed SOOAC para-aramid fabric was extracted with either ethanol, hexane, or 2:1 chloroform

methanol (Figure 13). After extraction, the reduction in color strength was observed to be the

greatest by chloroform methanol, followed by ethanol (Table 7). This was expected due to the

polar solvents' ability to dissolve the polar dye used in this process. The minimal change in

hexane extracted samples presents the effect of hydrogen bonding between the dye, fabric, and

formed resin that hexane is unable to disrupt due to being nonpolar. However, after extraction,

dye was still observable on the surface of polar solvent extracted samples. This presented

potential covalent interactions between the dye and fabric or resin on the surface of the fabric.

This was investigated through ATR FTIR analysis of both untreated and extracted para-aramid

fabric (Figure 14).

Ethanol and chloroform methanol extracted para-aramid fabric continued to present peaks

at 2926 cm^{-1} as well as 1734 cm^{-1}. These peaks show remaining soybean oil, believed to be

formed resin, due to 2928 cm^{-1} demonstrating the long alkyl chains in soybean oil as well as

1734 cm^{-1} demonstrating ester bonds connecting to glycerol backbone.

The extract solutions, after solvent evaporation, were separated with 1:1 hexane: distilled

water. It was found that all observable dye remained in the water phase, with the hexane phase

remaining colorless (Figure 15). This is due to the unbound polar dye being dissolved in the

polar solvent. However, it was observable that colored, insoluble material remained in the flasks

after removal of the solvents.

38
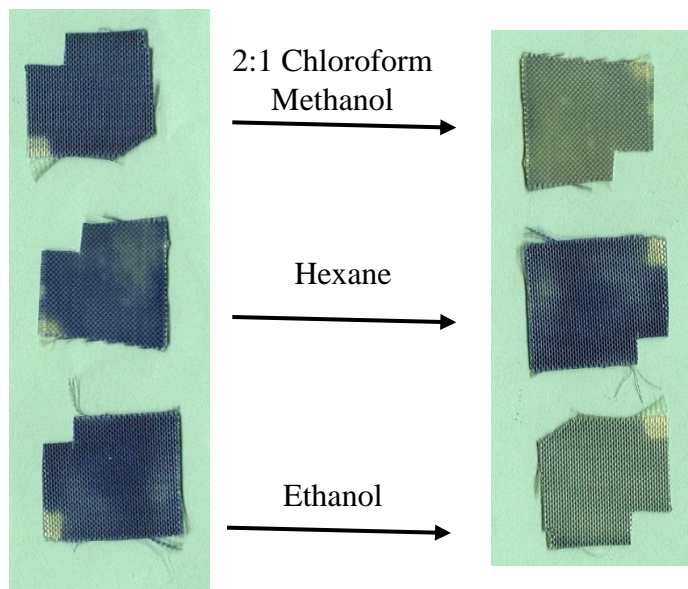
Figure 13. Scanned images of dyed para-aramid fabric samples before and after extraction in either ethanol, chloroform methanol, or hexane

Table 7. Color strength of dyed para-aramid fabric before and after extraction with ethanol. Hexane, or 2:1 chloroform methanol

Solvent	After Dye	Stdev	After Extraction	Stdev	K/S Reduction
Ethanol	7.80	0.155	2.75	0.049	5.05
Hexane	13.28	0.112	10.61	0.095	2.67
Chloroform Methanol	8.66	0.113	3.20	0.043	5.46
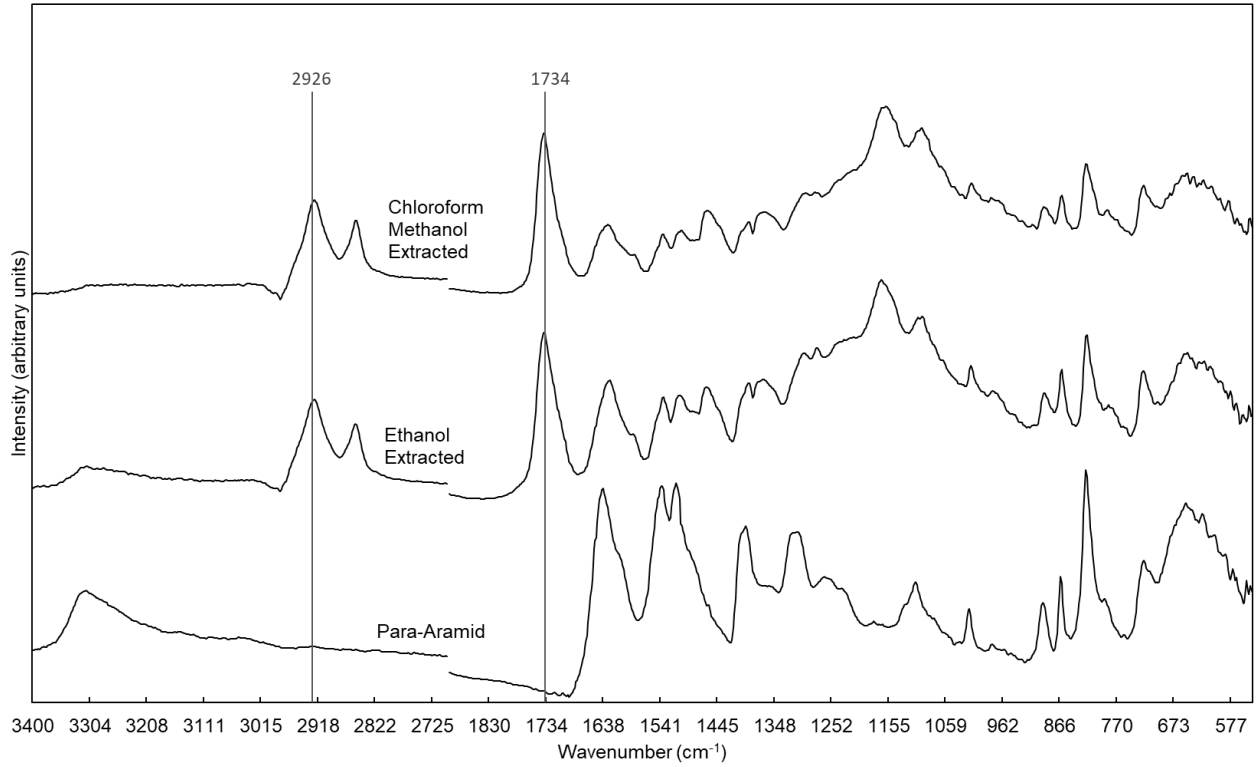
Figure 14. FTIR of untreated, ethanol, and 2:1 chloroform methanol extracted para-aramid fabric
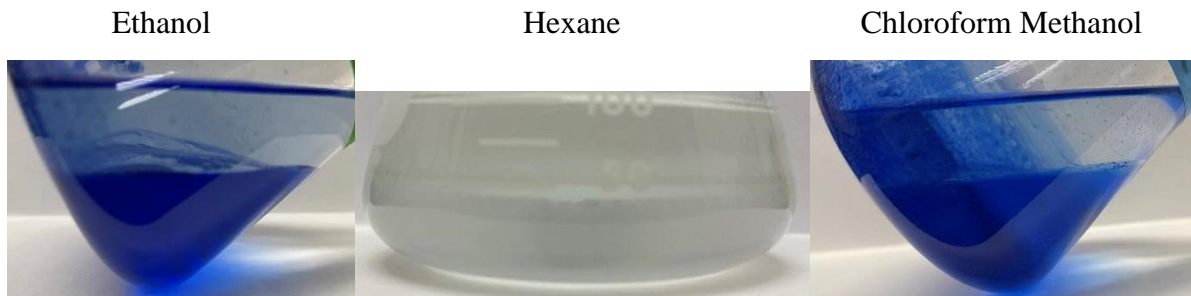
Figure 15. Hexane and water phase separation of dried, extracted material

The previously insoluble material was dissolved in DCM and separated with water. After separation, the observable dye remained in the DCM layer (Figure 16). This presented covalent bonding between the resin and Victoria Blue R dye, as if the dye had moved to the water fraction, it would be unbound from the resin. This also supports our theory of a complex between the fabric, resin, and dye as observed by the dye remaining on the fabric after extraction.

SEM observation of untreated, NTP treated, AESO, SOAAC, and GAAC pretreated para-aramid fabric for observation of treatment effect on surface morphology

For further observation of the effect of both the NTP treatment and the various pretreatment solutions, SEM was utilized to visualize the surface morphology of para-aramid fabric (Figure 17). There was minimal, if any, changes or etching to the para-aramid surface after 4 min of NTP, which would have been expected due to the reduction in break point observed after 3 min. However, as these samples were woven instead of individual yarn strands, it is possible that this provided some level of protection to strands by coverage, compared to the entire length of the treated region experiencing NTP.

The surface morphologies of dyed para-aramid fabric with various pretreatments were also observed. It was shown that, compared to AESO, the formed SOAAC was more rough and irregular. This is due to SOAAC being a mixture of reactions and polymerizations. Because of this, amorphous regions may form, resulting in the observed rough texture. This can also be observed in the GAAC system. While it is clear that the GAAC is more rough than AESO, it is less so than SOAAC. This is due to the smaller molecule size of glycerol compared to soybean oil. While there may be the same amount of polymerization, there is less bulk to protrude from the para-aramid strands.
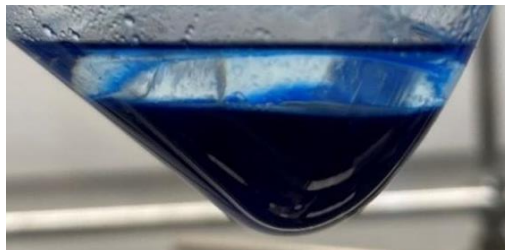
| Ethanol | Chloroform Methanol |

Figure 16. DCM and water phase separation of hexane and water insoluble material
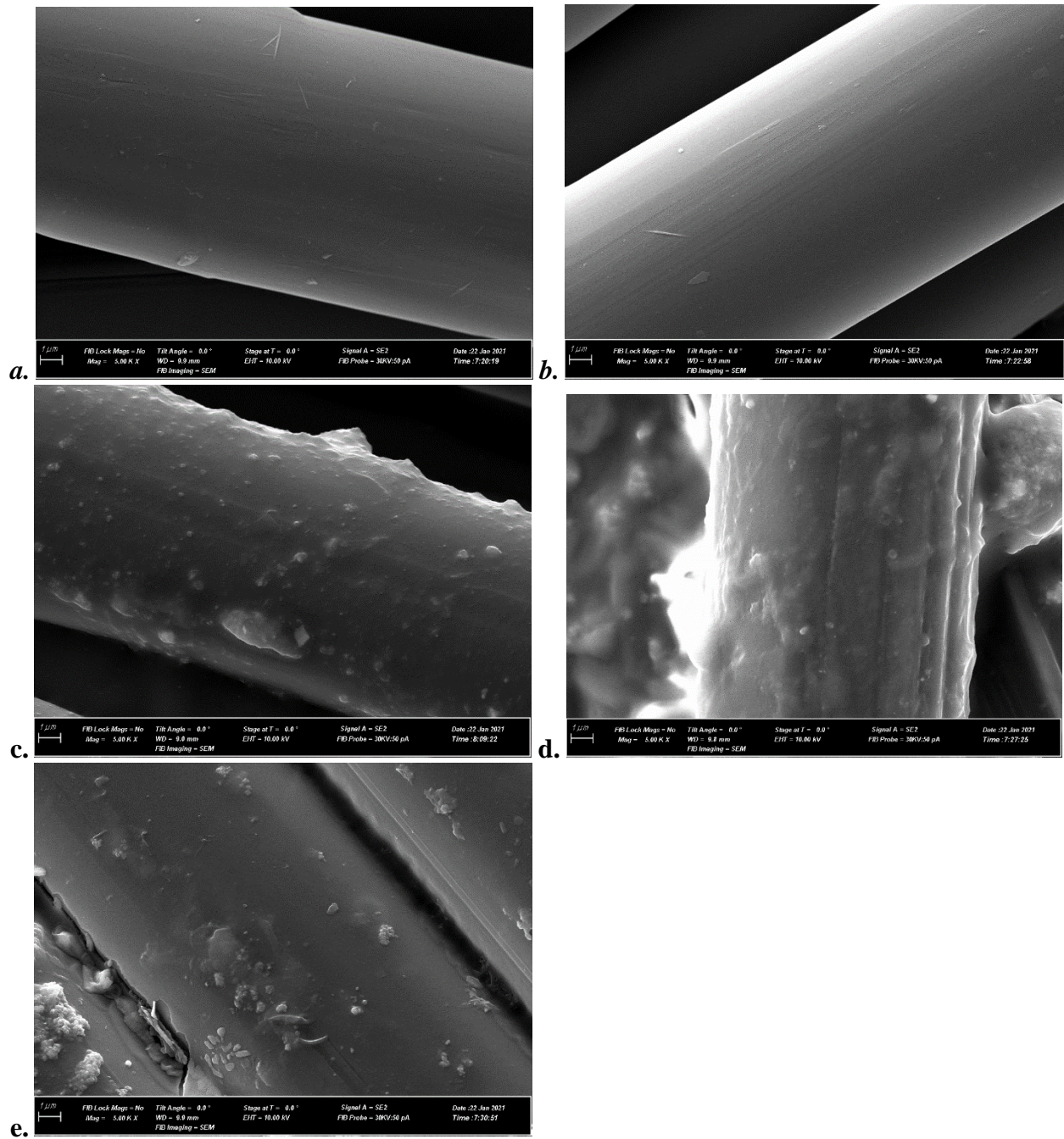
Figure 17. SEM with 5000x magnification of a. untreated, b. 4 min NTP treated, c. AESO pretreated and dyed, d. SOAAC pretreated and dyed, and e. GAAC pretreated and dyed, para-aramid fabric

Conclusion

From this investigation, it was found that SOAAC and GAAC both significantly increased the color strength of para-aramids dyed with Victoria Blue R dye. It was also observed that auxiliary components, specifically NaCl inclusion in the dye bath, was also effective in increasing the color strength of the para-aramid fabric. The processes necessary to achieve these color strengths resulted in no major reduction in strength of the material. Lastly, it was found that the predicted reactions between the SOAAC and GAAC were occurring, and further reacted to form covalent bonds with the para-aramids.

CHAPTER II
ENHANCING THE DYEING OF PARA-ARAMIDS BY TREATMENT WITH SOYBEAN OIL-BASED BIOPOLYMERS AND NONTHERMAL PLASMA IN AN AQEUOUS AND SUPERCRITICAL CARBON DIOXIDE DISPERSE DYE SYSTEM

The following chapter contains the work "Dyeing para-aramid fabrics in supercritical carbon dioxide with pretreatment of nonthermal plasma induced oil polymers" published in *J Am Oil Chem Soc.* **2022; 99(12): 1175– 1188.** All experiments were completed by me. Co-authors include Dr. Christopher Doona, Dr. Xiaofei Ye and Dr. Tong Wang advised this work.

Abstract

After complete investigation of dyeing para-aramids with a cationic dye system, the objective of this study was to investigate methods for increasing the color strength of para-aramid fabric dyed with Disperse Blue 14 in both an aqueous system, where the dye would dispersed, and supercritical carbon dioxide systems, a system where the dye would be dissolved. This was addressed in the aqueous system by observation of the effects of nonthermal plasma, pretreatment coatings consisting of soybean oil and acrylic acid, as well as by utilization of multiple auxiliary components. It was found that para-aramid fabric soaked in a molar ratio of 1.50 acrylic acid to commercial soybean oil, along with 480 seconds of nonthermal plasma treatment, and a 5 wt.% NaCl concentration in the dye bath presented the greatest color strength with a K/S value of 7.5. At these ideal conditions, an 11.1% reduction in color strength was recorded from washing the first to second detergent washes. For the supercritical system, the pressure and temperature of the supercritical fluid were varied for optimization. It was found that the greatest color strength was recorded at a temperature of 160°C and pressure of 2540 psig.

Abbreviations

Nonthermal plasma (NTP), acrylated epoxidized soybean oil (AESO), soybean oil and acrylic acid complex (SOAAC), supercritical CO_2 (SCCO2), attenuated total reflectance (ATR), Fourier

transform infrared (FTIR), mercury-cadmium-telluride (MCT), dichloromethane (DCM), hydrochloric acid (HCl)

Introduction

As found in chapter 1, with the ease in application and formation of the soybean oil and acrylic acid complex (SOAAC), as well as the long, alkyl chains present in soybean oil, SOAAC was investigated further as an intermediate between para-aramids and disperse dyes. Specifically Disperse Blue 14, a nonpolar, disperse dye (Figure 18), was used for the investigation of the success of the dyeing treatment due to the potential attraction from the nonpolar alkyl chains of soybean oil (Figure 2). To avoid the necessity of a surfactant for dye delivery in an aqueous system, glycerol is also being investigated as a method to disperse the dye in water, while also allowing for greater dyeing temperatures due to its higher boiling point.

While the aqueous system is being investigated, supercritical CO_2 (SCCO2) is also being investigated as a solvent for the disperse dye. While SCCO2 has been investigated by others due it being more green, as it takes the place of water therefore reducing the production of wastewater, SCCO2 is of our interest due to its hydrophobicity. SCCO2 is able to dissolve the hydrophobic dye, potentially supporting the delivery of disperse dye to the para-aramids, as well as enhance evenness of dyeing[5]. The supercritical state can be reached once a minimum temperature of 31°C and pressure of 1070 psig are met and maintained. In the supercritical state the solvent can still move like a gas, presenting better diffusion than water, but able to dissolve and therefore evenly spread the disperse dye[18]. Supercritical carbon dioxide has also been investigated for the swelling of polymer chains, a desirable property as para-aramids have very tight, crystalline chains[5]. Increasing pressure has also presented a positive effect on the color strength of meta-aramid fabric in multiple disperse dyes when in the supercritical system[18].
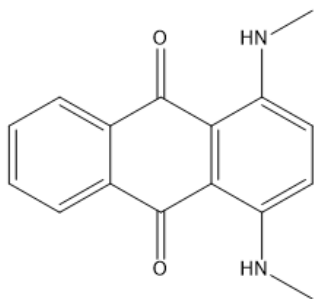
Figure 18. Chemical structure of Disperse Blue 14 dye

Therefore, the objectives of this study are to evaluate effective treatment strategies using NTP as a treatment, SOAAC as an intermediate reactive component along with NaCl to maximize the color strength and fastness of dye to para-aramid fabric, observe the differences between SCCO2 dyeing systems on color strength, and characterize the nature of the reactions occurring during the treatment process.

Materials and Methods

Pretreatment of Para-aramid Fabric

Soybean oil from a local grocery store (Crisco Pure Vegetable Oil) and acrylic acid (Sigma-Aldrich, St. Louis, MO, USA, CAS #: 79-10-7) were combined at various molar ratios of acrylic acid to soybean oil. To aid in the even distribution of the solution components onto the para-aramid surface, ethyl acetate (Sigma-Aldrich, St. Louis, MO, USA, CAS #: 41-78-6) was used as a solvent at a 3.00 molar ratio of ethyl acetate to acrylic acid. Para-aramid fabric samples were individually cut into approximately one-inch pieces and immersed in respective pretreatment solutions for 20 h.

Aqueous Dyeing of Para-aramid Fabric

A combination of Box Behnken response surface design and full factorial design were utilized for investigation and optimization of variables. A box Behnken design was utilized beyond full factorial design to further identify optimal concentrations of the three variables that presented the greatest impact on color strength, as well as identify potential interactions between the variables. Disperse Blue 14 dye solutions (0.1 wt.%) (Sigma-Aldrich, St. Louis, MO, USA, CAS #: 2185-86-6) in various mass ratios of glycerol (Sigma-Aldrich, St. Louis, MO, USA, CAS #: 56-81-5) to distilled water were prepared with various NaCl concentrations. Dye solutions

were loaded into 5mL glass conical vials, with stir bar included, and placed in a small reaction vial stirrer and heater (React-Thermo, Fisher Scientific, Waltham, Massachusetts, USA) for continuous agitation and heating.

Para-aramid samples, dried after removal from solvent solutions, were placed on a plexiglass platform for treatment with nonthermal plasma. Samples were rotated to promote even treatment by the NTP discharge, under coplanar dielectric barrier (Figure 4) for various times. Directly after NTP treatment, dye baths were raised to predetermined temperatures, and treated para-aramid samples were placed in dye vials while stirring for one hour.

SCCO2 Dyeing of Para-aramid Fabric

A hexagonal design of temperatures (80°C – 160°C) and pressure (1545 – 2810 psig) was utilized to determine the ideal experimental conditions for maximum color strength of SOAAC soaked para-aramid fabric. This range was selected due to constraints of the dyeing system (a maximum 3000 psig) as well as a hexagonal design utilized to fully observe the interactions between varying levels of the two factors investigated. To compare with the effect of SOAAC, raw para-aramids as well as soybean oil pretreated para-aramids, both with and without NTP treatment were dyed as well. 80 mg of Disperse Blue 14 was loaded along with magnetic stir bar to a non-circulating steel pressurization vessel along with 1 in^2 para-aramid samples. The vessel was then sealed and flushed with liquid CO_2 before pressurizing to 800 psig. At this point, the vessel was heated and pressurized to desired levels (80 – 160 °C, 1550 – 2800 psig), and once reached, stirred for 2 h. After completion, the vessel was removed from heat and left to cool overnight. The next day, the vessel was depressurized, and the dyed samples washed.

Para-aramid washing for removal of unbound dye

After dyeing was completed, samples were rinsed with warm, followed by cold water, for a total of 5 min to remove unbound dye. Wet samples were dried in convective oven, heated at a rate of 35°C /min to 150°C, and maintained for 2 min. When dried, the dyed fabric was tumbled with 12 g of detergent (ECOS Plus Stain-Fighting Enzymes) in 375 mL of 40°C distilled water for 30 min and the rinsing and drying process was repeated. The detergent wash, rinsing, and drying process was completed once more for a total of two detergent washes.

Color Strength Measurement of Dyed Para-aramid Samples and Fastness Test

The spectral reflectance (R) of dyed para-aramid fabric (NTP treated side) was recorded by refractometer (Spectro 1, Variable, Chattanooga, TN, USA) after the initial water rinse as well as after each detergent wash at 595 nm (maximum absorption wavelength of Disperse Blue 14). The recorded value was compared by conversion to K/S, the ratio of light absorption (K) to light scattering (S) by Kubelka-Monk equation (Equation 1). The dye fastness was measured by percent change in K/S between detergent washes[16].

Extraction of Dyed Para-aramid Fabric

To investigate the relationship among para-aramid fabric, formed resin, and Disperse Blue 14 dye, extraction of dyed para-aramid fabric was completed using solvents of varying polarity. Color strength of dyed para-aramid fabric was recorded prior to being placed in 40 mL of either hexane, a nonpolar solvent, ethanol, a polar solvent, or 2:1 chloroform methanol (v/v), containing both polar and nonpolar solvents, for 16 hours. After extraction, samples were dried at 150°C for 2 min before color strength was recorded.

Extract solutions were dried by rotary evaporation before being dissolved in 50mL of

hexane. As disperse dye would remain in the hexane phase along with other nonpolar material,

40mL of 6N hydrochloric acid (HCl) was added to protonate dye molecules, based on the

volume needed for entire movement 10mg of disperse dye into the water phase, allowing for

observation of unbound dye in the water phase (Figure 19). After separation, solvents were

decanted and the remaining material was dissolved by 20mL of dichloromethane (DCM),

followed by 20mL of 6N HCl for observation of dye movement.

Tensile Strength Analysis

Tensile strength analysis of para-aramid yarn was completed using a TA.XT plus texture

analyzer instrument (Stable Micro Systems, United Kingdom) by modification of ASTM D7269.

Para-aramid yarn 12 in in length of untreated, NTP treated, SOAAC pretreated and dyed, and

SOAAC pretreated and dyed with NaCl in the dye bath (both SOAAC treatments prepared at

ideal color strength conditions), para-aramid yarn were conditioned in a dry, airtight environment

for 3 days. After conditioning, one end of the yarn was wrapped around electrical wire, to

minimize slipping, and placed into the top clamp of the TA.XT system. The bottom, hanging end

of the yarn, was wrapped around electrical wire and then placed into the bottom clamp, totaling a

gauge length of 10 inches, decided due to length limitations of the TA.XT plus texture. The yarn

was then pulled apart with a pre-test speed of 0.5 mm/s, trigger force of 30 g, and test speed of 2

mm/s until the break point force (g) was observed. Each sample was completed in triplicate and

results compared by student's t-test comparison of means.

FTIR Analysis for Observation of Chemical Changes

Attenuated total reflectance (ATR) - Fourier Transform infrared (FTIR) analysis was

performed to obtain IR spectrums for reactants as well as SOAAC resin and dyed fabric for
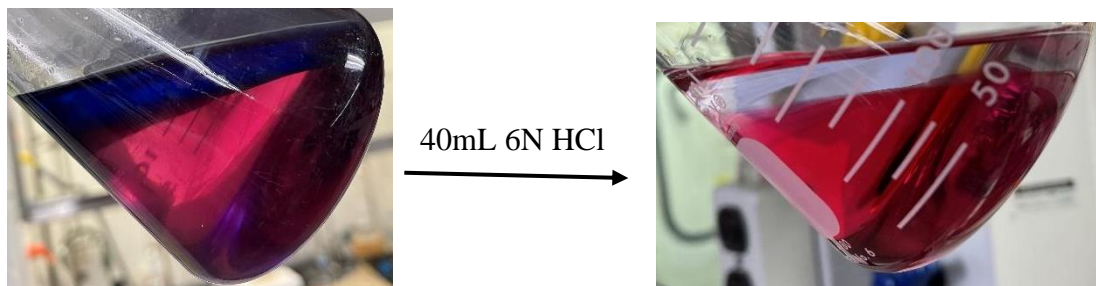
Figure 19. Disperse Blue 14 dye partially and entirely protonated with 6N HCl

observation of chemical changes occurring during the NTP and dyeing processes. A liquid nitrogen cooled Mercury-Cadmium-Telluride (MCT) detector with germanium crystal for ATR readings was used for recording the IR spectrum, with potassium bromide used as background for the samples.

Results And Discussion

Investigation of optimal dyeing conditions of the SOAAC pretreatment system in an aqueous dye system

To obtain the proper dyeing conditions for final optimization of the SOAAC system, a box Behnken and full factorial design experiment were completed. The initial box Behnken experiment aimed to identify if the SOAAC and NTP treatment times for the cationic dye were similarly effective in with the new dye, as well as identify the proper glycerol: water mass ratio for the dye bath (Table 8). Different from what was observed in the cationic dye system, the lowest molar ratio of acrylic acid to soybean oil was the most effective while NTP treatment times presented a minimal effect (Figure 20). Greater amounts of water in the dye bath presented greater color strength, which resulted in a mass ratio of 20 glycerol : 80 water moving forward.

From this point, a final dyeing condition exploration was completed for identifying the ideal dyeing temperature as well as investigate the effects of NaCl and the swelling agent benzyl alcohol (Table 9). Benzyl alcohol was investigated as it is a swelling agent, a dyeing aid that assists in greater dye penetration by "swelling" the chains of polymers[19]. Greater concentrations of NaCl were found to continue to be effective, while the inclusion of the swelling agent did not positively affect the color strength (Figure 21). A dyeing temperature of 140 °C was found to present greater color strength results.

Table 8. Box Behnken response surface experimental design for the molar ratio of acrylic acid to soybean oil, NTP treatment time, and glycerol to water mass ratio

Acrylic : Soy Molar Ratio	NTP Time (s)	Glycerol : Water Mass Ratio	K/S	dK/S[†] (%)
1.5	180	80 - 20	5.8	24.1
1.5	270	50 - 50	4.2	-3.9
1.5	270	100 - 0	2.8	21.3
1.5	360	80 - 20	4.0	13.2
3.25	180	50 - 50	3.8	20.2
3.25	180	100 - 0	2.5	20.0
3.25	270	80 - 20	3.1	27.0
3.25	270	80 - 20	2.6	15.6
3.25	270	80 - 20	2.1	21.1
3.25	270	80 - 20	3.9	10.7
3.25	270	80 - 20	2.3	26.4
3.25	360	50 - 50	5.8	7.3
3.25	360	100 - 0	4.6	9.5
5	180	80 - 20	6.0	28.2
5	270	50 - 50	4.1	-7.3
5	270	100 - 0	2.3	34.2
5	360	80 - 20	2.2	29.2

[†]"dK/S" indicates percent reduction in color strength from first to second detergent wash
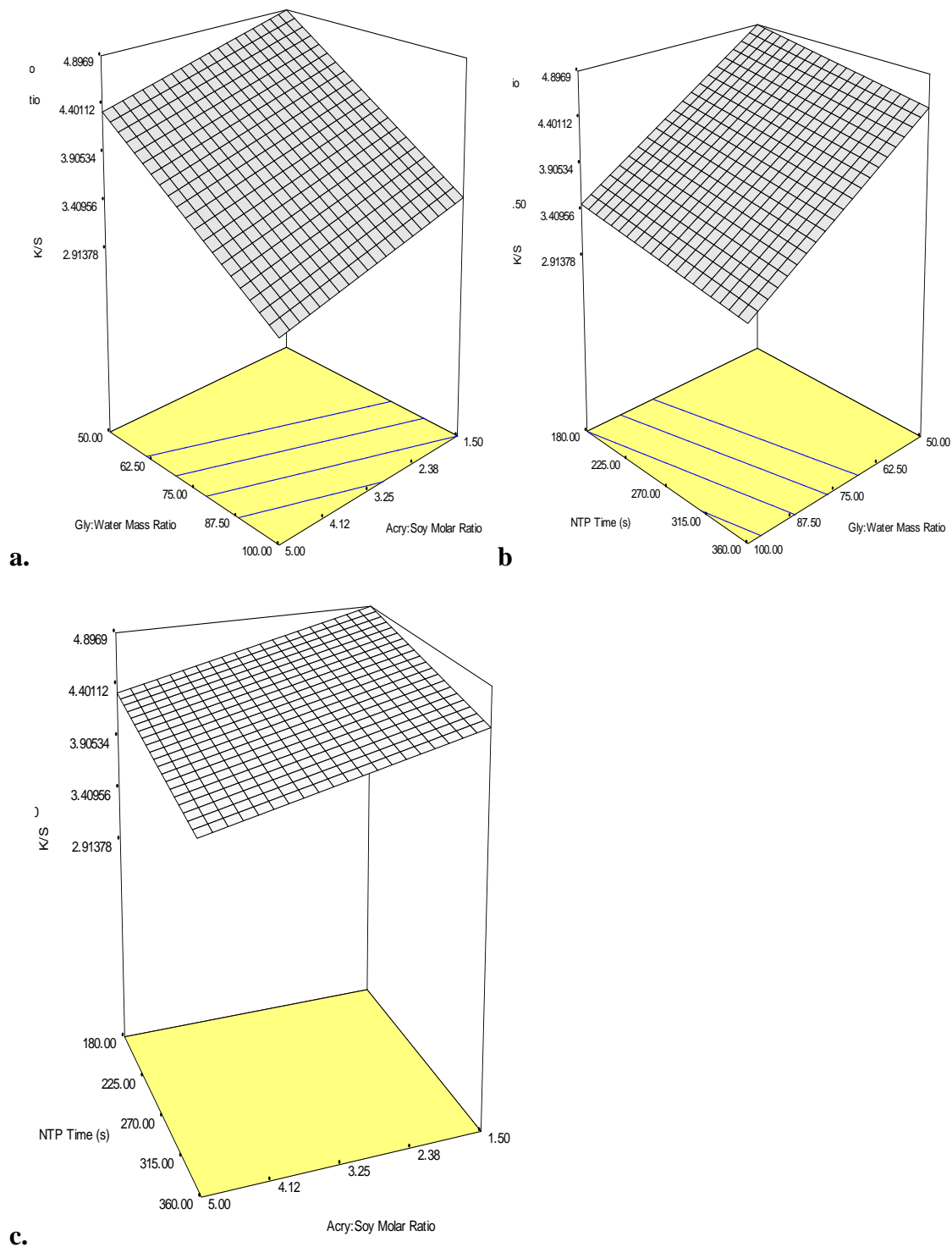
Figure 20. K/S value surface plot of SOAAC pretreatment after the first detergent wash with a. NTP treatment time held constant at 180 seconds, b. acrylic acid to soybean oil molar ratio held constant at 1.50, and c. glycerol to water mass ratio held constant at 50 ($r^2 = 0.7739$)

Table 9. Two level full factorial experimental design for dyeing temperature, NTP treatment time, NaCl concentration in the dye bath, and swelling agent concentration in the dye bath

Temperature (°C)	NTP Time (s)	NaCl (wt.%)	Swelling Agent (wt.%)	K/S	dK/S (%)
140	240	2	0	3.3	9.7
140	240	2	2	4.9	10.3
140	240	10	0	4.1	9.2
140	240	10	2	4.0	9.1
140	480	2	0	4.3	8.2
140	480	2	2	4.8	4.7
140	480	10	0	11.4	-0.2
140	480	10	2	4.8	6.9
190	240	2	0	2.6	11.1
190	240	2	2	3.1	15.6
190	240	10	0	3.4	7.9
190	240	10	2	3.8	10.9
190	480	2	0	3.0	6.6
190	480	2	2	3.9	9.6
190	480	10	0	4.2	6.9
190	480	10	2	4.4	7.6

[†]"dK/S" indicates percent reduction in color strength from first to second detergent wash
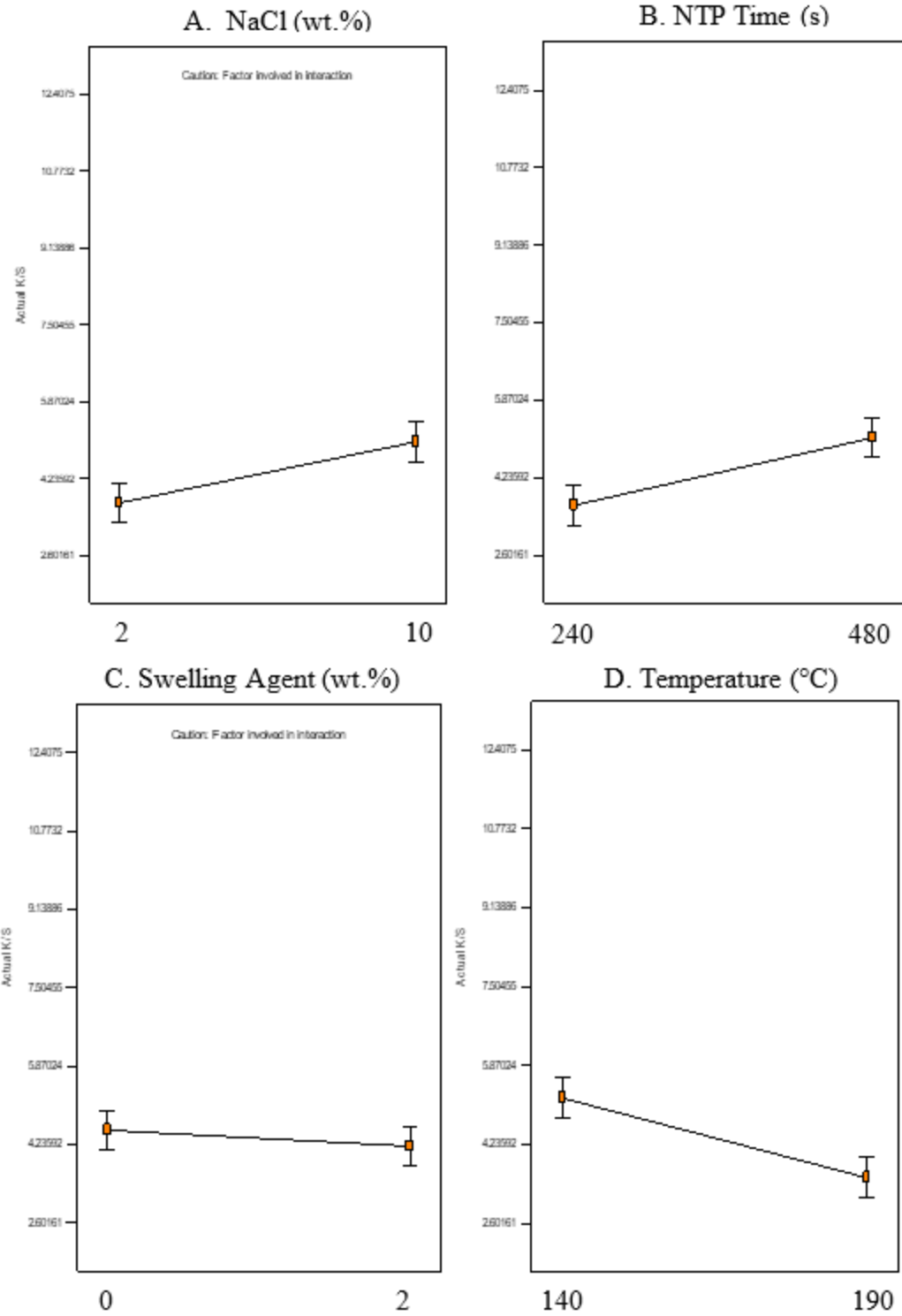
Figure 21. Main effect and interactions of swelling agent, NaCl, and NTP treatment, and temperature.
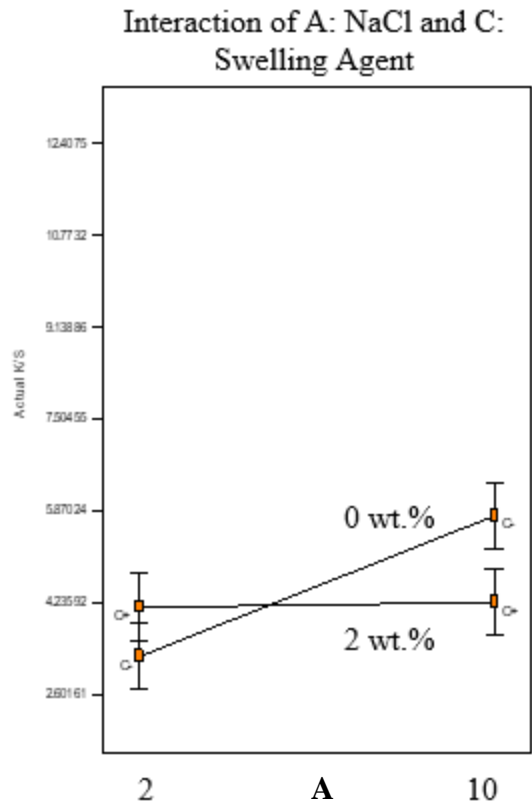
Figure 21 continued

Experimental optimization of the SOAAC pretreatment system in an aqueous dye system by

Box Behnken response surface design

The experiment optimization of soybean oil to acrylic acid molar ratio in the SOAAC pretreatment, NTP treatment times, and NaCl concentrations in the dye bath were investigated by a Box Behnken response surface design to find the ideal combination for maximum color strength values (K/S). The factors were investigated with constraints: acrylic acid to soybean oil molar ratios of 1.5, 3.25, and 5, NTP treatment times of 180, 330, and 480 s, and NaCl dye bath concentrations of 2, 5, and 8 wt.% (Table 10). As observed from the response surface plots, a quadratic model presented the greatest color strength at the experimental levels of acrylic acid to soybean oil molar ratio of 1.50 with 480 s of NTP treatment and 5 wt.% NaCl (Figure 22).

The impact of SOAAC may be explained by the increased presence of hydrophobic groups on the fabric to assist in binding of the disperse dye to the fabric. This could also explain the major impact of NTP treatment as longer times ensure that greater amount of acrylic acid was able to react with the soybean oil, potentially assisting in covalent bonding of the formed intermediate resin to the surface of the para-aramid fabric. It was also found that at these ideal experimental conditions, a dK/S (%), or the percent change in K/S after a second detergent wash, of 11.1% was observed.

Effect of vegetable oil pretreatments and NTP on para-aramid fabric dyed in a SCCO2 system

To fully investigate the impact that the SOAAC had in the SCCO2 system, raw para-aramid, as well as soybean and coconut oil treated samples were also included to be dyed in the SCCO2 system with and without NTP treatment. Raw para-aramid is used as a control to the pretreatments and NTP treatments, while soybean oil is of interest not only because it is a base

Table 10. Box Behnken response surface experimental design for soybean oil and acrylic acid as a pretreatment, NTP treatment time, and NaCl concentration in the dye bath

Acrylic : Soy Molar Ratio	NTP time (s)	NaCl in Bath (wt.%)	K/S	dK/S (%)
1.5	180	5	4.7	9.5
1.5	330	2	4.5	11.8
1.5	330	8	4.9	12.0
1.5	480	5	9.7	11.1
3.25	180	2	3.7	9.1
3.25	180	8	4.3	13.2
3.25	330	5	3.9	14.2
3.25	330	5	3.9	16.0
3.25	330	5	4.4	13.9
3.25	330	5	4.6	14.1
3.25	330	5	3.6	21.6
3.25	480	2	4.4	11.0
3.25	480	8	4.9	12.0
5	180	5	3.6	9.2
5	330	2	3.6	7.6
5	330	8	3.5	11.1
5	480	5	6.0	8.8

[†]"dK/S" indicates percent reduction in color strength from first to second detergent wash
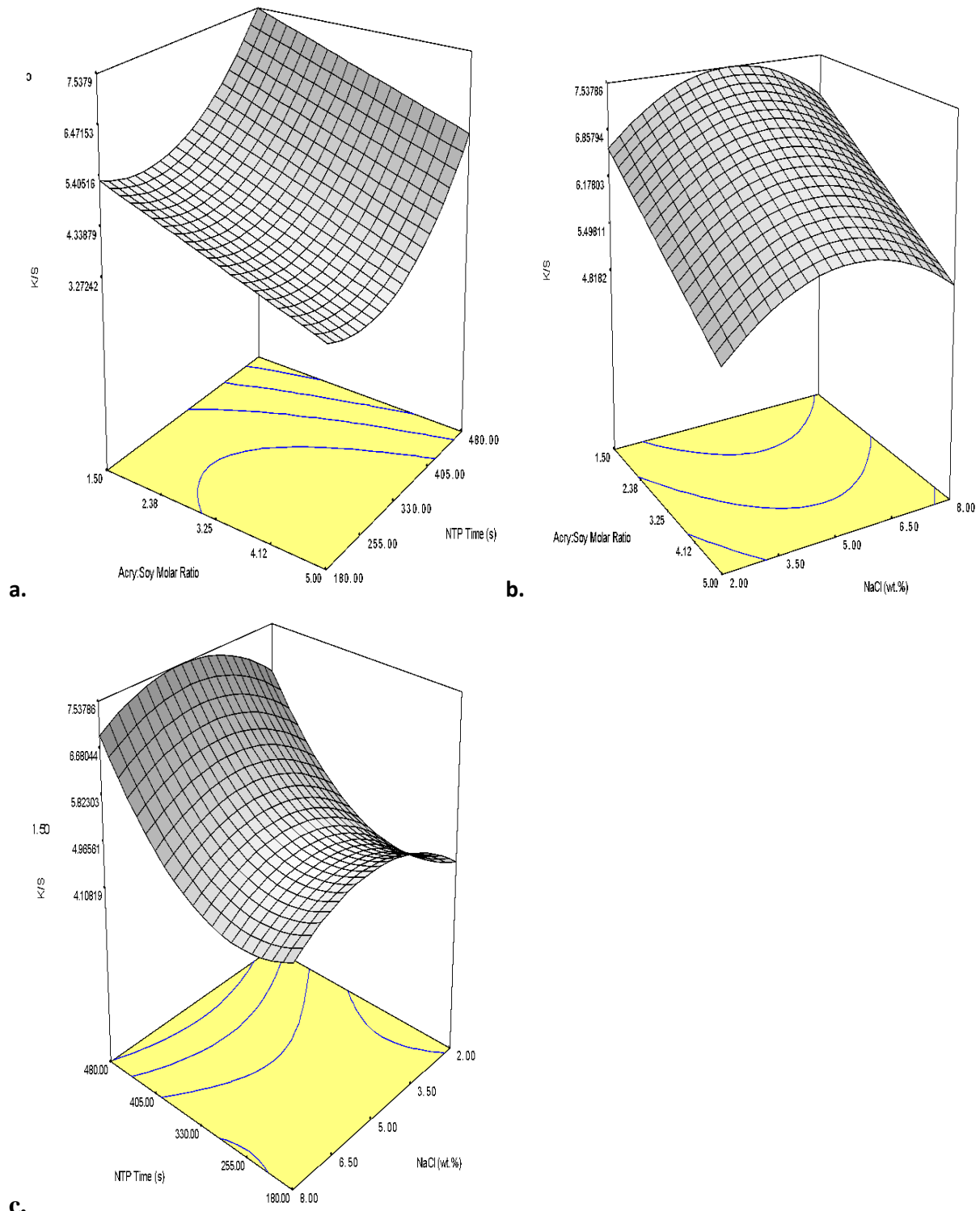
Figure 22. K/S value surface plot of molar ratio of soybean oil to acrylic acid, NaCl concentration, and NTP time after the first detergent wash with a. NaCl held constant at 5 wt.% b. NTP treatment time held constant at 480 s, and c. acrylic acid to soybean oil molar ratio held constant at 1.50 ($r^2 = 0.8251$)

component of the SOAAC system, but because it has shown positive color strength effects for para-aramids when treated with NTP[20]. Coconut oil was also included due to it containing the same triacyl glyceride (TAG) structure, but with less unsaturated bonds.

It was observed that in most temperature and pressure combinations, the color strength of para-aramids was greater after NTP treatment (Table 11). This is believed to be due to exposure of the crystalline structure to reactive species and radicals. When exposed to these materials, it is possible for the fabric to breakdown or react with the species in the environment. This may lead to a reduction in crystallinity, assisting in the penetration of dye. It also has the possibility to generate functional groups that could better interact with the dye or other materials in the environment. While there was no clear trend for the non-NTP treated samples, it could be observed that the greatest color strength was achieved for the NTP treated when at a maximum temperature of 160°C and 2540 psig (Figure 23).

Coconut and soybean oil were investigated as pretreatments for para-aramid fabric (Table 12). This was done due to the hydrophobicity of vegetable oils, which would in theory, better interact with the disperse dye due to attraction from Van der Waals forces between the dye and the alkyl chains. The increase in color strength due to this interaction could be observed in all the soybean oil-soaked fabric as well as in the NTP treated coconut oil. It was shown that soybean oil performed better overall, but specifically performed well after NTP treatment. This is due to the greater amount of unsaturated bonds on soybean oil compared to coconut oil. With a greater number of unsaturated bonds, there is more potential for interactions with both the atmospheric environment, as well as the dyeing environment and fabric, allowing for a greater attachment of the oil to the fabric. With observation on the impact of vegetable oils on the color strength of the

Table 11. K/S values for un-pretreated (raw) para-aramid fabric with and without NTP treatment for 3 minutes after SCCO2 dyeing

Temperature (°C)	Pressure (psig)	K/S	3 min NTP K/S
80	2275	0.3	0.3
100	1545	0.2	0.2
100	2810	0.2	0.3
120	1905	0.2	0.2
120	2185	0.2	0.3
140	1560	0.3	0.4
160	1730	n.a.	0.4
160	2540	0.3	0.5
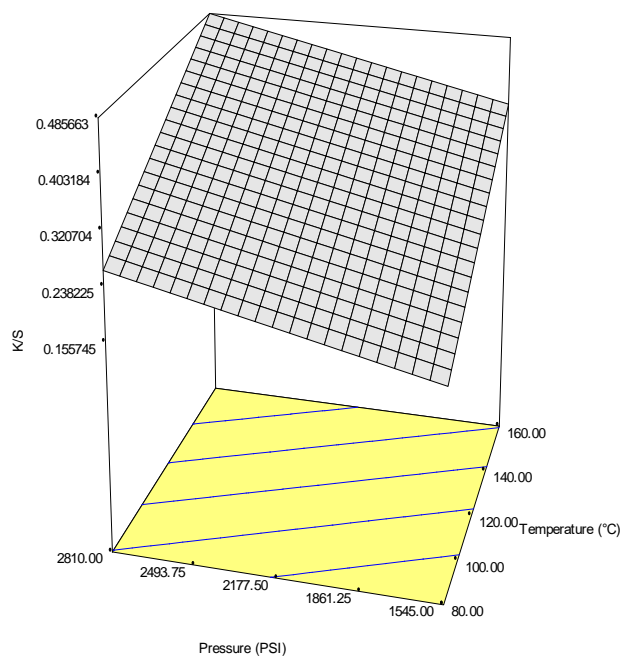
Figure 23. K/S surface plot of para-aramid fabric treated with three minutes of NTP dyed in SCCO2 at various pressures and temperatures ($r^2 = 0.7834$)

Table 12. K/S values for coconut and soybean oil pretreatment and NTP treatment for 3 minutes

Temperature (°C)	Pressure (psig)	Coconut Oil K/S	Coconut Oil w/ NTP K/S	Soybean Oil K/S	Soybean Oil w/ NTP K/S
80	2275	0.2	0.4	0.4	2.0
100	1545	0.2	0.3	0.9	4.0
100	2810	0.2	0.4	0.9	5.1
120	1905	0.2	2.3	1.8	4.7
120	2185	1.2	1.4	1.6	4.7
140	1560	0.3	0.5	2.3	4.7
160	1730	1.7	3.4	2.6	4.3
160	2540	0.5	0.8	2.7	4.6

para-aramid fabric, SOAAC was then observed to show how the addition of acrylic acid can increase the overall effectiveness of the pretreatment.

Experimental optimization of SCCO2 system conditions with the SOAAC pretreatment with Disperse Blue 14

With para-aramid samples pretreated in the previously determined ideal conditions for color strength for SOAAC in the aqueous system, molar ratio 1.50 acrylic acid to soybean oil and a NTP treatment time of 480s, the conditions of the SCCO2 system were optimized to assist in further increasing the color strength. It was found that at a temperature of 160 °C and pressure of 2540 psig the maximum color strength was achieved (Table 13).

To further understand the effect of NTP, the pretreatment was also included without NTP treatment. At each temperature and pressure combination, the NTP treated fabric presented a greater color strength. This is due to polymerization and attachment of the SOAAC to the fabric from the NTP treatment. With greater polymerization of the formed resin, greater attachment is possible, increasing the concentration of material on the surface for dye to interact with, such as nonpolar alkyl chains. Without this treatment, it is easier for the pretreatment solution to be removed during the dyeing process, therefore reducing the color strength as less disperse dye can interact with the fabric's surface (Figure 24).

Pressure had a relatively smaller impact compared to temperature on the color strength. This can likely be attributed to the higher energy of the dyeing environment due to the higher dyeing temperature, allowing for greater movement of dye molecules, and therefore more opportunities for dye to contact the fabric in an ideal orientation[21]. With increased pressure, the density of the SCCO2 system would also increase, increasing the solubility of the dye system[22].

Table 13. K/S values of para-aramids soaked in SOAAC with and without NTP treatment for 480 s after SCCO2 dyeing

Temperature (°C)	Pressure (psig)	K/S w/o NTP	K/S w/ 480 s NTP
80	2275	2.0	2.9
100	1545	2.0	2.8
100	2810	2.0	5.7
120	1905	1.4	8.9
120	2185	0.4	8.3
140	1560	1.1	9.3
160	1730	n.a.	7.6
160	2540	n.a.	9.7
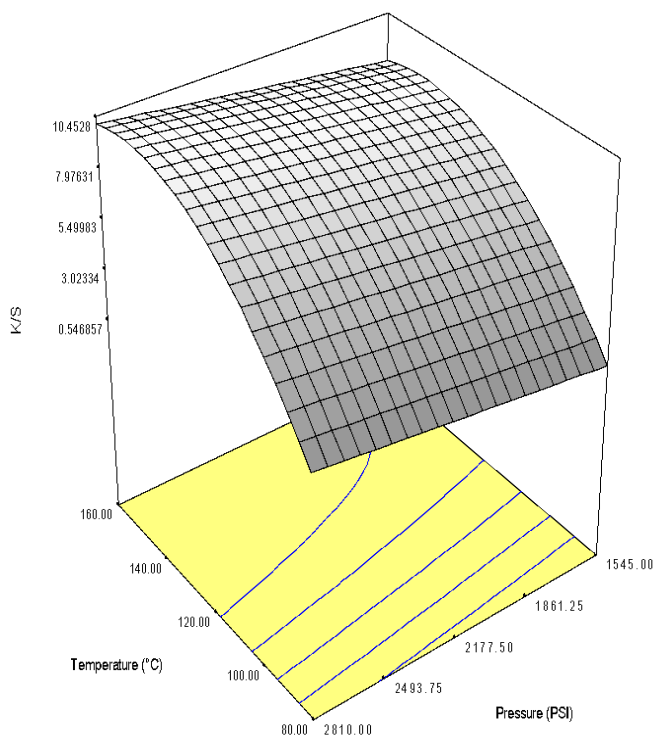
Figure 24. K/S surface plot of SOAAC pretreated and 6 min NTP treated para-aramid fabric dyed in SCCO2 at set pressures and temperatures ($r^2 = 0.8518$)

67

This increased uptake of the dye may explain the slight increase overall, but did not present a large impact as the majority of the dye in the system was already dissolved.

The SCCO2 system was able to achieve the same color strength of 9.7 as the aqueous system, while also providing consistently high color strength values over a range of temperatures and pressures. The SCCO2 system was also able to effectively dye the para-aramid fabric with both the vegetable oils to some extent (Table 14).

Tensile Strength Analysis of NTP Treated and Dyed Para-aramid Yarn

To investigate the impact of NTP treatment and dyeing on the strength of para-aramid fabric, a tensile strength analysis for observation of break point (g) was completed (Figure 25). There was no significant difference found among any treated sample, except for the 3 min NTP treated samples in both the aqueous and SCCO2 systems. This is believed to be due to continued exposure to reactive species and radicals, causing breakdown and changes in the chemical structure of the fabric.

SOAAC treated para-aramid yarn was dyed with Disperse Blue 14, both with and without 5 wt.% NaCl included in the dye bath. NaCl was included as a factor due to its importance found during the experimental process, but also because of the potential for aqueous chlorine solutions to cause a degradation in the para-aramid structure[23]. However, there was no significant reduction in any sample containing NaCl. This can be explained by the occurrence of para-aramid degradation being common in the presence of sodium hypochlorite solutions, not ionic chlorine.

Table 14. Scans of para-aramid fabric with various pretreatments at 160°C and 2540 psig

Treatment Conditions	Scanned Photograph
Raw Para-Aramid	
Coconut Oil – 180 s NTP	
Soybean Oil – 180 s NTP	
SOAAC – 480 s NTP SCCO2 System	
SOAAC – 480 s NTP Aqueous system	
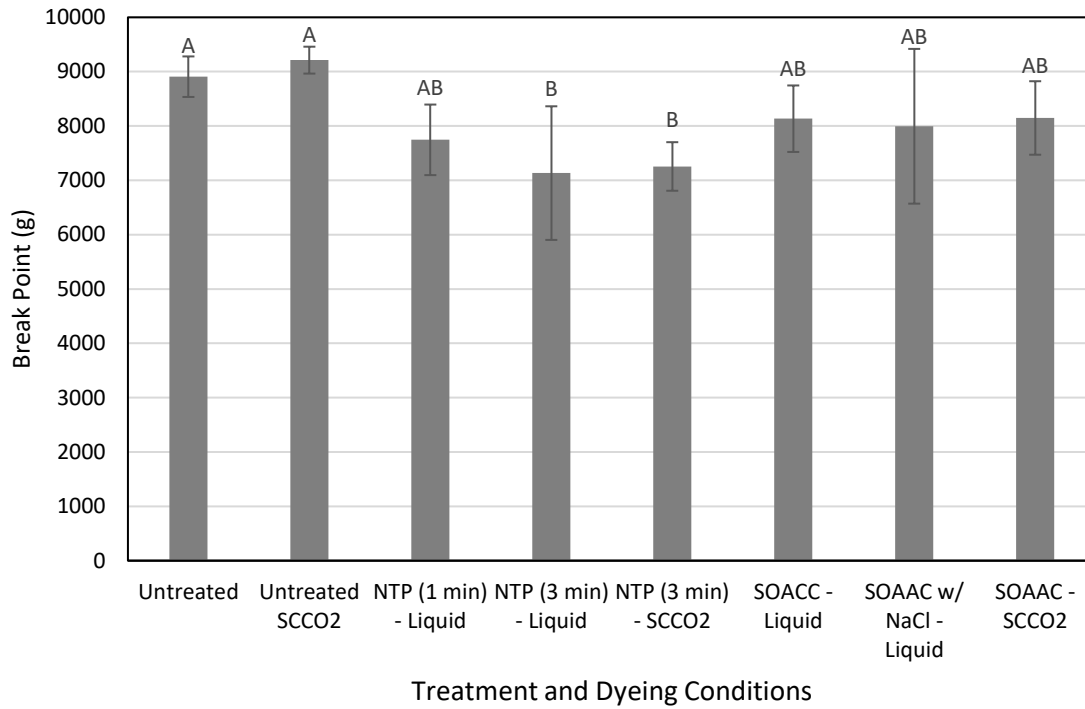
Standard deviation based on triplicate analysis
Significance determined by Tukey-Kramer HSD

Figure 25. Break point (g) comparison of untreated, NTP, and SOACC treated para-aramid fabric from both aqueous and SCCO2 Disperse Blue 14 systems

Extraction of Dyed Para-aramid Fabric for Characterization of the Interactions Between

Para-aramid Fabric, Formed Resin, and Disperse Blue 14 Dye

To investigate the interactions among para-aramid fabric, SOAAC, and Disperse Blue 14 dye, extraction of dyed para-aramid fabric was completed using ethanol, hexane, and 2:1 chloroform: methanol (Figure 26). It was found that of the solvents, chloroform methanol presented the greatest color strength reduction (Table 15). This is due to not only dissolving the nonpolar dye, but also removing unbound or unreacted lipid from the surface of the para-aramid fabric because of this mixture containing both polar and nonpolar solvents. Hexane, however, did not entirely remove the disperse dye from the surface of the fabric. While this solvent should have disrupted the nonpolar interactions between the dye and fabric / intermediate, it is evident that this may have only occurred to a minor extent as it presented the smallest reduction in color strength.

The initial solutions were dried and redissolved in hexane, upon which time 6N HCl was added for protonation of the disperse dye in the hexane layer (Figure 27). Upon complete protonation, it was found that all three solvent systems displayed dye in both the hexane and water layers, presenting a covalent interaction between the dye and the removed material. This was further investigated by observation of the undissolved material in the ethanol and chloroform methanol flasks.

After dissolving in DCM and addition of HCl, it was observed that the protonated dye remained entirely in the DCM layer. This assists observation in showing that there was covalent interaction between the dye and removed material as otherwise the protonated dye would be present in the water phase. This also explains the dyed material remaining on the surface of the hexane extracted para-aramid material.
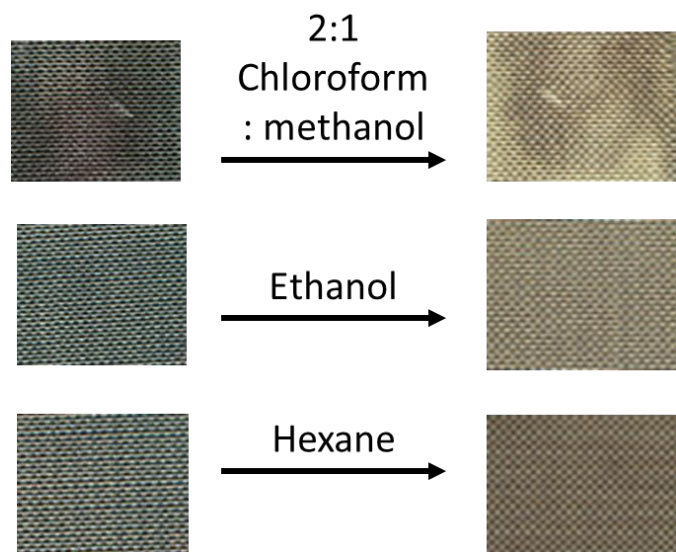
Figure 26. Scanned images of aqueous dyed para-aramid fabric samples before and after ethanol, chloroform methanol, or hexane extraction

Table 15. Color strength of aqueous dyed para-aramid fabric before and after ethanol, chloroform methanol, or hexane extraction

Solvent	K/S After Dyeing	K/S After Extraction	K/S Reduction	% Reduction
Chloroform Methanol	6.7	1.3	5.4	80.6
Ethanol	3.4	1.7	1.7	50.0
Hexane	4.1	2.3	1.9	46.3

b.

c.
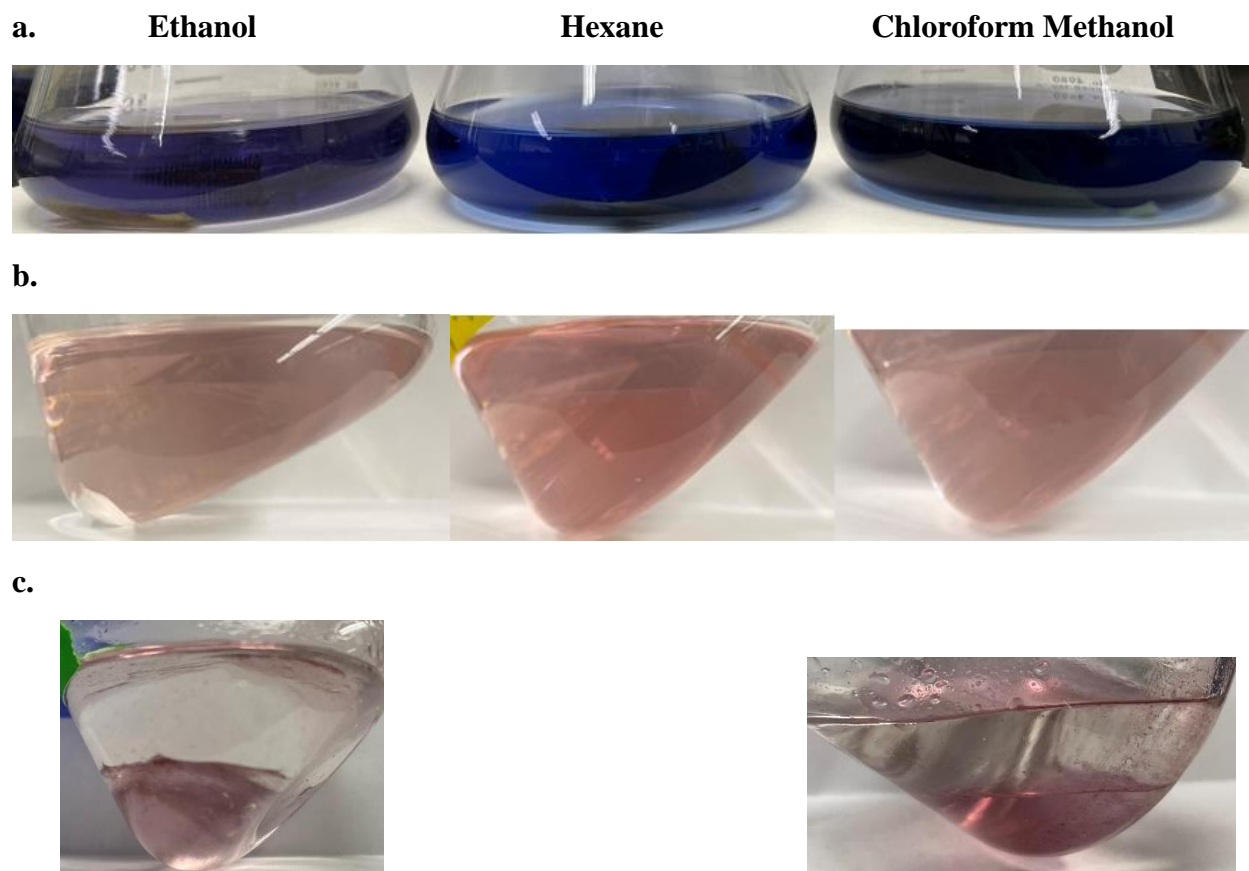
Figure 27. Aqueous dyed ethanol, hexane, and 2:1 chloroform: methanol Disperse Blue 14 extract solutions a. dissolved in hexane. b. after addition of 6N HCl, and c. separation of remaining material by DCM and water

The same process was completed for the SCCO2 dyed para-aramid fabric (Figure 28). It was found that the fabric extracted with chloroform: methanol presented the greatest reduction in color strength, which was expected as the mixture is comprised of both polar and nonpolar solvents (Table 16). Hexane and ethanol presented similar percent reductions in color strength, while ethanol did have the least reduction, which was also expected due to the dye being a nonpolar dye.

The extracted material of each solvent was then concentrated by rotary evaporation before addition of 30 mL of hexane and 6M HCl (Figure 29). It was observed that the protonated dye, now pink in color due to the protonation, moved into the aqueous phase while the majority of the hexane phase was clear, except for a slight color noticeable in the ethanol and chloroform: methanol separations. This result is similar to what was observed in the aqueous dye system. However, with less of a color observed in the hexane layers, it can be assumed that there was less unbound dye present on the SCCO2 samples compared to the aqueous samples.

After decanting the separations, material remained in both the ethanol and chloroform: methanol flasks, believed to be the formed resin that was not able to be entirely dissolved by hexane or water. The remaining material was dissolved with 20 mL of DCM and 6M HCl. In both flasks, the majority of the dyed material remained in the DCM phase while very little was observable in the aqueous phases. This further presents the belief that there is a covalent bond between the extracted resin and the Disperse Blue 14 as otherwise the color observed would have entirely moved in the aqueous phase.

To further observe the relationship between the dye, SOAAC, and para-aramid fabric, FTIR of extracted SCCO2 dyed samples were completed (Figure 30). It was found that in each solvent system, the saturated C-H bonds (2930 cm^{-1}) and ester linkages of the glycerol backbone
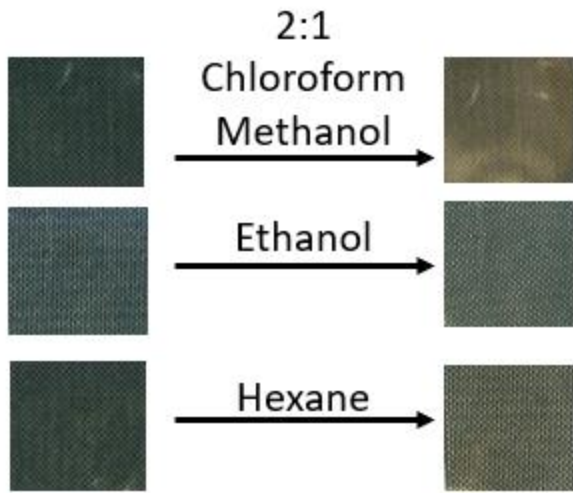
Figure 28. Scanned images of SCCO2 dyed para-aramid fabric samples before and after ethanol, chloroform methanol, or hexane extraction

Table 16. Color strength of SCCO2 dyed para-aramid fabric before and after ethanol, chloroform methanol, or hexane extraction

Solvent	K/S After Dyeing	K/S After Extraction	K/S Reduction	% Reduction
Chloroform-Methanol (2:1)	9.5	2.8	6.7	70.8
Ethanol	9.7	5.8	3.9	39.3
Hexane	8.8	5.0	3.8	43.7
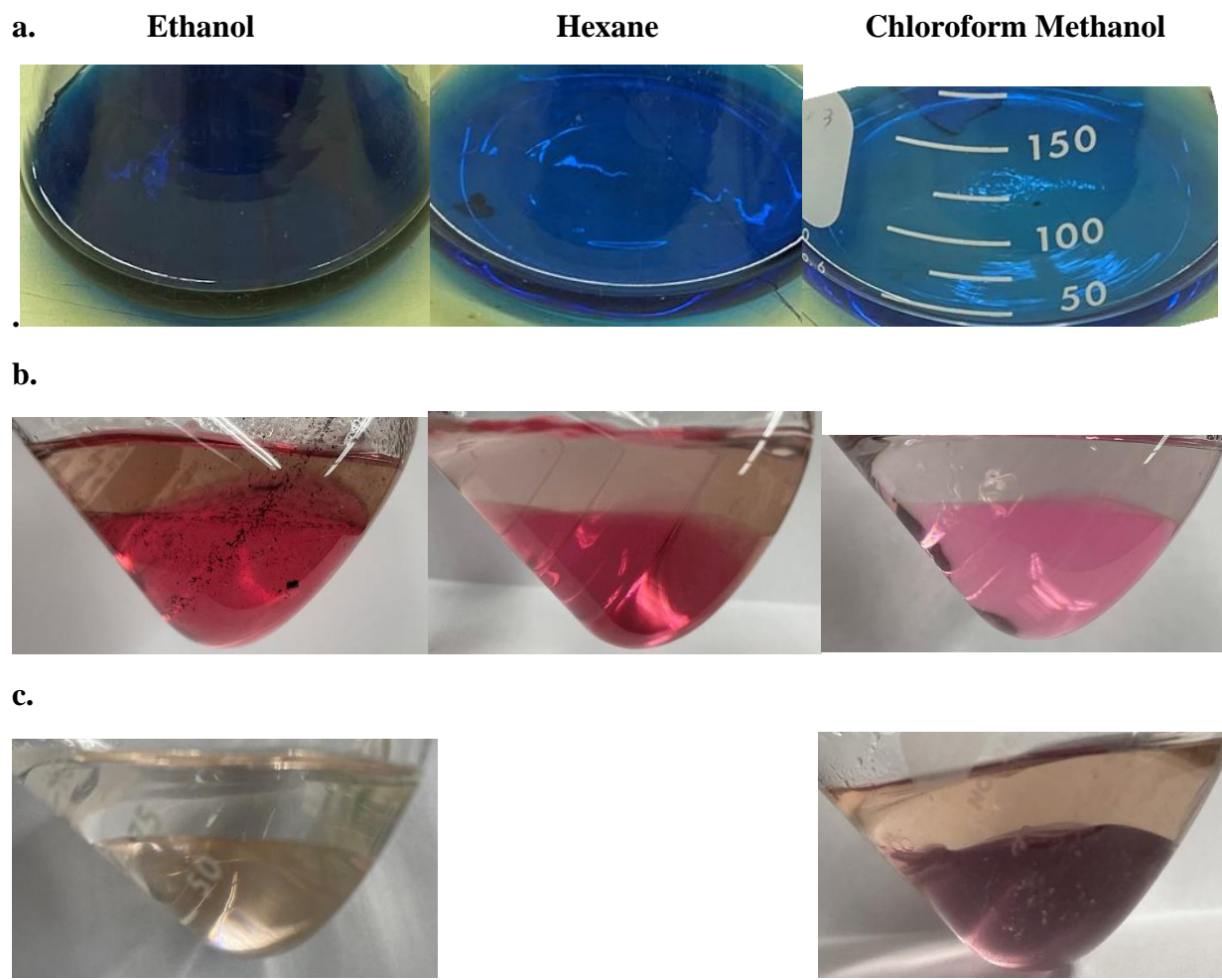
Figure 29. SCCO2 dyed ethanol, hexane, and 2:1 chloroform: methanol Disperse Blue 14 extract solutions a. dissolved in hexane. b. after addition of 6N HCl, and c. separation of remaining material by DCM and water
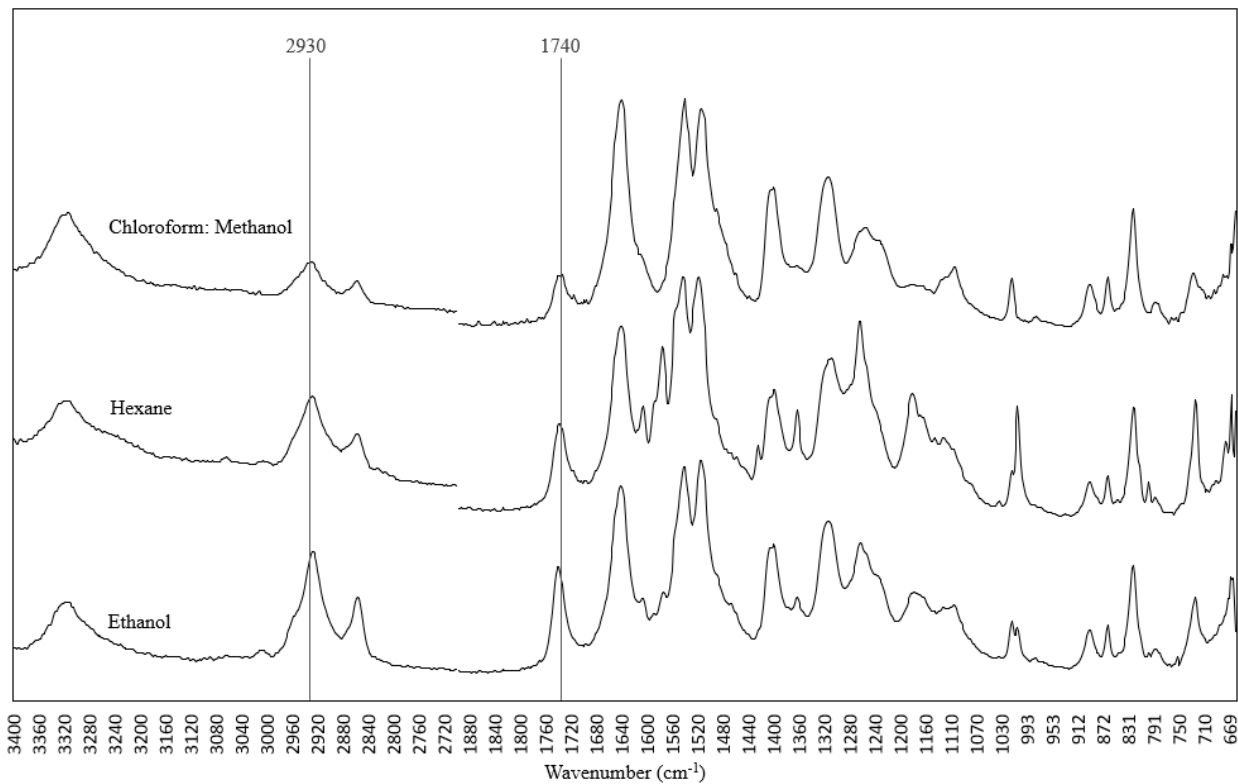
Figure 30. FTIR of, ethanol, hexane, and 2:1 chloroform methanol extracted SCCO2 dyed para-aramid fabric

(1740 cm^{-1}) of soybean oil could still be observed after extraction. With the dye remaining on the surface of the fabric, as well as still presenting the presence of the remaining soybean oil, it is theorized that there is formation of a covalent complex between the para-aramid fabric, SOAAC, and Disperse Blue 14 dye.

FTIR Analysis to determine chemical changes during NTP treatment and dyeing

For further exploration of chemical changes that occurred during NTP treatment as well as during dyeing, FTIR was utilized (Figure 31). It was found that the SOAAC mixture after NTP treatment presented an entire reduction at 1700 cm^{-1} while increasing at the 1735 cm^{-1} position. This was expected as the reduction corresponds to the carboxylic acid groups present on the acrylic acid and their conversion into esters, the groups present at 1735 cm^{-1}, which was the expected pathway of addition to the soybean oil. This same evidence is also present at the peaks of 1425 cm^{-1} and 1100 cm^{-1} [15]. 1425 cm^{-1}, similarly to 1700 cm^{-1}, also corresponds to carboxylic acid, hence the reduction at 1425 cm^{-1}, the same reduction in carboxylic acids due to formation of esters by addition to alkenes on the soybean oil alkyl chain. 1100 cm^{-1} supports this claim by presenting an increase in alkoxy groups after NTP treatment. By formation of more carbon – oxygen bonds through the esterification process, this peak also increased. Cross polymerization of the resin specifically could be observed at the peak at 1460 cm^{-1}. The increase correlated with an increase in alkanes, which would occur due to reaction of the acrylic acid's terminal alkenes with each other. For each consumed alkene, two alkanes would be created, making it possible for observation of this peak to occur.
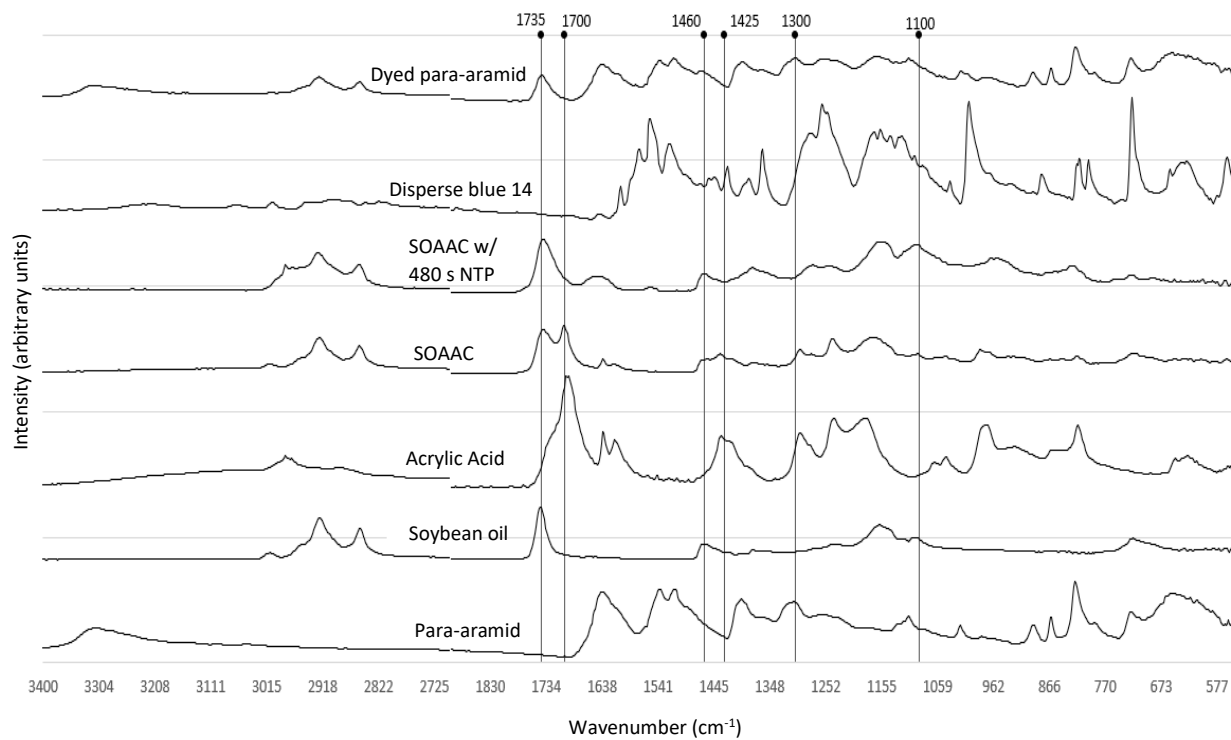
Figure 31. FTIR of para-aramid fabric, soybean oil, acrylic acid, SOAAC mixture before and after NTP treatment, Disperse Blue 14, and dyed para-aramid

Conclusion

Pretreatment with SOAAC increased the color strength of para-aramids in both the aqueous and SCCO2 disperse dye systems. The SCCO2 system presented a relatively more even dyeing compared to the aqueous system. The treatment process of either system did not result in a significant reduction of para-aramid strength based on tensile testing. Both the aqueous and SCCO2 systems presented possible covalent bonding between the para-aramids, SOAAC, and Disperse Blue 14 based on the remaining dye after solvent extraction.

CHAPTER III
SYNTHESIS AND EVALUATION OF ANTIMICROBIAL BIOBASED WAXES

The following chapter contains the work "Synthesis and Evaluation of Antimicrobial Biobased Waxes as Coating Materials" published in *ACS Appl. Bio Mater.* **2023***, 6, 2248–2256*. All experiments were completed by me with technical assistance from other co-authors. Co-authors include Dr. Francisco Leyva Gutierrez, Dr. Bonnie Ownley, Dr. Jeremiah Johnson, and Mary Wakim. Dr. Xiaofei Ye and Dr. Tong Wang advised this work.

Abstract

The objective of this study was to synthesize and evaluate the efficacy of antimicrobial waxes to be used as both physical and biological protection to perishable fruits and vegetables. The existing wax materials used in postharvest coating applications do not provide this desirable functionality. One class of antimicrobial waxes was obtained by covalently linking quaternary ammonium compounds (QACs) featuring alkyl, benzyl, and stearyl ester hydrophobic side groups to the terminal position of a bromo stearyl ester. A second class was obtained by linking these QACs to the pendant hydroxyl group of an aliphatic diamide made of 12-hydroxystearic acid, stearic acid, and ethylene diamine. In total, six distinct structures having three different QAC groups were synthesized. Compounds containing QACs with C_8 alkyl groups exhibited potent inhibition towards the growth of both bacteria and fungi. Notably, the complete inhibition of *Penicillium italicum* and *Geotrichum candidum*, two fungi detrimental to the postharvest quality of fruits, as well as the complete destruction of viable cells for gram-positive and gram-negative bacteria was observed when these organisms were incubated in contact with QAC waxes or dispersed in an aqueous system at a concentration of 1.0 mM; compared to benzalkonium chloride with an alkyl chain length of 10 that can completely inhibit *S. aureus* at a concentration of 1.44 mM. The properties of the attached hydrophobic groups appeared to exert a strong influence on

antimicrobial activity presumably due to differences in molecular orientation, size, and differences among cellular structures.

Abbreviations

Quaternary ammonium compounds (QAC), pyridinium chlorochromate (PCC), dichloromethane (DCM), dimethylformamide (DMF), lithium aluminum hydride (LiAlH$_4$), tetrahydrofuran (THF), sodium hydroxide (NaOH), sodium iodide (NaI), sodium bromide (NaBr), nuclear magnetic resonance (NMR), differential scanning calorimetry (DSC), valley to peak ratio (VTP), optical density (OD), Luria-Bertani (LB), potato dextrose agar (PDA), potassium tert-butoxide (KOtBu), dimethyl amino pyridine (DMAP), pyridinium dichromate (PDC), terminal alkyl wax (TAW), terminal benzyl wax (TBW), terminal ester wax (TEW), pendant alkyl wax (PAW), pendant benzyl wax (PBW), pendant ester wax (PEW), fully hydrogenated soybean oil (FHSO)

Introduction

Commercial waxes consisting of natural or synthetic lipid mixtures are used in myriad industrial products such as cosmetics as well as, food, drug, and paperboard coatings.[24],[25] Their widespread utilization is due in part to the hydrophobic nature of the aliphatic chain which functions as a barrier to moisture and gas permeation, in addition to physical stresses from the environment. For these reasons, the postharvest coating of perishable fruits and vegetables represents a significant market for natural and synthetic waxes. Although virtually all fruits and vegetables possess a functional native wax layer, handling, storage, and transport require that fresh fruits and vegetables be coated postharvest to retard transpiration and microbial attack.[12] Most commercial waxes, however, are neither biocidal nor biostatic.[26] Waxes with antimicrobial activity have received little attention in the literature despite the clear and present need for such functionality in the industry.

Quaternary ammonium compounds (QACs) are a ubiquitous class of broad-range antimicrobials.[13] QACs interact directly with the negatively charged microbial cell membrane by means of the positive charge present on the quaternized nitrogen atom.[27] These ionic interactions disrupt the cell wall or membrane and result in the leakage of cytoplasmic material leading to cell death.[28] Addition of hydrophobic groups to QACs can enhance their antimicrobial activity. Alkyl and benzyl groups, which can vary in chain length and structure, have been reported to act by penetrating the cell membrane allowing facile access to negatively charged phospholipids.[29] This effect appears to have some restrictions, however. For example, Lv et al.[7] found that increasing the alkyl chain length beyond seven carbon atoms (C_7) to eight or nine (C_8-C_9) resulted in a reduction in the zone of inhibition from 13.34 to 9.14 mm for *Candida albicans* and 9.16 to 8.28 mm for *Aspergillus fumigates*, both species representing pathogenic fungi. The authors attributed this behavior to the "burying" of the charged groups by the longer alkyl chains due to their increasing conformational freedom (i.e., bending-in of the chain).[30] For QAC-containing synthetic polymers, it has likewise been reported that the length and structure of the alkyl chain linked to the quaternized nitrogen atom plays an important role in the antimicrobial activity of the material, as does the molecular weight and hydrophobicity of the polymer chain.[31] In contrast to the flexibility of alkyl chains, benzyl groups are rigid and planar. The benzyl group may provide a different method of access to the cellular membrane, although given the differences between microbial cellular membranes, its mechanistic effect remains elusive. For example, substitution of a substituent benzyl group with a methyl group for a series a QACs has been reported to increase the toxicity against the gram-negative marine bacterium, *Vibrio phosphoreum,* and even planktonic organisms .[32] Additionally, and perhaps of more practical importance, the benzyl group has been reported to increase the adsorption of QACs to wastewater sludge, therefore

84

limiting their release into the environment, while still rendering the molecule biodegradable in aqueous media.[33, 34,] Addition of C_{16}-C_{18} ester or ester-amide hydrophobic groups to QACs can reportedly ensure biodegradability while also exerting potent antimicrobial activity. These groups also serve to increase the molecular weight and hydrophobicity of QACs, two important features associated with antimicrobial activity in synthetic polymers. Inclusion of multiple quaternized nitrogen atoms into a single compound has also been investigated as a method to increase the interactions between QACs and bacterial cell membranes. This approach intended to increase the net positive charge of QACs but resulted in high water solubility,[35] a feature which may or may not be desirable for certain applications.

We therefore hypothesized that functionalizing wax materials with the aforementioned structural features might result in a novel class of antimicrobial postharvest coating waxes which may improve food quality and reduce the waste associated with microbial spoilage. The main objective of this work was to synthesize wax materials (the term "wax" will henceforth be used to refer to long-chain aliphatic compounds such as fatty acyl esters and amides) functionalized with QAC groups and evaluate their antimicrobial activity against bacteria and fungi that represent a nuisance in the agricultural industry. We further sought to limit ourselves to some biobased building blocks such as stearic acid and 12-hydroxystearic acid for the synthesis of these wax materials to highlight the potential for commercialization and ensure biodegradability. QACs with alkyl, benzyl, and stearyl (octadecanoic) ester hydrophobic side groups were investigated. Alkyl and benzyl groups were chosen as these have exhibited antimicrobial activity in polymers and other small molecules. The stearyl ester group was chosen due to its low cost and biobased origin. Further, as a high melting point (>60°C) is a desirable property for wax, the position of the QAC was also investigated by designing wax backbones with terminal and pendant

attachments. These two structural motifs would be expected to have a different ability to pack closely together in the solid state and therefore affect the melting point, as well as other physical properties of the materials. This work will serve to further the utilization of wax materials derived in part from biobased building blocks and introduce new material technologies to the agricultural sector.

Materials and Methods

General. All compounds, solvents, and reagents were purchased from commercial sources (Acros Organics, TCI, Alfa Aesar, MilliporeSigma) and used as received unless otherwise noted. ^{1}H and ^{13}C NMR spectra were acquired using a Varian 500 MHz spectrometer using CDCl$_3$ with 1% tetramethylsilane (TMS) as solvent. Chemical shifts are reported relative to TMS signal. Thin layer chromatography (TLC) was performed on silica gel 60 coated plates and visualized with ceric ammonium molybdate (CAM). Flash chromatography was performed on silica gel 60.

Synthesis of QAC waxes

Scheme 1 depicts the general synthetic route used to access QAC waxes. Terminal and pendant chain wax backbones were prepared. Three distinct tertiary amines, *N,N*-dimethyloctan-1-amine, *N*-benzyl-*N*-methyloctan-1-amine, and 2,2'-(methyl azanediyl)bis(ethane-2,1-diyl) distearate, were likewise prepared for subsequent quaternization.
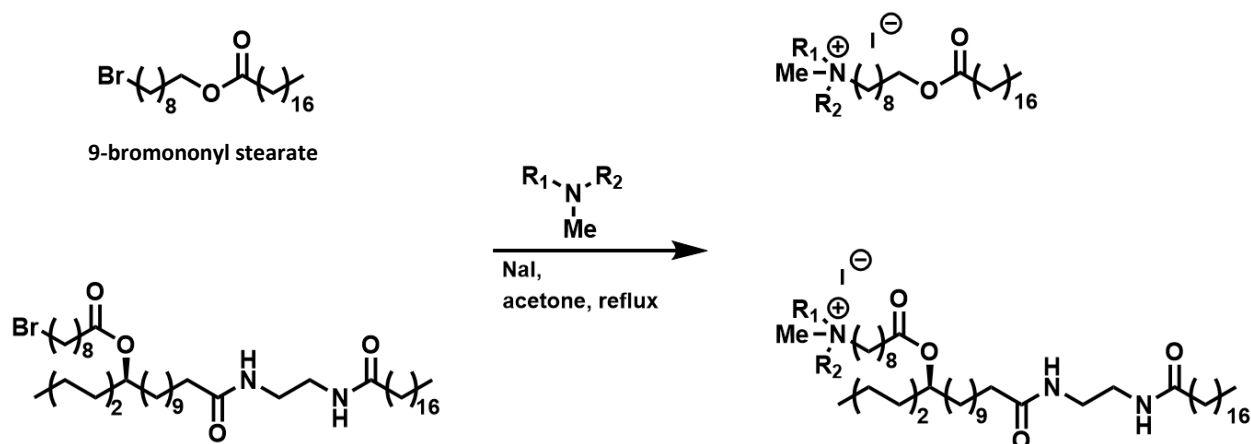
Scheme 1. General synthetic scheme used to access QACs from terminal and pendant wax backbones. For identity of hydrophobic groups attached to quaternized nitrogen atom, refer to Table 17.

For terminal wax backbones, 9-bromononyl stearate was first prepared by the esterification of stearic acid with 9-bromononan-1-ol. The terminal bromo functional group was then displaced by the previously prepared tertiary amines in the presence of NaI to obtain a QAC-functionalized ester. Iodide was utilized as counterion due to increased reactivity which was necessary for displacement of some tertiary amines, and has been shown to present comparable antimicrobial behavior to other halide counterions.[36] The tertiary amines featured alkyl, benzyl, and stearyl ester hydrophobic side groups. The final structures were denoted as terminal alkyl wax (TAW), terminal benzyl wax (TBW) and terminal ester wax (TEW).

For pendant chain wax backbones, 9-bromononanoic acid was first converted into the acid chloride and then esterified to a previously synthesized diamide composed of 12-hydroxystearic acid, stearic acid, and ethylenediamine. The terminal bromo functional group was then displaced by the same previously prepared tertiary amines in the presence of NaI to obtain a QAC-functionalized pendant ester. The final structures were denoted as pendant alkyl wax (PAW), pendant benzyl wax (PBW) and pendant ester wax (PEW).

87

Preparation of terminal and pendant wax backbones

Terminal wax backbone (9-bromononylstearate). A 100 mL round-bottom flask was charged with, 9-bromononan-1-ol (4.70 g, 20.7 mmol), stearic acid (5.94 g, 20.9 mmol), and Amberlyst-15 acid catalyst (0.36 g). The mixture was heated to 80°C into a melt and stirred under vacuum for 6 h. The reaction was monitored by TLC. Upon completion, the mixture was dissolved in ethanol, vacuum filtered to remove the catalyst, and recrystallized from ethanol at 4°C. The ω-bromo ester was collected by vacuum filtration and dried under vacuum to obtain a white powder (9.65 g, 95% yield). ^{1}H NMR (500 MHz, CDCl$_3$) δ 4.05 (t, J = 6.7 Hz, 2H), 3.40 (t, J = 6.9 Hz, 2H), 2.28 (m, J = 7.5 Hz, 2H), 1.85 (m, J = 14.7, 6.9 Hz, 2H), 1.61 (p, J = 7.1 Hz, 4H), 1.42 (m, J = 7.4 Hz, 2H), 1.37 – 1.22 (m, 34H), 0.88 (t, J = 7.0 Hz, 3H).

Pendant wax backbone (18-oxo-18-((2-stearamidoethyl)amino)octadecan-7-yl 9-bromononanoate). A 100 mL, 2-necked round-bottom flask with condenser was charged with ethylene diamine (10 mL, 149 mmol) and Amberlyst-15 acid catalyst (1.67 g). The mixture was heated to 70°C with stirring and methyl stearate flakes (5.18g, 16.8 mmol) added gradually over the course of 3 h at an approximate rate of 0.1 mmol/min to prevent formation of diamide. The mixture was stirred at 70°C for an additional 3 h, filtered through a pad of Celite, and recrystallized from hexanes at 4°C[37] to afford the pure monoamide, *N*-(2-aminoethyl)stearamide, as a white powder (5.05 g, 92% yield).

Subsequently, a dry 50 mL round-bottom flask was charged with methyl 12-hydroxyoctadecanoate (1.01 g, 3.2 mmol), *N*-(2-aminoethyl)stearamide (1.04 g, 3.2 mmol), Amberlyst-15 (0.28 g) and toluene (15mL). The mixture was refluxed with stirring for 12 h. The hot mixture was filtered through a pad of silica to remove the catalyst and recrystallized from ethyl

acetate at 4°C to afford the diamide, 12-hydroxy-*N*-(2-stearamidoethyl)octadecanamide, as a white powder (1.85 g, 95% yield)

The resulting diamide, 12-hydroxy-*N*-(2-stearamidoethyl) octadecanamide (0.74 g, 1.2 mmol) in THF (10 mL) was then added a 0°C solution of 9-bromononanoyl chloride in THF (10 mL) prepared from 9-bromononanoic acid (0.30 g, 1.2 mmol) and oxalyl chloride (0.11 mL, 1.2 mmol) in the presence of dry dimethylformamide (DMF; 0.01 mL, 0.1 mmol). The mixture was warmed to 22°C and stirred overnight or until TLC confirmed full conversion. The mixture was quenched with deionized water (30 mL), diluted with chloroform (15 mL), partitioned, and extracted with additional chloroform (10 mL ×4). The pooled organic layers were washed with deionized water (10 mL) and brine (30 mL ×2), dried over $MgSO_4$, and concentrated under vacuum to afford a white powder (0.92 g, 93 % yield).

Preparation of tertiary amines with alkyl, benzyl, and stearyl ester groups

Tertiary amine with alkyl group (N,N-dimethyloctan-1-amine). This compound was commercially available and used as purchased.

Tertiary amine with benzyl group (N-benzyl-N-methyloctan-1-amine). This compound was not commercially available and was synthesized from commercially available *N*-benzylmethylamine based on a reported procedure.[38] A dry, 50 mL round-bottom flask flushed with Ar, was charged with octanoic acid (3.12 g, 21.6 mmol), dry DMF (0.17 mL), dry dichloromethane (10 mL) and cooled to 0°C. Oxalyl chloride (1.85 mL, 21.8 mmol) was added slowly to the mixture. After the evolution of gas bubbles ceased, *N*-benzylmethylamine (2.57 g, 21.4 mmol) was added dropwise via a syringe and the mixture monitored by TLC. After ~27 h, the mixture was quenched with deionized water (30 mL), diluted with chloroform (30 mL), partitioned, and extracted with additional chloroform (10 mL ×4). The pooled organic layers were

washed with deionized water (10 mL) and brine (30 mL ×2), dried over MgSO4, and concentrated under vacuum to afford a yellow oil.[38]

The resulting amide was then reduced to the tertiary amine based on a reported procedure.[39] A flame-dried, three-necked, 250-mL round-bottom flask equipped with a reflux condenser was charged with lithium aluminum hydride solution in THF (13 mL, 31.4 mmol) and diluted with additional dry THF (20 mL). The amide was dried by passing through alumina, dissolved in dry THF (15 mL), and added dropwise to the flask at 0°C. After complete addition, the solution was refluxed for 9 h or until completion as determined by TLC. The mixture was quenched with water and 10% NaOH according to the Fieser workup. The aluminum salts were filtered, the organic extract was dried over MgSO4, filtered, and concentrated under vacuum to afford a yellow oil.[39] (4.35 g, 87% yield). ^{1}H NMR (500 MHz, CDCl3) δ 7.34 – 7.20 (m, 5H), 3.48 (s, 2H), 2.38 – 2.33 (m, 2H), 2.18 (s, 3H), 1.28 (br, 11H), 0.88 (t, J = 6.8 Hz, 3H).

Tertiary amine with stearyl ester groups ((methylazanediyl)bis(ethane-2,1-diyl) distearate). A 100 mL round-bottom flask was charged with stearic acid (2.73 g, 9.6 mmol) and Amberlyst-15 (0.08 g). The mixture was heated to 100°C and commercially available *N*-methyldiethanolamine (0.54g, 4.6 mmol) added dropwise to the melt. The mixture was stirred under vacuum 2 h. The mixture was dissolved in chloroform (15 mL), filtered to remove the acid catalyst. The filtrate was concentrated and dissolved in ethanol. Excess stearic acid was recrystallized from ethanol, filtered, and the mother liquor concentrated to afford the desired product as a white powder (2.76 g, 92% yield). ^{1}H NMR (500 MHz, CDCl3) δ 3.88 – 3.83 (m, 4H), 2.99 – 2.94 (m, 4H), 2.67 (s, 3H), 2.32 (t, *J* = 7.6 Hz, 4H), 1.62 (p, *J* = 7.5 Hz, 4H), 1.37 – 1.19 (br, 59H), 0.88 (t, *J* = 6.9 Hz, 6H).

Quaternization of tertiary amines with terminal or pendant wax backbones

General procedure for quaternization of wax backbones. The wax backbone (1 eq) was dissolved in dry acetone in the presence of anhydrous NaI (1.2 eq) and refluxed for 2-4 h. The clear solution gradually became turbid white due to halide exchange.[40] The tertiary amine (1.2 eq) was added to the refluxing reaction mixture and left to stir overnight or until completion as determined by TLC. The QAC wax products were purified by column chromatography by gradient elution with one column length (125 mL) of hexanes, 90:10 hexane: ethyl acetate, 50:50 acetone: hexane, and lastly acetone. The product was collected from the acetone flush and concentrated under vacuum to afford white to off-yellow powders (45-60% yield).

Characterization of physical properties of synthesized waxes

Thermal analysis. The melting temperatures of synthesized materials were analyzed by differential scanning calorimetry (DSC) (TA instruments) by the following temperature program: equilibrate at 20°C, ramp to 100°C at 10°C/min, hold for 3 min, cool to 20°C at 5°C/min, followed by heating to 100°C at 5°C/min. The relative degree of crystallinity (%) was calculated by dividing the enthalpy of the melting endotherms by 293 J/g, the enthalpy for a hypothetical 100% crystalline polyethylene sample.[41] Melting onset and peak temperatures were recorded.

Textural analysis. Hardness and cohesiveness are two physical properties that determine the range of applications for wax materials. These physical properties were measured using a TA.XT Plus (Stable Micro Systems) texture analyzer instrument equipped with a 2.5-mm cylinder probe. The following parameters were used: pre-test and post-test speed of 2.0 mm/s, probe movement speed of 0.5 mm/s, and compression distance of 4.0 mm. Tests were performed on 9 mm diameter x 9 mm height cylinder samples prepared by pouring molten material into a mold.

Hardness was measured as the greatest compressive force recorded. Cohesiveness was measured by two traits; the rate of deformation, i.e., the slope directly after the maximum peak is reached, and the valley to peak ratio (VTP), i.e., the ratio of the force at the valley after the drop-off to the force at the peak.[42] High hardness, high VTP, and low rate of deformation values are desirable.

Hydrophobicity analysis. To observe the effect of the addition of QACs on the hydrophobicity of wax materials, the surface contact angle was measured using a Kruss FM40 Easydrop (Kruss Scientific Instruments, Inc.) instrument. A drop of deionized water (~10 µL) was dropped onto the flat surface of samples after casting from the melt (~1 g) onto a pre-heated glass slide. The resulting samples surfaces were generally flat. The droplet shape was captured 10 s after drop and surface contact angle calculated by the instrument's data acquisition software. This measurement was repeated for three separate locations on the surface of the samples to account for any possible surface morphological differences after casting from the melt.

Evaluation of antimicrobial activity

Microorganisms that commonly contaminate fruit and vegetables during and postharvest (e.g., handling, processing, transport, and storage) were used to evaluate the antimicrobial activity of our QAC waxes. Three foodborne bacterial pathogens *Escherichia coli* O157:H7, *Listeria monocytogenes* LM10403S, and *Staphylococcus aureus* (ATCC 25923), the latter being commonly found in the nasopharynx of humans [43] and a source of contamination during handling, were examined. Two fungi that commonly cause spoilage of harvested fruit, *Penicillium italicum*[44] and *Geotrichum candidum,* were likewise examined.

Antibacterial activity by incubation with bacterial species of interest. Prior to conducting antibacterial activity assays, growth curves (Appendix Figure 33) for *E. coli* O157:H7,

L. monocytogenes, and *S. aureus* were generated using bacterial cultures (150 μL) in Luria-Bertani (LB) broth at a starting absorbance (A_{600}) of 0.01 for *E. coli* and *S. aureus,* or 0.05 for *L. monocytogenes*. Cultures were grown aerobically in 96-well plates at 37°C with agitation and A_{600} recorded every 10 min for up to 10 h to identify pre, mid, and late log phase and stationary phase of each bacteria.

The antibacterial activity was initially measured by recording the A_{600} of cultures at various growth stages in the presence of each wax. To achieve this, QAC wax solutions in ethanol (100 μL, 0.1 g/mL) were loaded into individual wells of a 96-well plate and the solvent removed by heating in an oven at 50°C for 1 h. This resulted in the deposition of a homogenous wax film in each well. As a negative control, a paraffin wax solution in hexanes (100 μL, 0.1 g/mL) was used. For growth curve determination, bacterial cultures (150 μL) in LB broth at either a starting A_{600} of 0.01 for *E. coli* and *S. aureus*, or 0.05 for *L. monocytogenes* were added to the coated wells. The inoculated 96-well plates were then sealed with Parafilm and incubated at 37°C until each previously identified time point was reached (1, 2, 3, and 5 h for *E. coli* O157:H7 and *L. monocytogenes*, and 2.5, 5, 7, and 9 h for *S. aureus*). At these time points, cultures were removed and transferred to a new well plate to record the A_{600} values as the opaque waxes were not optically clear and would lead to unreliable absorbance. The onset of stationary phase as determined by the control bacteria growth curves was identified and only data at these times were presented and compared for cell growth. These specific times or growth stages were also used for subsequent viability testing as it yielded the greatest difference between the negative control and QAC wax.

Viable bacterial cells were quantitated at the onset of the stationary phase of growth by determining the number of colony forming units (CFU/mL) in the presence of each QAC wax. This was performed to assess whether the samples were bacteriostatic and inhibited growth or

whether they were bactericidal and directly reduced cell viability. To achieve this, bacterial cultures (100 μL) from each wax incubation was transferred to sterile 1X phosphate buffered saline (PBS, 900 μL), serially diluted, and spread on LB plates. Plates were incubated at 37°C for 24 h and colonies were counted. This experiment was conducted twice in technical triplicate.

Antifungal activity using wax-infused media and surface inoculation.
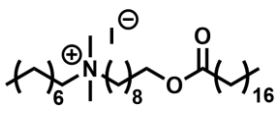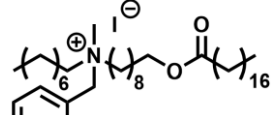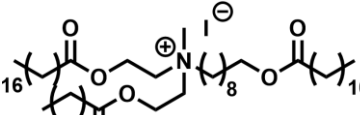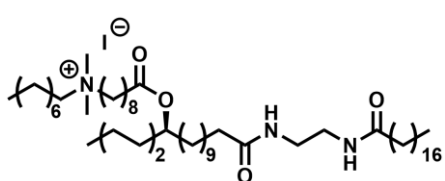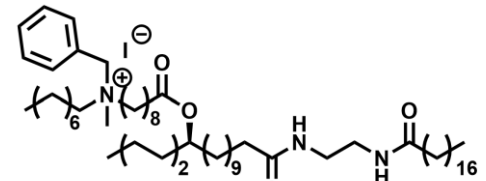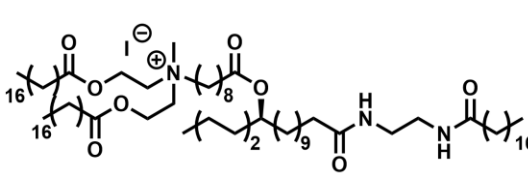
The antifungal activity was measured by growth diameter of fungi cultured in QAC wax-infused media. The commercial antifungal agent Imazalil and a commercial QAC, FS Amine Z, (ZEP, Atlanta, GA,) were used as positive controls. The positive controls and QAC waxes were dissolved in ethanol (1 mL) and added to hot potato dextrose agar (PDA, 15 mL) immediately after autoclaving to obtain a uniform dispersion with a final concentration of 1.0 mM before dispensing into 85-mm petri dishes. It is presumed the ethanol solvent was removed from the agar by the high temperature (~110°C) of the media upon addition. Once the media solidified, spore suspensions of *P. italicum* and *G. candidum* in deionized water (100 μL) were pipetted onto the center of the petri dish and incubated at 25°C. Growth diameter measurements and photographs were recorded every 24 h for 3 d. Duplicate analyses were performed and differences among samples determined by Tukey HSD comparison of means.

Results and Discussion

Synthesis of QAC waxes

The compounds listed in Table 17 were easily accessed via condensation and Menshutkin reaction conditions. An example of confirmed structural confirmation is found in Appendix Figure 34. Additional synthetic routes were explored with limited success, however; in this section we report some observations to assist in future synthetic methodologies.

Table 17. Quaternary ammonium compound waxes synthesized and their abbreviations.

Position	Tertiary amine substituents		
	Alkyl	**Benzyl**	**Ester**
Terminal	Terminal alkyl wax (TAW)	Terminal benzyl wax (TBW)	Terminal ester wax (TEW)
Pendant	Pendant alkyl wax (PAW)	Pendant benzyl wax (PBW)	Pendant ester wax (PEW)

The pendant wax backbones were initially envisioned as featuring a 9-bromononyl aliphatic ether rather than a 9-bromononanoate ester functional group in an effort to increase the hydrophobicity of the molecule. To this end, the pendant hydroxyl group of the 12-hydroxystearyl moiety was first converted into the corresponding tosylate in the presence of DMAP and tosyl chloride, and subsequently displaced by the 9-bromononanolate nucleophile generated from 9-bromononan-1-ol and a strong base (e.g., potassium *tert*-butoxide, NaH). This procedure was sluggish at room temperature, and upon refluxing in toluene resulted in a mixture of products consisting of the pendant aliphatic ether (minor product), 9-bromononyl 12-hydroxyoctadecanoate (major product), and various polymers (trace). Additionally, polar aprotic solvents (e.g., MeCN, THF, DCM) were screened with little to no success. Mitsunobo conditions were entirely avoided due to the use of the relatively higher toxicity phosphines and azodicarboxylates. For these reasons, we settled for the more direct condensation of 9-bromononanyl chloride (generated from 9-bromononaoic acid in the presence of DMF and oxalyl chloride) with the hydroxyl group of the 12-hydroxystearyl moiety.

As previously stated, *N*-benzyl-*N*-methyloctan-1-amine was not commercially available and therefore needed to be synthesized. This was initially completed by alkylating *N*-benzylmethylamine with 8-bromooctane under Menshutkin reaction conditions. However, this resulted in over alkylation and afforded a mixture of secondary, tertiary, and quaternary amines, which were difficult to purify during scale-up. This was addressed by first generating a tertiary amide using octanoic acid and then reducing to the corresponding tertiary amine with LiAlH$_4$.

Physical properties of QAC waxes

Thermal properties. We hypothesized that wax backbones which feature long aliphatic chains would readily crystallize and result in high (>60°C) melting temperatures. Although the

melting temperatures (Appendix Figures 35-40) and calculated degree of crystallinity did not follow any clear trends, there is some support for this hypothesis. For example, the TAW structure may be regarded as a 37 carbon aliphatic chain if we consider the fact that the van der Waal radii of internal nitrogen (-NH-; ~1.70 Å) and oxygen (-O-; 1.29 Å) atoms are smaller than that of the methylene group (-CH$_2$-; ~2.0-2.2 Å), and that carbonyl oxygen atoms do not significantly affect the packing of neighboring aliphatic chains.[45] TAW exhibited an intermediate melting point (~44.5°C) and the highest degree of crystallinity (44.5%) of all QAC waxes. For TAW, the van der Waals radii of methyl groups (-CH$_3$; 2.0 Å) protruding from the quaternized nitrogen atom as well as the iodide counter anion (I$^-$; ~2.0-2.2 Å) presumably exerted a strong influence on the ability of the molecule to pack closely together. The benzyl and stearyl ester hydrophobic groups may have exacerbated this effect, as evidenced by the decrease in melting temperature and degree of crystallinity for TBW (39.4°C, 14.8%) and decrease in degree of crystallinity for TEW (3.4%), the latter best characterized as an amorphous solid. The higher melting temperature for TEW (53.5°C), a feature consistently observed on multiple heating cycles, may be explained by the increase in bulk intermolecular forces (i.e., cohesive energy density) introduced by the two stearyl esters.

The pendant QAC waxes, PAW and PBW, exhibited a low degree of crystallinity (1.4 and 5.43%, respectively) yet high melting temperatures (55.9°C and 75.8°C, respectively). In contrast, PEW was entirely amorphous at room temperature. While the increased melting points seem to indicate an ideal coating material, the low crystallinity directly counteracts the goal of a wax coating. The more crystalline the wax, the greater the reduction in water vapor permeability, therefore these amorphous materials would do little to prevent the loss of moisture from coated fruits and vegetables.[41]

Textural properties. Hardness is a factor of molecular packing while cohesiveness is intrinsic to intermolecular interactions and molecular entanglement. Overall, QAC waxes attached at the terminal position provided greater hardness, compared to the pendant position counterparts. The increased amorphous structure due to the pendant addition created much softer waxes. TEW had shown the greatest hardness of the synthesized materials, similar to that of paraffin, but did not show high levels of cohesiveness (the lower the slope values and the higher the VTP ratio values, the better the cohesiveness). However, both the TAW and PAW presented high levels of cohesiveness, as observed from the high VTP. Both TBW and PBW had only rising peaks with no descent to form the valley until the measurement was complete (3.999 – 4.0 mm), a feature likely due to the softness of the materials. The low hardness and low surface contact angle observed in PEW may also relate to the antifungal effectiveness observed. From these textural measurements, we identified that TAW and TEW may be useful coating materials due to the high cohesiveness and hardness values observed, respectively.

Hydrophobicity. In general, a surface is deemed as hydrophobic when the surface contact angle is >90°, and images are presented in Appendix Figure 41. Addition of the charged quaternized nitrogen atom group to wax backbones was expected to lower the hydrophobicity (i.e., surface contact angle) due to the potential increase in polar interactions. This was shown to be true for all QAC waxes relative to paraffin and other postharvest coating materials such as carnauba wax (71.2°) or beeswax (58.5°). Of the terminal waxes, the least hydrophobic to most followed the trend of TAW, TEW, and then finally to TBW. TAW was the least hydrophobic of the terminal waxes likely due to a smaller number of hydrophobic groups to counter for the charge generated by the charged quaternary nitrogen atom. With the multiple branching chains of the TEW, the increased amorphous region may make the material less crystalline, and behave more dispersible

98

compared to TBW. The surface contact angle for the pendant QAC waxes was lower than that of terminal QAC waxes. This is due to the fact that the branched chain structure with pendant groups precludes an ordered molecular packing relative to that of the straight chain QAC waxes with addition at the terminal position. This same general trend was observed of surface contact angle with increasing complexity of ammonium substituent in the pendant waxes. With increased complexity, the already branched wax backbone had more bulk protruding, lowering the crystallinity, showing the trend of PAW, PBW, and lastly PEW with decreasing contact angle. While low hydrophobicity is not a desirable quality of wax coatings, it is an expected outcome of addition of positively charged groups to wax structures. The charged QACs are likely to interact with water in a polar environment.

Overall, none of the QAC waxes exhibited similar bulk physical properties as paraffin wax or other commercial waxes used in the postharvest coating of fresh fruits and vegetables (e.g., carnauba wax, beeswax) and therefore are unlikely to directly replace these bulk materials (Table 18). The relationship between structure and physical properties of carnauba wax and beeswax has been explored elsewhere.[17, 21] However, for our target application of postharvest coatings, waxes are not used as bulk materials but rather formulated into aqueous micro- and nano emulsions which are spray coated on the surface of fruits and vegetables. This practice is also common in the coating of paperboard products. Typically, these aqueous wax emulsions are supplemented with antimicrobial agents such as Imazalil and thiabendazole at concentrations of ~2000 ppm,[46] equivalent to ~6.7 and ~9.9 mM, respectively. As demonstrated in the proceeding sections, our QAC waxes exhibit antimicrobial activity at lower concentrations. We formulated our QAC waxes into carnauba wax and beeswax blends at up to 50 wt% and observed only a minor 1-5°C decrease in the melting point of these materials and no significant phase separation as judged by the enthalpy

Table 18. Physical properties of common waxes used in postharvest coatings and synthesized QAC waxes in this work.

Entry	Melting Onset (°C)	Melting Point (°C)	Degree of Crystallinity (%)	Hardness (g)	Rate of Deformation (slope)	VTP (ratio)	Surface Contact Angle (°)
Paraffin	52.4	67.6	53.8	7091.9 ± 42.6^b	1440.4 ± 283.3^b	0.48 ± 0.03^{bcd}	117.1 ± 1.6^b
Carnauba wax	71.2	83.4	62.3	21100.6 ± 3030.0^a	19928.5 ± 4237.9^a	0.14 ± 0.17^d	$154 \pm 5.0^{*a}$
Beeswax	46.0	64.0	44.7	5788.2 ± 87.2^{bc}	3316.2 ± 413.9^b	0.96 ± 0.00^a	$129 \pm 3.0^{*b}$
TAW	42.4	44.5	21.2	1262.3 ± 99.8^d	899.5 ± 66.7^b	0.78 ± 0.02^{abc}	39.1 ± 6.6^d
TBW	34.2	39.4	14.8	2663.2 ± 60.2^b	no break	-	97.0 ± 0.6^c
TEW	50.1	53.5	3.4	6957.7 ± 474.4^{bc}	6152.8 ± 118.0^b	0.39 ± 0.17^{cd}	79.6 ± 0.7^c
PAW	53.0	55.9	1.4	846.6 ± 30.4^d	650.8 ± 41.1^b	0.76 ± 0.06^{ab}	24.0 ± 1.7^{de}
PBW	65.6	75.8	5.4	278.4 ± 16.5^d	no break	-	13.4 ± 4.2^e
PEW	30.5	36.5	0.3	-	-	-	12.7 ± 3.6^e

Significance determined by duplicate analysis with Tukey HSD comparison of means at P = 0.05.

All wax abbreviation can be found in Table 1.

"-" indicates no value recorded due to softness of material.

"*" indicates value obtained from [47].

of melting (Appendix Figures 42-43). Therefore, our QAC waxes may be formulated into wax blends or existing emulsions to curtail the pervasive use of Imazalil, for example, as there exist environmental and biological concerns with its use due to bioaccumulation.[48]

Antimicrobial activity of QAC waxes

Antibacterial activity. Absorbance (A_{600}) values were recorded to quantitate differences in growth between uninhibited bacteria incubated in the presence of a negative control (paraffin wax) and QAC waxes coated at the bottom of wells in a 96-well plate (Table 19). A_{600}, or the cell density measured by spectrophotometer, is used to characterize the degree of growth that can be observed due to the increase, or lack of increase, in cell density over time. Since the wax coatings are not optically clear, the bacterial cultures were transferred to new 96-well plates prior to measuring A_{600}. Nevertheless, several of the QAC cultures yielded higher A_{600} values than control cultures (Table 19). These elevated A_{600} values were due to small quantities of QAC waxes being transferred, which resulted in unreliable measurements. While addressed by transferring to another well plate, the small quantities that were not able to be removed continued to falsely describe the actual density.

All QAC waxes reduced the number of viable cells for all bacteria relative to the negative control (uninhibited growth), with TAW and PAW resulting in complete elimination of viable cells for both gram-positive and gram-negative bacteria, even when compared against the initial bacterial inocula (Table 20). Their activity can therefore be characterized as bacteriocidal. Both TAW and PAW feature the C_8 alkyl chain extending from the quaternized nitrogen atom. In agreement with previous reports, we hypothesize the C_8 alkyl chain may be long enough to penetrate and disrupt cell membranes yet short enough to position the charged quaternary nitrogen atom in such a way to exhibit significant bactericidal activity. The surface contact angle of these

Table 19. Absorbance (A600) values of bacteria after incubation to the onset of stationary phase.

Entry	*S. aureus* (at 9 h)	*L. monocytogenes* (at 5 h)	*E. coli* (at 5 h)
Initial concentration	0.086 ± 0.00	0.087 ± 0.001	0.088 ± 0.001
Paraffin	0.290 ± 0.034	0.201 ± 0.001	0.306 ± 0.028
TAW	1.204 ±1.561	1.196 ± 1.541	1.044 ± 1.344
TBW	0.187 ± 0.134	0.139 ± 0.029	0.181 ± 0.125
TEW	0.244 ± 0.041	0.106 ± 0.003	0.180 ± 0.040
PAW	0.112 ± 0.007	0.207 ± 0.067	0.102 ± 0.014
PBW	0.678 ± 0.438	0.569 ± 0.358	0.558 ± 0.106
PEW	0.241 ± 0.015	0.128 ± 0.032	0.207 ± 0.046

Significance determined by duplicate analysis with Tukey HSD comparison of means at P = 0.05 and no significant difference.
All wax abbreviations can be found in Table 17.

Table 20. Log10 CFU/mL of bacteria after incubation to the onset of stationary phase.

Entry	*S. Aureus* (at 9 h)	*L. monocytogenes* (at 5 h)	*E. coli* (at 5 h)
Initial concentration	6.81 ± 0.05[a]	8.13 ± 0.10[a]	6.87 ± 0.11[b]
Paraffin	9.33 ± 0.78[a]	8.98 ± 0.22[a]	9.06 ± 0.19[a]
TAW	0.00	0.00	0.00
TBW	6.50 ± 0.00[ab]	8.63 ± 0.62[a]	7.90 ± 1.41[ab]
TEW	1.61 ± 2.27[c]	5.66 ± 1.53[ab]	7.93 ± 0.11[ab]
PAW	0.00	0.00	0.00
PBW	0.00	3.46 ± 4.89[bc]	0.00
PEW	2.78 ± 3.93[bc]	7.12 ± 0.51[ab]	8.78 ± 0.05[a]

Significance determined by duplicate analysis with Tukey HSD comparison of means at P = 0.05.
Different superscripts indicate significant difference among treatments in the same column.
All wax abbreviations can be found in Table 17.

two materials ($<90°$) suggests they are not hydrophobic and that the C_8 alkyl chain is not buried by the wax backbones in the bulk material. Accordingly, the position of attachment, either terminal or pendant, exhibited the same level of activity for this particular pair QAC waxes.

When comparing TBW and PBW, it appeared that attachment to the pendant position resulted in a stronger bactericidal effect compared to attachment at the terminal end. In this case, the molecular packing and orientation of functional groups on the wax surface may have contributed to the antimicrobial activity QAC waxes. By being at the pendant position to the wax backbone, it may have allowed greater access of the QAC to bacteria in the environment. For the TEW and PEW pair, the stearyl esters may have introduced too much disorder in the bulk material, precluding the direct interaction of the quaternized nitrogen atom with the cell membrane. The low surface contact angles and amorphous nature of both TEW and PEW support this hypothesis. Other studies have similarly reported that the antimicrobial activity of QACs is attenuated by the presence of very-long alkyl hydrophobic groups or spacers, as well as large hydrophobic substituents on the quaternized nitrogen atom.[13] [49]

The orientation of hydrophobic groups in the bulk materials might play an important role in antimicrobial activity. For TAW, the C_8 alkyl group attached to the quaternized nitrogen atom may be considered as a linear extension of the wax backbone, as previously mentioned. The length and relatively "straight chain" nature of this compound may have allowed for only partial access to the cell membrane. For PAW, we hypothesize the pendant position on the wax backbone allows a relatively more facile access to the cell membrane. This is likewise observed for and supported by the TBW and PBW pair, in which the pendant position exhibited higher activity. Once again, because of the "straight chain" nature of these compounds, crystallization may have rendered the active groups inaccessible and unable to interact with the cell membrane. When the quaternized

nitrogen atom group is pendant to the diamide backbone, the active groups may have had more access to cell membrane. The same behavior has been observed in other large QACs known as "esterquats", compounds that are commonly used as emulsifiers in cosmetics and detergents.[50] For example, an *N*-hexyl,*N*-methyl *N,N*-diundecanoyl methyl ester QAC, which may be considered as possessing a pendant C_8 alkyl chain, was reported to exhibit a potent antimicrobial effect. This positioning may have resulted in facile access to the cell membrane by the "pendant" alkyl chain.[13] As for lengths of alkyl substituents investigated, small QACs that contain longer alkyl chains have been shown to provide greater antimicrobial effect, whereas for longer QACs, smaller alkyl substituents have been shown to present greater antimicrobial effect.[30] Due to the large wax structures utilized for this study, C_8 alkyl chains were selected. Further investigation of other chain lengths attached to the synthesized materials would need to be completed to further verify this theory.

Antifungal activity. An initial investigation on the antifungal effect of the QAC waxes was completed with each wax held at a constant concentration of 8.7 mM in PDA. It was found that all fungal growth was inhibited except for *P. italicum* when in the presence of the TBW. To further observe and understand the differences among waxes, the concentration of each wax dispersed in agar was reduced to 1.0 mM.

As shown in Figure 32, and Table 21 and 22, TAW and PEW completely inhibited fungal growth at 1.0 mM concentration. The least inhibition was observed for PAW and *P. italicum,* and for TEW and *G. candidum* system. TAW was the lowest molecular weight structure relative to all other QAC waxes and exhibited the greatest antifungal activity against both species. As observed for TBW, the next lowest molecular weight structure, the replacement of a methyl group by a benzyl group attenuated the antifungal activity against *G. candidum*, although the activity was
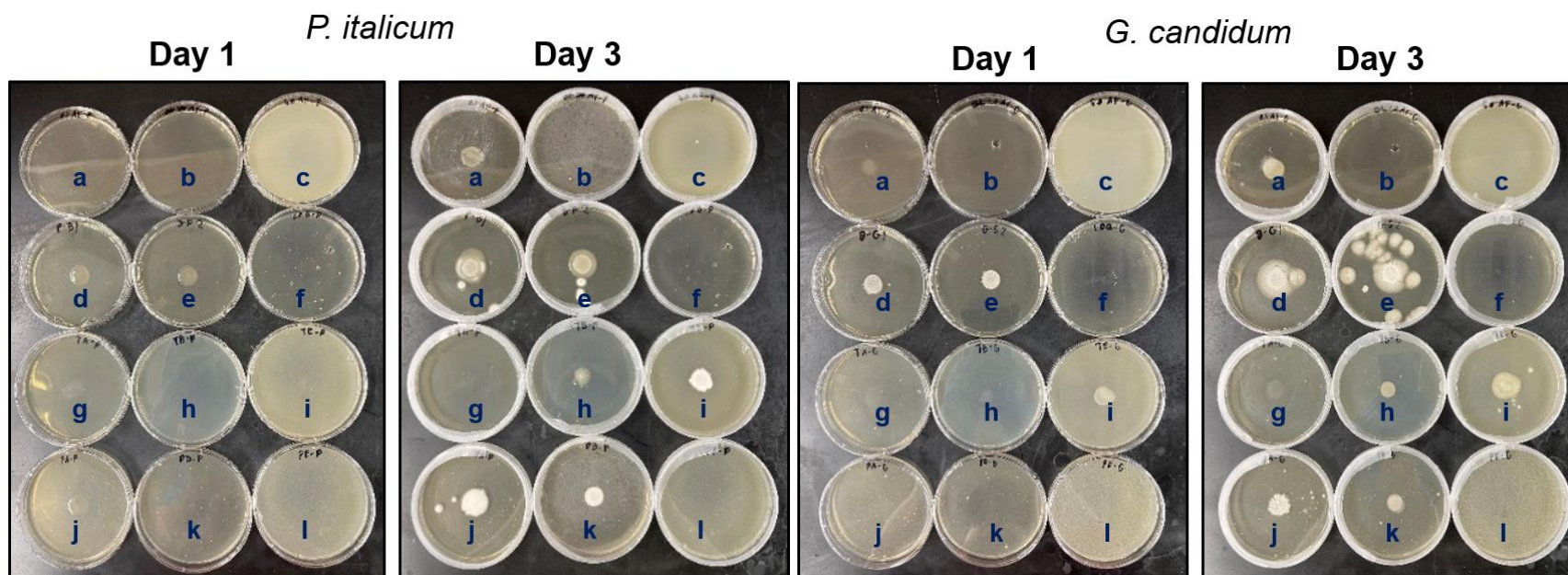
Figure 32. Growth of *P. italicum* (top) and *G. candidum* (bottom) on PDA with 1.0 mM QAC wax inclusions at day 1 and day 3. Legend: a = 0.1 mM Imazalil (positive control); b = 1.0 mM Imazalil (positive control); c = 5.0 mM Imazalil (positive control); d,e = blank replicate 1 and 2; f = FS Amine Z (positive control); g = 1.0 mM terminal alkyl wax (TAW); h = 1.0 mM terminal benzyl wax (TAW); i = 1.0 mM terminal ester wax (TEW); j = 1.0 mM pendant alkyl wax (PAW); k = 1.0 mM pendant benzyl wax (PBW); l = 1.0 mM pendant ester wax (PEW).

Table 21. Diameter (mm) of growth of *P. italicum* over three days on 1.0 mM wax-infused potato dextrose agar (PDA) media.

Entry	P. italicum		
	Day 1	Day 2	Day 3
Blank 1	15.60 ± 0.42^a	19.55 ± 1.66^a	25.05 ± 1.73^a
Blank 2	16.40 ± 0.49^a	18.00 ± 0.77^{ab}	22.20 ± 1.34^{ab}
0.1 mM Imazalil	0.00^c	15.15 ± 1.31^{abc}	17.45 ± 1.45^{cd}
1.0 mM Imazalil	0.00^c	0.00^d	0.00^e
FS Amine Z	0.00^c	0.00^d	0.00^e
TAW	0.00^c	0.00^d	0.00^e
TBW	0.00^c	0.00^d	12.40 ± 5.23^d
TEW	0.00^c	13.10 ± 0.78^{bc}	14.95 ± 1.38^{cd}
PAW	12.65 ± 0.25^b	16.50 ± 1.27^{abc}	19.10 ± 1.56^{bc}
PBW	0.00^c	11.10 ± 1.06^c	14.15 ± 1.38^d
PEW	0.00^c	0.00^d	0.00^e

Significance determined by duplicate analysis with Tukey HSD comparison of means within the same column at $P = 0.05$. Different superscripts indicate significant difference among treatments in the same column.
All wax abbreviations can be found in Table 17.

Table 22. Diameter (mm) of growth of *G. candidum* over three days on 1.0 mM wax-infused potato dextrose agar (PDA) media.

Entry	G. candidum		
	Day 1	Day 2	Day 3
Blank 1	14.1 ± 1.06^{ab}	23.15 ± 0.49^a	31.1 ± 1.48^a
Blank 2	13.55 ± 0.53^b	22 ± 2.12^a	29.3 ± 0.71^a
0.1 mM Imazalil	11.45 ± 0.88^{bc}	15.1 ± 0.28^b	16.6 ± 0.85^c
1.0 mM Imazalil	0.00^d	0.00^d	0.00^e
FS Amine Z	0.00^d	0.00^d	0.00^e
TAW	0.00^d	0.00^d	0.00^e
TBW	10.1 ± 0.77^c	11.25 ± 0.53^c	12.1 ± 0.28^d
TEW	18.00 ± 0.64^a	20.55 ± 0.88^a	21.15 ± 0.15^b
PAW	0.00^d	14.55 ± 0.81^{bc}	16.65 ± 0.53^c
PBW	0.00^d	13.15 ± 1.23^{bc}	13.80 ± 0.64^{cd}
PEW	0.00^d	0.00^d	0.00^e

Significance determined by duplicate analysis with Tukey HSD comparison of means within the same column at $P = 0.05$. . Different superscripts indicate significant difference among treatments in the same column.
All wax abbreviations can be found in Table 17.

comparable to a low dose (0.1 mM) of the fungicide Imazalil. The formation of spores of *P. Italicum* was seemingly delayed by TBW compared to other treatments as there were no signs of sporulation after three days. It is possible that the smaller structure allowed for greater access to the growing fungi due to less encumbrance when the wax was finely dispersed in the agar, resulting in an increased antifungal effect. The attenuation in antifungal activity appeared to be reversed for PAW and PBW, however. For TEW, increasing the molecular weight of the structure by introducing the stearyl ester groups appeared to further attenuate the antifungal activity compared to TAW and TBW. For PEW, nonetheless, the stearyl esters exerted an astonishing antifungal activity compared to PAW, PBW and even a low dose of Imazalil. In agreement with previous reports, the length of alkyl chain, specifically C_8, does exert influence on the biocidal activity of our QAC waxes. Although it has been reported that longer alkyl chains may attenuate the activity of other QACs, we observed the long stearyl ester groups of TEW and PEW were capable of exhibiting potent–antifungal activity. This feature is promising as the stearyl ester moiety is biobased in origin and increases the likelihood for biodegradability.

These antimicrobial activity against fungi differed from that of bacteria, possibly due to how the waxes were used (solid surface vs. dispersed) and differences in the cell wall or membranes of fungi and bacteria. When coated on the wells for the antibacterial tests, there may have existed a preferred molecular orientation and different surface properties. However, as the waxes were dispersed in an aqueous medium (i.e., agar for antifungal tests) with fine particles interacting predominantly by polar interactions, it may be the case that the molecular orientation at the interface of the media was different. Because of this, it is possible that the quaternized nitrogen atom in PEW was less buried by the two stearyl ester groups due to self-association of the hydrophobic substituents in an aqueous system, thereby providing the quaternized nitrogen

atom greater access to the cell membrane. There may be a difference in the mode of action of QACs against fungi as well as between different fungal species. It is believed that the prevailing method of antifungal action is due to "reversal" of the charge on the surface of the cell membrane.[51] This would point to the accessibility of the positive charge being a more important characteristic compared to penetration by hydrophobic groups present in the molecule. Further studies are warranted to differentiate the proposed mode of action. Nevertheless, this study serves as validation that QACs can be attached to wax backbones, and the resulting materials can still exhibit antimicrobial activity.

Conclusions

The development of QAC waxes with proven antimicrobial activity represents a potentially new technology for application in the postharvest coating of perishable fruits and vegetables. In this study, the antimicrobial activity of QACs with alkyl, benzyl, and stearyl hydrophobic groups attached to either the terminal or pendant positions of wax backbones was investigated. The physical properties were likewise characterized to determine whether the materials could be used in postharvest coating applications. The C_8 alkyl group, exhibited a general and potent antimicrobial effect against bacteria and fungi. The stearyl ester groups exhibited astonishing antifungal activity. The attachment of QACs at the pendant position resulted in a more pronounced antimicrobial effect compared to the terminal position. Although none of the synthesized QAC waxes had desirable physical properties comparable to that of commercial waxes, blends with carnauba wax and beeswax suggested broad compatibility. This may in turn curtail the use of antimicrobial agents such as Imazalil, which are widely used in the postharvest coating industry. Further, the utilization of biobased feedstocks such as stearic acid may potentially bode well for the biodegradability of these materials. The intermediate size of these QAC waxes, relative to small QACs and QAC polymers, warrants further exploration to create new applications.

a. *S. aureus*
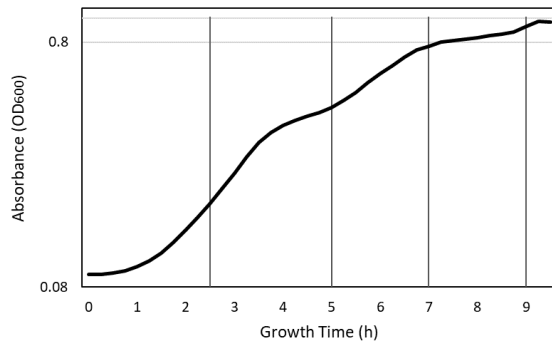
b. *L. monocytogenes*
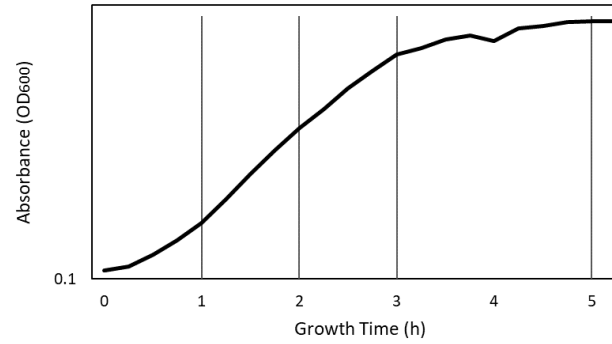
c. *E. coli*
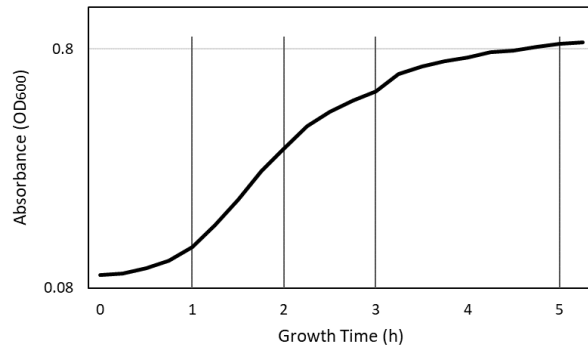
Figure 33. Growth curves of *S. aureus* (a), *L. monocytogenes* (b), and *E. coli* (c) from the beginning of growth to the onset of stationary phase with vertical lines indicating data collection time point.
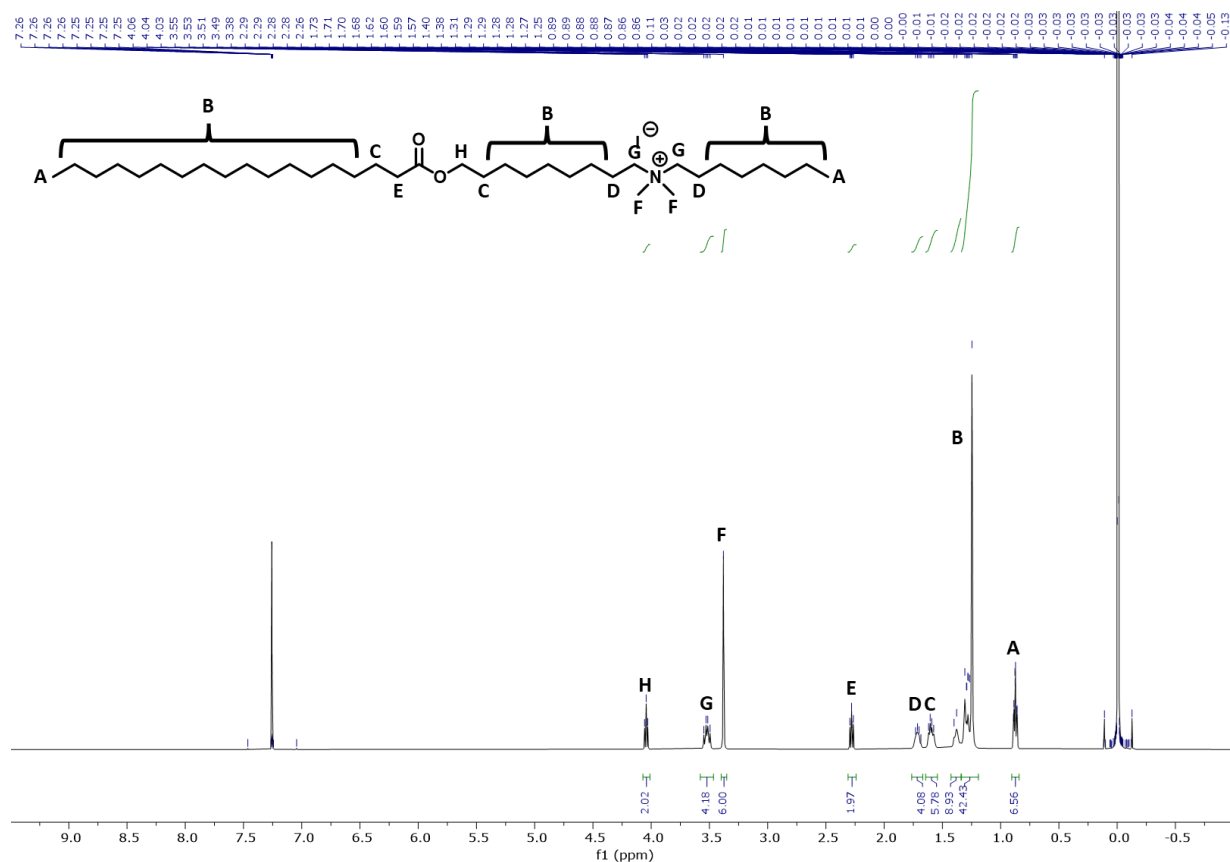
Figure 34. 1H NMR of TAW: ^{1}H NMR (500 MHz, cdcl$_3$) δ 4.04 (t, J = 6.8 Hz, 2H), 3.58 – 3.46 (m, 4H), 3.38 (s, 6H), 2.28 (dd, J = 8.1, 7.1 Hz, 2H), 1.71 (q, J = 8.0 Hz, 4H), 1.60 (dd, J = 14.4, 7.5 Hz, 6H), 1.39 (d, J = 11.1 Hz, 9H), 1.28 (d, J = 30.6 Hz, 42H), 0.90 – 0.84 (br, 7H).

Enthalpy (normalized): 62.061 J/g
Onset x: 42.40 °C

Peak temperature: 44.47 °C
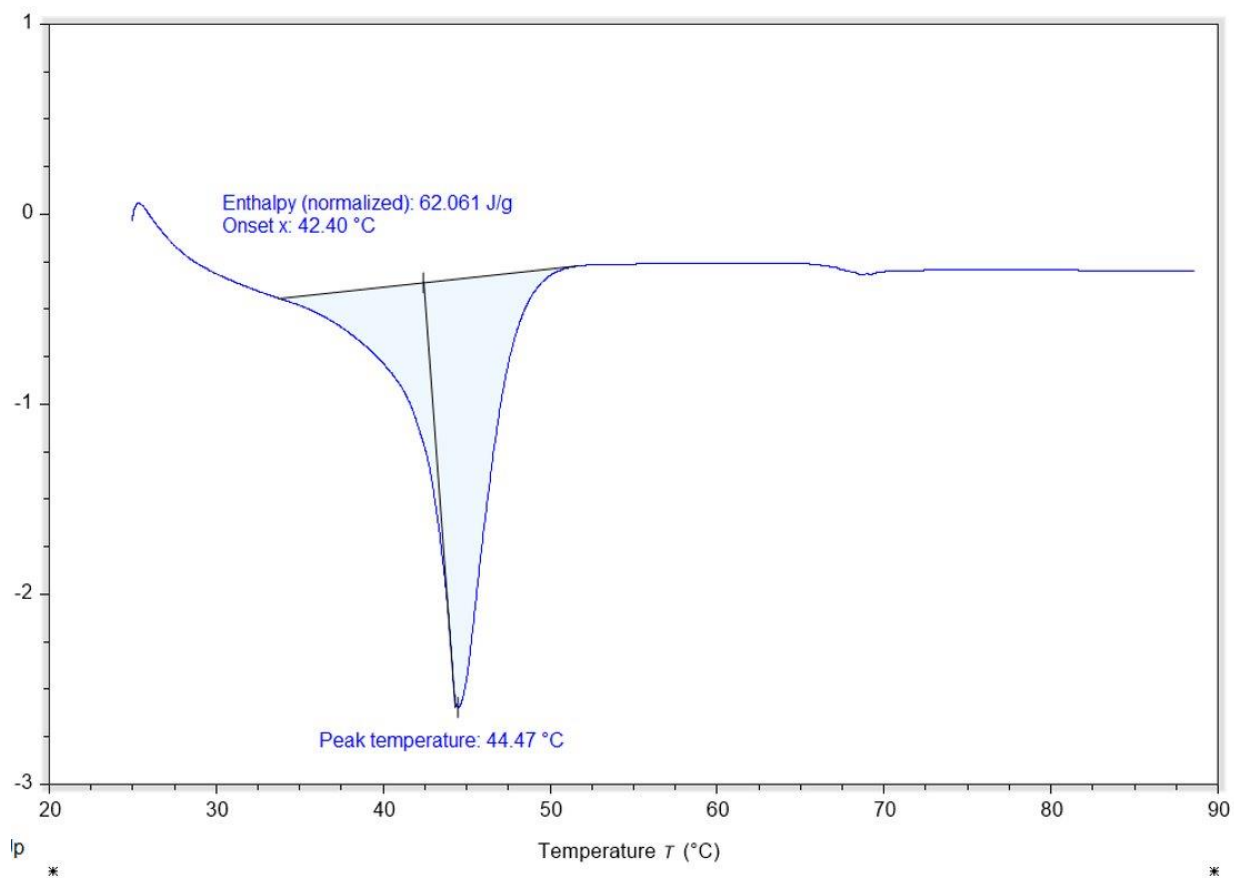
Figure 35. DSC melting curve of TAW

Enthalpy (normalized): 43.451 J/g
Onset x: 34.21 °C

Peak temperature: 39.40 °C
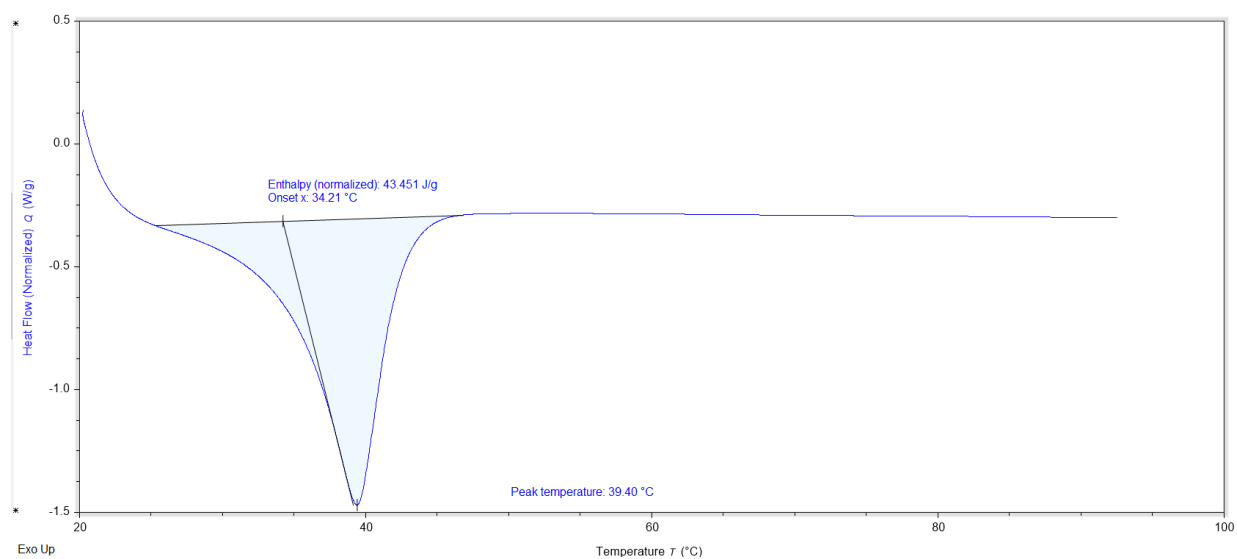
Figure 36. DSC melting curve of TBW

111
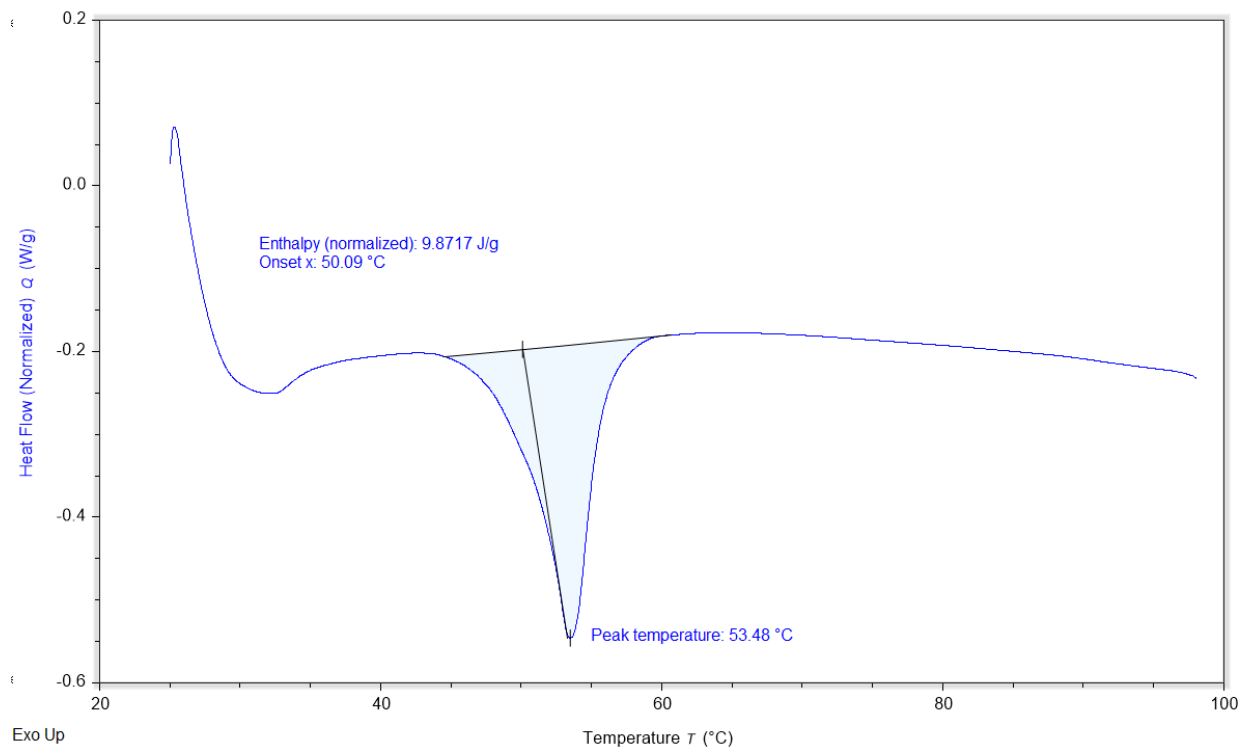
Figure 37. DSC melting curve of TEW
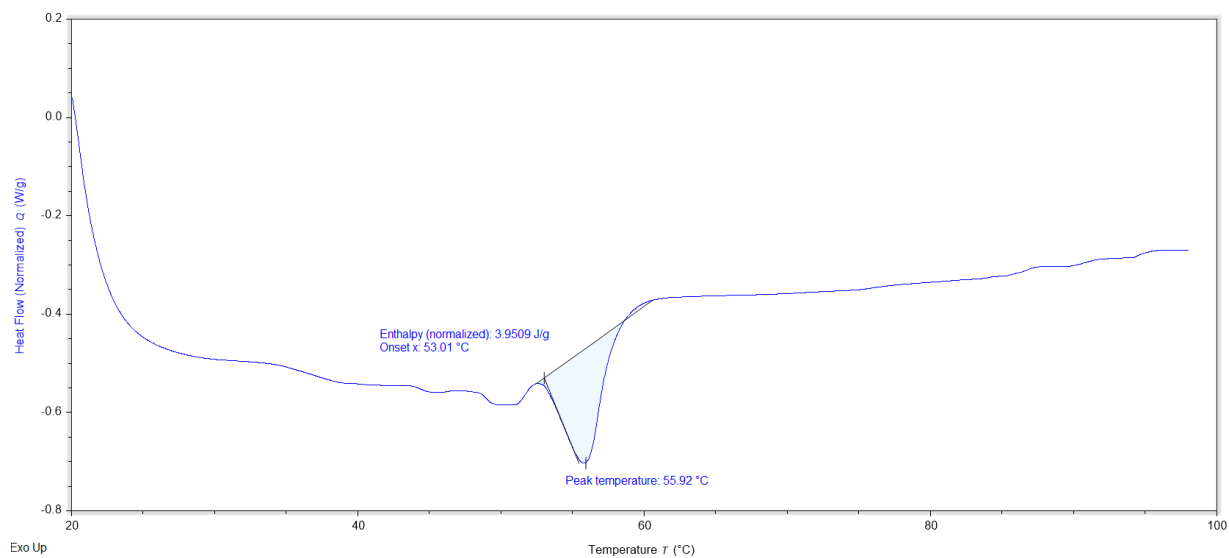
Figure 38. DSC melting curve of PAW

112
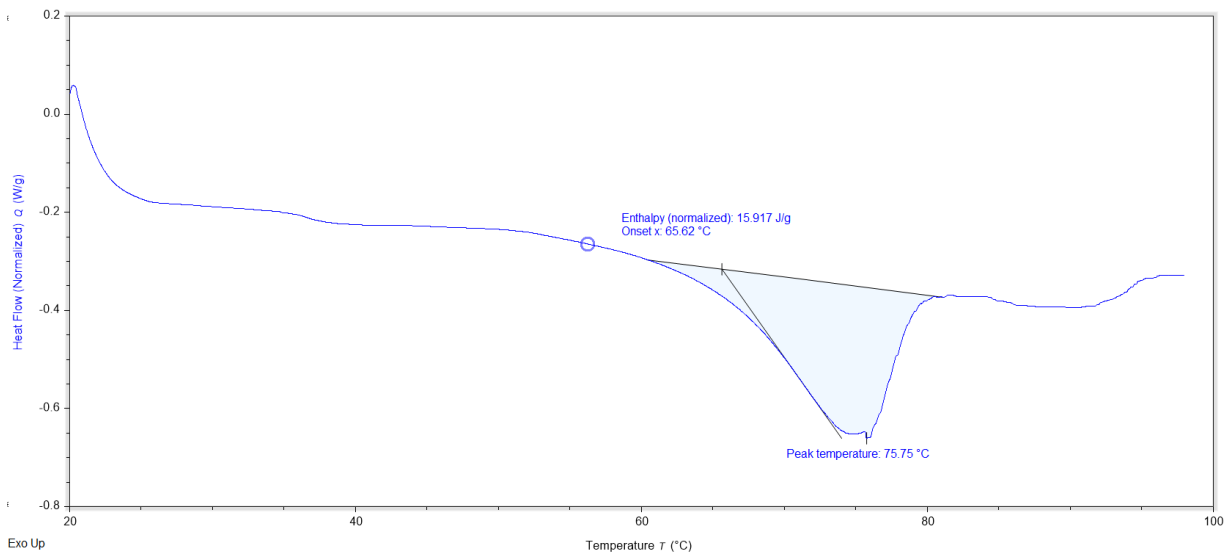
Figure 39. DSC melting curve of PBW
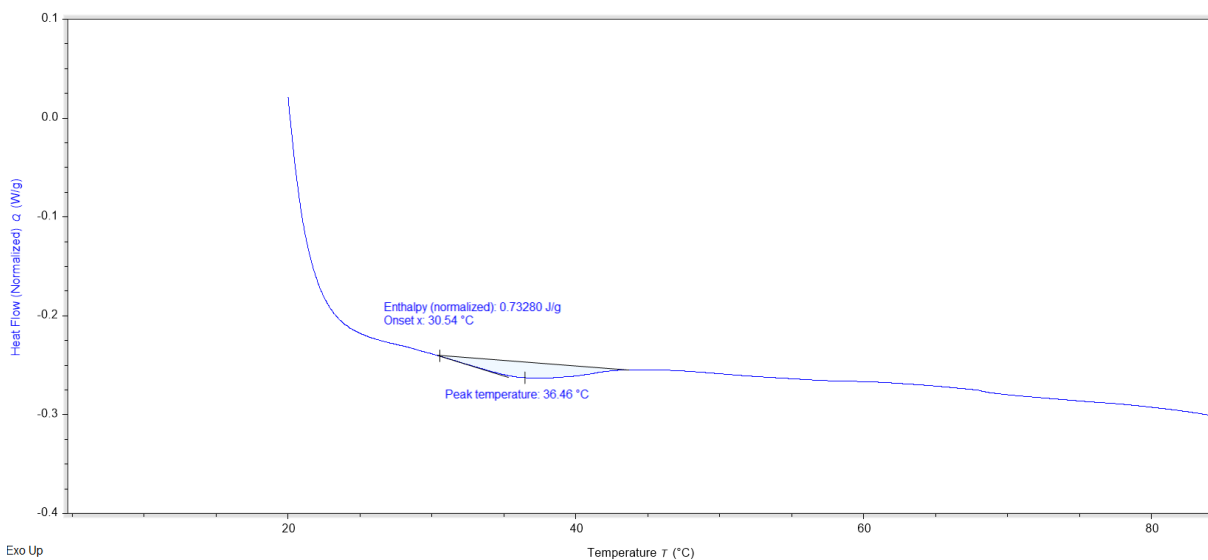
Figure 40. DSC melting curve of PEW

113

a. Paraffin   b. TAW
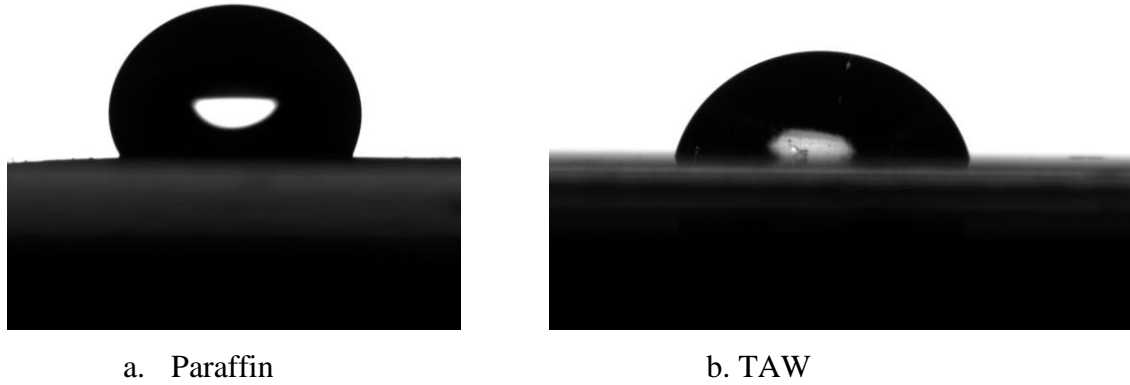
Figure 41. Surface contact angle images of paraffin and TAW with 10 µL of deionized water deposited on the surface.
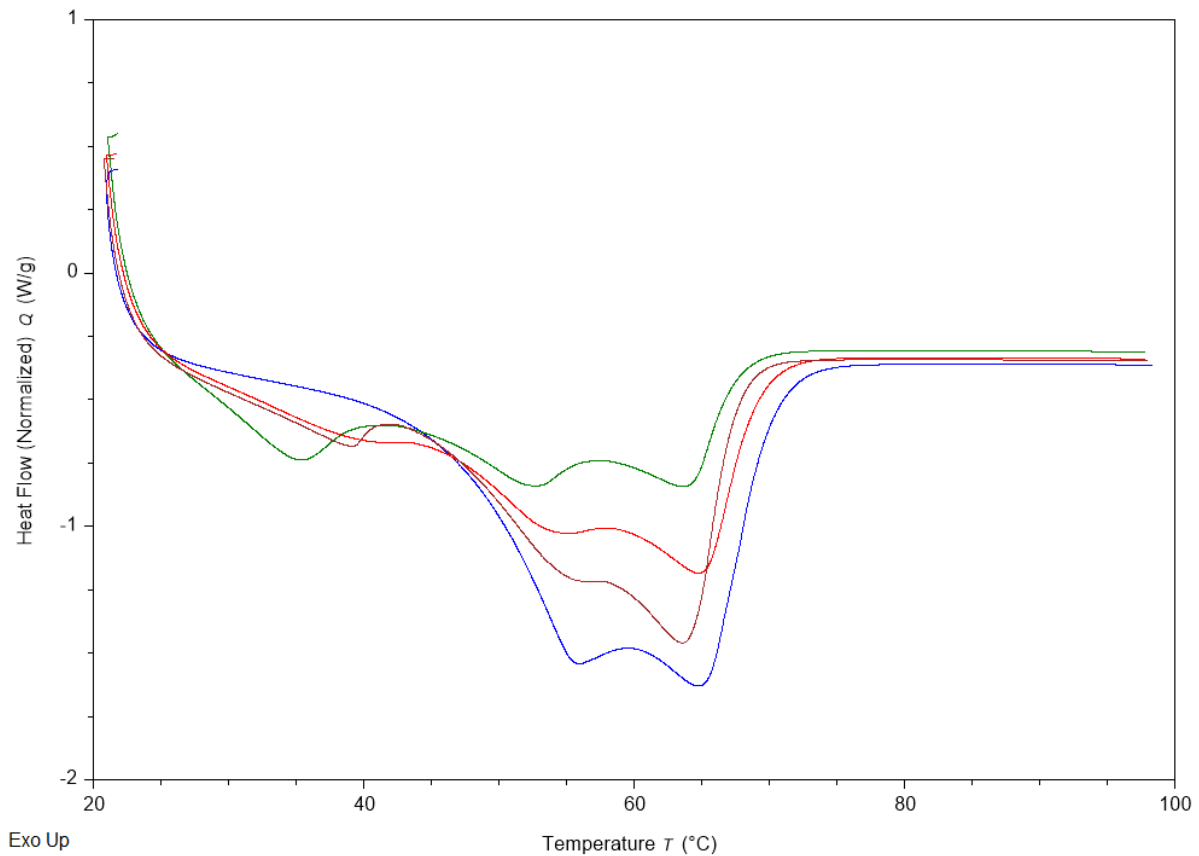
Figure 42. DSC melting curve of beeswax (blue), with TAW included at 15 (brown), 30 (red), and 50 wt.% (green)
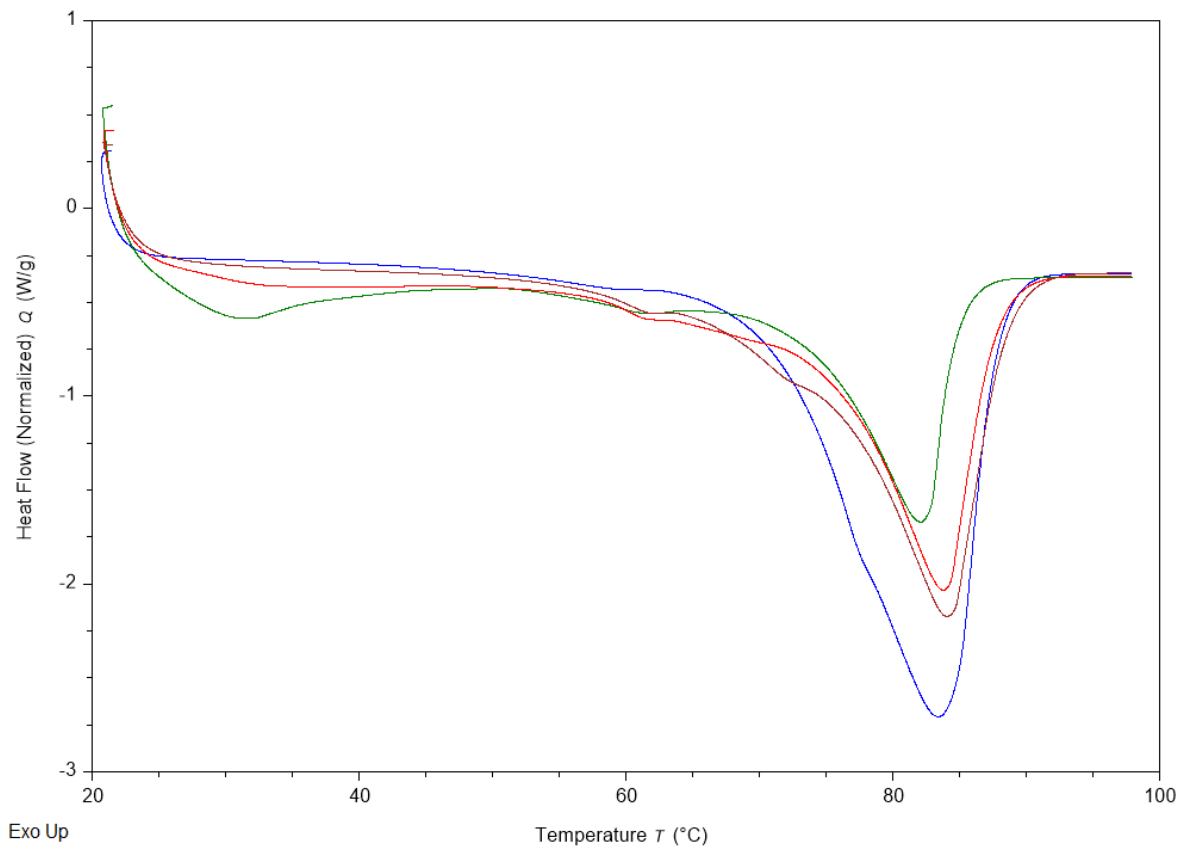
Figure 43. DSC melting curve of carnauba wax (blue), with TAW included at 15 (brown), 30 (red), and 50 wt.% (green)

REFERENCES

1.   U.S. Imports 1970-2022.
2.   American Agricultural Exports Shattered Records in 2021.
3.   Global vegetable oil production set to reach new record highs | Biofuels International Magazine.
4.   Kertesz, M., Pancake Bonding: An Unusual Pi-Stacking Interaction. *Chemistry – A European Journal* **2019,** *25* (2), 400-416.
5.   Jia, C.; Yuan, C.; Ma, Z.; Du, Y.; Liu, L.; Huang, Y., Improving the Mechanical and Surface Properties of Aramid Fiber by Grafting with 1,4-Dichlorobutane under Supercritical Carbon Dioxide. *Materials* **2019,** *12* (22), 3766.
6.   Xia, D.; Wang, L. J., Sulfuric Acid Treatment of Aramid Fiber for Improving the Cationic Dyeing Performance. *Advanced Materials Research* **2012,** *627*, 243-247.
7.   Dave, H.; Ledwani, L.; Nema, S. K., Nonthermal plasma: A promising green technology to improve environmental performance of textile industries. In *The Impact and Prospects of Green Chemistry for Textile Technology*, Elsevier: 2019; pp 199-249.
8.   Behera, D.; Banthia, A. K., Synthesis, characterization, and kinetics study of thermal decomposition of epoxidized soybean oil acrylate. *Journal of Applied Polymer Science* **2008,** *109* (4), 2583-2590.
9.   Hernandez, S.; Vigueras, E., Acrylated-Epoxidized Soybean Oil-Based Polymers and Their Use in the Generation of Electrically Conductive Polymer Composites. In *Soybean - Bio-Active Compounds*, El-Shemy, H., Ed. InTech: 2013.
10.   Bevilacqua, A.; Corbo, M. R.; Sinigaglia, M., *The Microbiological Quality of Food: Foodborne Spoilers*. Elsevier Science & Technology: Cambridge, UNITED KINGDOM, 2016.
11.   Barth, M.; Hankinson, T. R.; Zhuang, H.; Breidt, F., Microbiological Spoilage of Fruits and Vegetables. Springer New York: 2009; pp 135-183.
12.   Chan, M., The Coat on Fruits – Wax? **2016**.
13.   Yasa, S. R.; Kaki, S. S.; Poornachandra, Y.; Kumar, C. G.; Penumarthy, V., Synthesis, characterization, antimicrobial and biofilm inhibitory studies of new esterquats. *Bioorganic & Medicinal Chemistry Letters* **2016,** *26* (8), 1978-1982.
14.   Attri, P.; Yusupov, M.; Park, J. H.; Lingamdinne, L. P.; Koduru, J. R.; Shiratani, M.; Choi, E. H.; Bogaerts, A., Mechanism and comparison of needle-type non-thermal direct and indirect atmospheric pressure plasma jets on the degradation of dyes. *Scientific Reports* **2016,** *6* (1), 34419.
15.   Nasirizadeh, N.; Dehghanizadeh, H.; Yazdanshenas, M. E.; Moghadam, M. R.; Karimi, A., Optimization of wool dyeing with rutin as natural dye by central composite design method. *Industrial Crops and Products* **2012,** *40*, 361-366.
16.   Hunterlab Advanced Organic Spectroscopy Tools for Beginning Organic Spectroscopists.
17.   Ferrero, F.; Periolatto, M., Glycerol in comparison with ethanol in alcohol-assisted dyeing. *Journal of Cleaner Production* **2012,** *33*, 127-131.
18.   Zheng, H.; Zheng, L., Dyeing of Meta-aramid Fibers with Disperse Dyes in Supercritical Carbon Dioxide. *Fibers Polym* **2014,** *15*, 1627-1634.

19. Islam, M. T.; Aimone, F.; Ferri, A.; Rovero, G., Use of N-methylformanilide as swelling agent for meta-aramid fibers dyeing: Kinetics and equilibrium adsorption of Basic Blue 41. *Dyes and Pigments* **2015,** *113*, 554-561.

20. Morris, M.; Ye, X. P.; Doona, C. J., Dyeing Para-Aramid Textiles Pretreated with Soybean Oil and Nonthermal Plasma Using Cationic Dye. *Polymers* **2021,** *13* (9), 1492.

21. Long, J.-J.; Xiao, G.-D.; Xu, H.-M.; Wang, L.; Cui, C.-L.; Liu, J.; Yang, M.-Y.; Wang, K.; Chen, C.; Ren, Y.-M.; Luan, T.; Ding, Z.-F., Dyeing of cotton fabric with a reactive disperse dye in supercritical carbon dioxide. *The Journal of Supercritical Fluids* **2012,** *69*, 13-20.

22. Lee, J. W.; Min, J. M.; Bae, H. K., Solubility Measurement of Disperse Dyes in Supercritical Carbon Dioxide. *Journal of Chemical & Engineering Data* **1999,** *44* (4), 684-687.

23. Akdag, A.; Kocer, H. B.; Worley, S. D.; Broughton, R. M.; Webb, T. R.; Bray, T. H., Why Does Kevlar Decompose, while Nomex Does Not, When Treated with Aqueous Chlorine Solutions? *J. Phys. Chem. B* **2007,** *111* (20), 5581-5586.

24. Fei, T.; Walker, J. A.; Vickerman, K. L.; Stanley, L. M.; Jarboe, D.; Wang, T., Synthesis and characterization of soybean oil-based waxes and their application as paraffin substitute for corrugated coating. *Journal of Industrial and Engineering Chemistry* **2018,** *58*, 113-122.

25. Kim, E. J.; Kim, M.-K.; Jin, X.-J.; Oh, J.-H.; Kim, J. E.; Chung, J. H., Skin Aging and Photoaging Alter Fatty Acids Composition, Including 11,14,17-eicosatrienoic Acid, in the Epidermis of Human Skin. *J Korean Med Sci* **2010,** *25* (6), 980-983.

26. Zeisler-Diehl, V. V.; Barthlott, W.; Schreiber, L., Plant Cuticular Waxes: Composition, Function, and Interactions with Microorganisms. Springer International Publishing: 2018; pp 1-16.

27. Antimicrobial finishes for textiles | Elsevier Enhanced Reader. **2015**.

28. Tavakolian, M.; Jafari, S. M.; van de Ven, T. G. M., A Review on Surface-Functionalized Cellulosic Nanostructures as Biocompatible Antibacterial Materials. *Nano-Micro Lett.* **2020,** *12* (1), 73.

29. Grigoras, A. G., Natural and synthetic polymeric antimicrobials with quaternary ammonium moieties: a review. *Environ Chem Lett* **2021**.

30. Lv, X.; Liu, C.; Song, S.; Qiao, Y.; Hu, Y.; Li, P.; Li, Z.; Sun, S., Construction of a quaternary ammonium salt platform with different alkyl groups for antibacterial and biosensor applications. *RSC Adv.* **2018,** *8* (6), 2941-2949.

31. Dizman, B.; Elasri, M. O.; Mathias, L. J., Synthesis and antimicrobial activities of new water-soluble bis-quaternary ammonium methacrylate polymers. *Journal of Applied Polymer Science* **2004,** *94* (2), 635-642.

32. García, M. T.; Ribosa, I.; Guindulain, T.; Sánchez-Leal, J.; Vives-Rego, J., Fate and effect of monoalkyl quaternary ammonium surfactants in the aquatic environment. *Environ Pollut* **2001,** *111* (1), 169-75.

33. Boethling, R. S.; Sommer, E.; Difiore, D., Designing Small Molecules for Biodegradability. *Chemical Reviews* **2007,** *107* (6), 2207-2227.

34. Zhang, C.; Cui, F.; Zeng, G. M.; Jiang, M.; Yang, Z. Z.; Yu, Z. G.; Zhu, M. Y.; Shen, L. Q., Quaternary ammonium compounds (QACs): a review on occurrence, fate and toxicity in the environment. *Sci Total Environ* **2015,** *518-519*, 352-62.

35. Minbiole, K. P. C.; Jennings, M. C.; Ator, L. E.; Black, J. W.; Grenier, M. C.; LaDow, J. E.; Caran, K. L.; Seifert, K.; Wuest, W. M., From antimicrobial activity to

mechanism of resistance: the multifaceted role of simple quaternary ammonium compounds in bacterial eradication. *Tetrahedron* **2016,** *72* (25), 3559-3566.

36.   Ingalsbe, M. L.; Denis, J. D. S.; McGahan, M. E.; Steiner, W. W.; Priefer, R., Development of a novel expression, ZIMAX/KZI, for determination of the counter-anion effect on the antimicrobial activity of tetrabutylammonium salts. *Bioorganic & Medicinal Chemistry Letters* **2009,** *19* (17), 4984-4987.

37.   Fei, T.; Jarboe, D.; Wang, T., Soybean oil as feedstock for the synthesis and characterization of a carnauba substitute and a study of the structure–function relationships. *Journal of Industrial and Engineering Chemistry* **2018,** *57*, 416-423.

38.   Salmon, R.; Efremov, I. V., Oxalyl Chloride. *Encyclopedia of Reagents for Organic Synthesis* **2008**.

39.   Tsoungas, P.; Assimomytis, N.; Sariyannis, Y.; Stavropoulos, G.; Varvounis, G.; Cordopatis, P., Anionic ortho-Fries Rearrangement, a Facile Route to Arenol-Based Mannich Bases. *Synlett* **2009,** *2009* (17), 2777-2782.

40.   Finkelstein, H., Darstellung organischer Jodide aus den entsprechenden Bromiden und Chloriden. *Berichte der deutschen chemischen Gesellschaft* **1910,** *43* (2), 1528-1532.

41.   Leyva-Gutierrez, F. M. A.; Wang, T., Crystallinity and Water Vapor Permeability of <i>n-</i>Alkane, Alcohol, Aldehyde, and Fatty Acid Constituents of Natural Waxes. *Industrial & Engineering Chemistry Research* **2021,** *60* (41), 14651-14663.

42.   Yao, L.; Wang, T., Textural and Physical Properties of Biorenewable "Waxes" Containing Partial Acylglycerides. *Journal of The American Oil Chemists Society - J AMER OIL CHEM SOC* **2012,** *89*, 156-157.

43.   Sakr, A.; Brégeon, F.; Mège, J. L.; Rolain, J. M.; Blin, O., Staphylococcus aureus Nasal Colonization: An Update on Mechanisms, Epidemiology, Risk Factors, and Subsequent Infections. *Front Microbiol* **2018,** *9*, 2419.

44.   Palou, L., Chapter 2 - Penicillium digitatum, Penicillium italicum (Green Mold, Blue Mold). In *Postharvest Decay*, Bautista-Baños, S., Ed. Academic Press: San Diego, 2014; pp 45-102.

45.   Dorset, D. L. In *Crystallography of the Polymethylene Chain: An Inquiry into the Structure of Waxes*, 2005.

46.   Cabras, P.; Schirra, M.; Pirisi, F.; Garau, V.; Angioni, A., Factors Affecting Imazalil and Thiabendazole Uptake and Persistence in Citrus Fruits Following Dip Treatments. *Journal of agricultural and food chemistry* **1999,** *47*, 3352-4.

47.   Gupta, S.; Ivvala, J.; Grewal, H. S., Development of natural wax based durable superhydrophobic coatings. *Industrial Crops and Products* **2021,** *171*, 113871.

48.   Jurak, G.; Bošnir, J.; Đikić, D.; Ćuić, A. M.; Prokurica, I. P.; Racz, A.; Jukić, T.; Stubljar, D.; Starc, A., The Risk Assessment of Pesticide Ingestion with Fruit and Vegetables for Consumer's Health. *International Journal of Food Science* **2021,** *2021*, 1-8.

49.   Thorsteinsson, T.; Másson, M.; Kristinsson, K. G.; Hjálmarsdóttir, M. A.; Hilmarsson, H.; Loftsson, T., Soft Antimicrobial Agents: Synthesis and Activity of Labile Environmentally Friendly Long Chain Quaternary Ammonium Compounds. *Journal of Medicinal Chemistry* **2003,** *46* (19), 4173-4181.

50.   Landeck, L.; Baden, L. A.; John, S. M., Detergents. In *Kanerva's Occupational Dermatology*, John, S. M.; Johansen, J. D.; Rustemeyer, T.; Elsner, P.; Maibach, H. I., Eds. Springer International Publishing: Cham, 2020; pp 1131-1143.

51.   Kwaśniewska, D.; Chen, Y.-L.; Wieczorek, D., Biological Activity of Quaternary Ammonium Salts and Their Derivatives. *Pathogens* **2020,** *9* (6), 459.

CONCLUSION

Oleochemicals continue to be a growing commodity of need that are utilized across a multitude of industries. While the United States continues to export an ever-increasing quantity of oleochemicals, an ever-increasing quantity also continues to be imported. Therefore, the work described aimed to innovate and develop further functionality for domestic oleochemicals.

The first two chapters of this work examined the use of oleochemicals as dyeing pretreatments for para-aramids aiming to improve the color strength after dyeing with either cationic or disperse pigments. The first chapter details the sequential design utilized for investigation of the ideal molar ratios of soybean oil or glycerol and acrylic acid along with NTP treatment to improve the color strength in an aqueous cationic dye system. The second chapter details the sequential design necessary to complete the same task with disperse dye in both an aqueous and supercritical CO_2 dyeing system. NTP treatment and dyeing did not result in any major reduction in tensile strength of dyed para-aramids. There was evidence in both the cationic and disperse dye systems of covalent linkages formed between the para-aramid fabric, the SOAAC intermediate, and the dye molecules.

Of the dye systems investigated, the cationic dye system with the SOAAC pretreatment resulted in the greatest color strength of all dye systems investigated. This provides an effective method to successfully dye the extremely commercially relevant para-aramids utilizing an already common aqueous dyeing method. However, the success of the $SCCO_2$ dyeing system cannot be overstated. This method provides a renewable utilization of the CO_2 dyeing medium, while also completely removing the production of wastewater, the largest unit of waste in the textile industry. Also, the $SCCO_2$ method resulted in the smallest observed reduction in fastness (dK/S of 2.18 % compared to the aqueous disperse of 11.1 %, and aqueous cationic of 10.3 %),

therefore providing a better fixation of dye to the para-aramids compared to the other methods. Overall, this work assisted in identifying green solutions to the difficult to dye para-aramids, while also further expanding the very limited knowledge of this material in the dyeing industry.

The last chapter of this work detailed the use of oleochemicals to synthesize antimicrobial coating materials, specifically for fruits and vegetables. With successful synthesis and analysis of the QAC wax products, covalent attachment of QAC's to a wax backbone presented a feasible method to feasibly generate significant antimicrobial effect on green, domestic wax materials. This also laid the foundation for further exploration of intermediate sized QAC's, as both small QAC salts, and large QAC polymers have been extensively researched. By utilization of these oil-based wax materials, it is also possible to obtain the hydrophobic property of QAC polymer coatings while still maintaining the biodegradability of the ester functional groups.

VITA

Caleb Matthew Metzcar was born in Greenville, Ohio. At age 4 he moved with his parents and brother to Omaha, Nebraska where he stayed for 5 years before moving to Cincinnati, Ohio, where he attended both middle and high school. He majored in food science and technology at The Ohio State University. He also worked as an intern for American Foods Group, Cargill, and Coca-Cola in product development and operations management during this time. In 2020, he joined the research group of Dr. Tong Wang at The University of Tennessee Knoxville while being co-advised with Dr. Xiaofei Ye. He was given the opportunity to support research related to lipid chemistry and applications.